UNCLASSIFIED

BOILING AND CONDENSATION IN A LIQUID-FILLED ENCLOSURE

by

Avram Markowitz
B. Sc. and M. Sc.
Massachusetts Institute of Technology
(1968)

Submitted in Partial Fulfillment
of the Requirements for the Degree of
Doctor of Philosophy
at the

MASSACHUSETTS INSTITUTE OF TECHNOLOGY
January 1971

Signature of Author. . . . . .
Department of Mechanical Engineering, January 15, 1971

Certified by . . . . . .
Thesis Supervisor

Accepted by . . . . . .
Chairman, Departmental Committee on Graduate Students

UNCLASSIFIED

BOILING AND CONDENSATION IN A LIQUID-FILLED ENCLOSURE

by

Avram Markowitz

Submitted to the Department of Mechanical Engineering on January 15, 1971 in partial fulfillment of the requirements for the degree of Doctor of Philosophy

ABSTRACT

A combined experimental and analytical investigation of boiling and condensation in a liquid-filled enclosure, with water and Freon-113 as the working fluids, is described. The operating characteristics of a boiling system, utilizing a condenser submerged in the fluid, are presented and related to specific operational modes and thermal transport mechanisms.

A lower bound of operation, corresponding to natural convection heat transfer at both the heated and condenser surfaces, is identified. Similarly, for the commonly encountered range of system operation, a condensive upper bound is identified and shown to correspond to vapor space condensation.

A nondimensional vapor bubble collapse length, L_c/W, is found to govern the rate and mechanism of heat transfer at the submerged condenser surface. Values of $\frac{L_c}{W} << 1$ are associated with natural convection heat transfer at the submerged condenser. For $\frac{L_c}{W} \sim 1$ the presence of a substantial vapor fraction in the bulk liquid leads to augmented convection, while for values of $\frac{L_c}{W} >> 1$ condensation is found to dominate thermal transport at the condenser surface.

A possible technique for augmenting condensation heat transfer on horizontal surfaces is examined in an attempt to raise the condensive upper bound of submerged condenser operation. A doubly-rippled surface with small, constant radius of curvature undulations is shown to yield a factor of two increases in the rate of vapor space condensation based on the projected area of the condenser surface.

A systematic design procedure for submerged condenser systems utilizing the proposed models and correlations is described and related to typical design considerations.

Thesis Supervisor: A. E. Bergles
Title: Associate Professor of Mechanical Engineering

ACKNOWLEDGMENTS

The thesis investigation described herein was supported by Raytheon Company, Missile Systems Divisions, and performed at the MIT Heat Transfer Laboratory.

Special thanks are extended to Professor A. E. Bergles, thesis supervisor, for his guidance and support during all phases of this investigation.

I am indebted to Professors B. B. Mikic, P. Griffith, W. M. Rohsenow, and A. Sonin, members of the thesis committee, as well as D. L. Cochran and A. Owens of Raytheon Company, MSD, for their encouragement and assistance.

The generous help of F. Johnson and J. Horowitz in assembling and instrumenting the test apparatus is gratefully acknowledged.

The successful completion of this thesis investigation is due in large measure to the love and affectionate understanding of my wife, Annette. The last stages of this work were happily brightened by the smiles and babbling of my newborn son, Barak, who graciously allowed me the use of his desk.

I also wish to thank Annette Markowitz and the Raytheon, MSD, Publications Department for their efforts in preparing the manuscript.

NOMENCLATURE

a - Acceleration

A - Area

B - Bubble collapse parameter, $Ja^2 \frac{K}{R_o} \sqrt{\frac{\rho}{\Delta\rho}}$

c - Arbitrary constant

c_p - Specific heat at constant pressure

c_{sf} - Boiling constant

c_d - Bubble departure constant

D - Diameter

De - Equivalent diameter, (4 x flow area)/(wetted perimeter)

D_o - Bubble departure diameter

F' - Buoyant force per unit volume

Fr - Froude number $v/\sqrt{gr_o}$

Gr - Grashof number, $g \beta (\Delta T) L^3 \rho^2/\mu^2$

g - Gravitational acceleration

g_o - Gravitational constant, 32.17 lb_m ft/lb_f sec^2

h - Heat transfer coefficient

h_{fg} - Latent heat of condensation or evaporation

h'_{fg} - $h_{fg} + 0.68 c_p (T_s - T_c)$

Ja - Jacob number, $c_p \rho (T_s - T_b)/h_{fg} \rho_v$

k - Thermal conductivity

K - Thermal diffusivity, $k/\rho c_p$

L - Length

L_c - Bubble collapse length

n - Exponent

Nu - Nusselt number, $\frac{hL}{k}$ or $\frac{hD}{k}$

Nu^* - Augmentation parameter, Nu_{aug}/Nu_{nc}

P	-	Pressure
Pr	-	Prandtl number $\frac{c_p \mu}{k}$
q	-	Rate of heat transfer
q''	-	Heat flux
Q	-	Volumetric flow rate
r_o	-	Radius of curvature of undulation
R_o	-	Bubble departure radius
Ra	-	Rayleigh number, Gr Pr
R_t	-	Thermal resistance
S	-	Distance along curved surface
T	-	Temperature
t	-	Time
t_c	-	Bubble collapse period
V	-	Volume
V_e	-	Enclosure Volume
v	-	Velocity
v_b	-	Bubble rise velocity
v_j	-	Vapor jet velocity
W	-	Separation distance between heated and condenser surfaces
We	-	Weber number, $r_o \rho v^2/\sigma g_o$
x, y	-	Coordinate axes
z	-	Independent variable
α	-	Volumetric vapor fraction
α	-	Angle
β	-	Thermal coefficient of volumetric expansion
β	-	Bubble contact angle
Γ	-	Mass rate of condensate flow per unit width
γ	-	Bubble collapse ratio, D/D_o
γ	-	Condensate film thickness in undulation trough
δ	-	Condensate film thickness on undulation crest
η	-	Vapor generation parameter
θ	-	Configuration factor

λ - Modified configuration factor

$\hat{\lambda}$ - Nondimensional condensate film thickness

μ - Absolute viscosity

ρ - Mass density

σ - Surface tension

τ - Nondimensional bubble collapse period

ϕ - Nondimensional parameter

ψ - Angle

$\hat{\psi}$ - Nondimensional angle

Subscripts

b - Bulk

c - Cold surface, condenser surface

e - External

f - Fluid

h - Hot surface, heater surface

i - Internal

l - Liquid

m - Mean

nc - Natural convection

s - Saturation

T - Total

v - Vapor

Note: Unsubscripted fluid properties refer to the liquid phase.

TABLE OF CONTENTS

TABLE OF CONTENTS (Cont.)

LIST OF ILLUSTRATIONS

LIST OF ILLUSTRATIONS (Cont.)

1. INTRODUCTION

1.1 Electronic Cooling

The advent of modern, high speed, high power electronic components has generated growing interest in boiling heat transfer for electronic cooling. Most first-generation electronic devices and some of today's standard units are adequately cooled by the natural circulation of ambient air. The cooling requirements of many others can be met by the forced flow of air or other standard fluids in conjunction with highly conductive thermal paths through appropriate structural elements (so-called cold-plates, cold-bars, etc.). However, a growing number of thermal and electrical constraints can be met only by direct immersion of the components and/or devices in a dielectric coolant chosen to provide boiling heat transfer at the heated surfaces. This technique can be applied in two distinct electronic device categories differing widely in dissipated power per unit. The first is typified by high-voltage power supplies for ground and airborne radar transmitters typically dissipating 1-5 kilowatts which must operate successfully over a wide range of environmental conditions and where volumetric and weight considerations are paramount [1]. The second is comprised of solid-state devices in high speed, data processing, logic and memory equipment typically dissipating 200-800 milliwatts where the need to reduce wiring delays [2] and the increased power consumption per gate associated with high switching frequency [3] have led to more compact devices and heat fluxes at the substrate level approaching 200 $W/in.^2$ [4].

In both of the above categories, the relatively small temperature differences inherent in boiling transfer, play a crucial role in reducing thermal cycling. Substantial spatial and temporal power variations can thus be tolerated without increasing component failure rates. In the cooling of high-power components as, for example, in temperature sensitive power tubes, the nearly constant surface temperature is essential to proper operation. In many memory units the maintenance of a relatively narrow temperature range

at the core, despite variations in power dissipation, facilitates precise determination of the required driving current. This in turn reduces power input to the system while, simultaneously, decreasing heat dissipation within the memory by eliminating special circuits otherwise required to compensate for thermal drift [1, 5].

1.2 Pool Boilers

In the design of pool boilers for electronic assemblies, the coolant may be considered expendable or unexpendable. In the expending type the vapor generated is allowed to escape through a pressure control valve [6]. Obviously, the use of such a system is limited to tasks in which the required life is short, since the supply of liquid is rapidly depleted and as the liquid level falls, components are exposed to vapor. For systems requiring a high level of reliability and longer operating life, the generated vapor must be condensed and recirculated.

Initially, such cooling systems had been designed with remote condensers or condensing surfaces placed in the vapor space above the boiling fluid as shown in Fig. 1. There are, however, two major drawbacks associated with a vapor space condenser: packaging height is limited to the liquid height at minimum temperature and the presence of even small quantities of noncondensables (e.g., air) can cause a dramatic degradation in condenser performance [7] leading to higher system pressures and temperatures. Consequently, elaborate filling and degassing procedures must be specified for these systems, thus increasing maintenance costs and decreasing overall reliability.

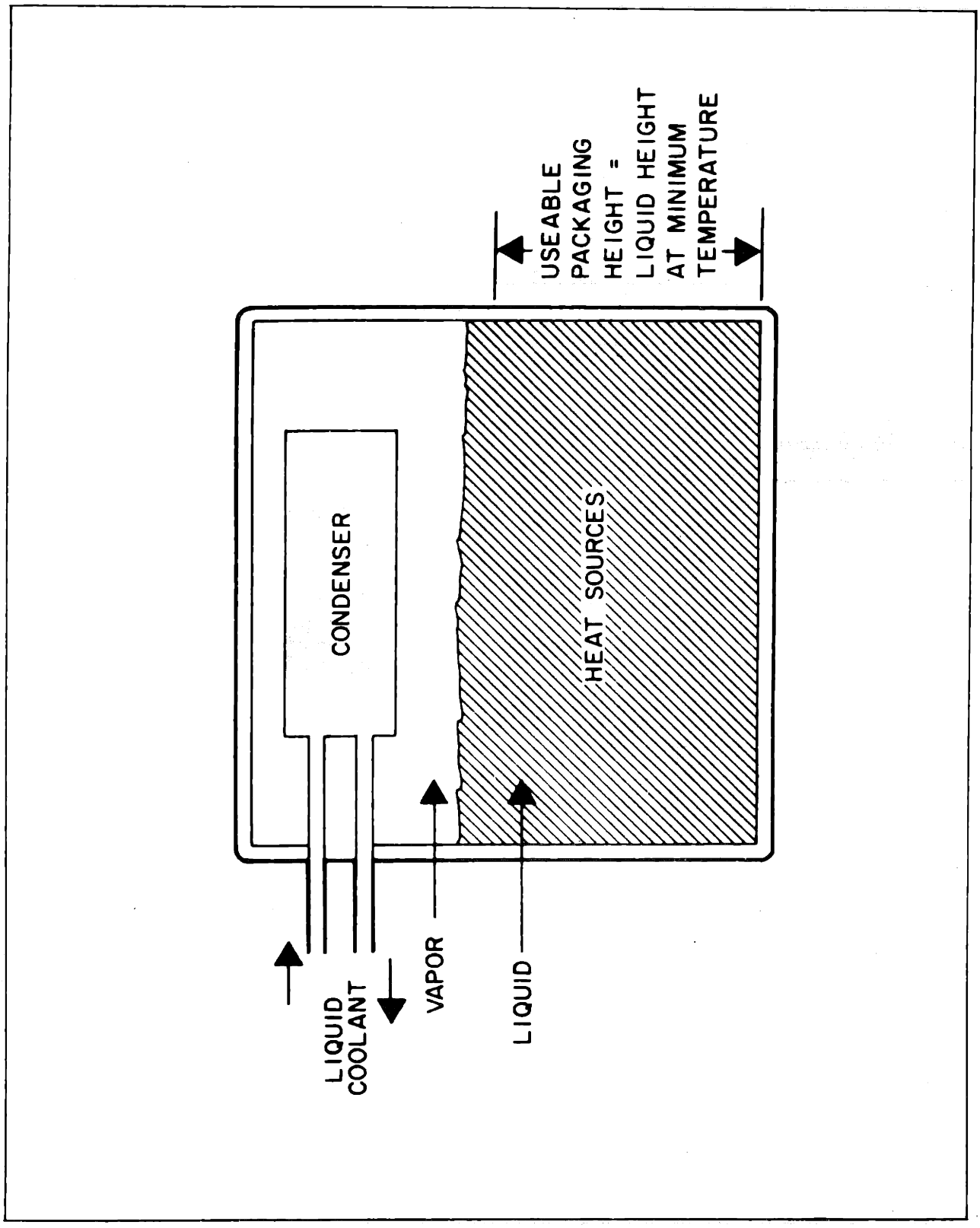

Fig. 1 - Pool Boiler for Electronic Components with Vapor Space Condenser (1)

1.3 Submerged Condenser

It is possible, though to overcome these drawbacks by completely filling the pool boilder and incorporating an expansion chamber in the design, as shown in Fig. 2. The condenser is thus submerged at all times in the liquid and liquid level variations with temperature are eliminated. In this configuration, the condenser surface serves primarily to subcool the liquid in the pool boilder and vapor bubbles generated at the surfaces of the dissipative electronic components rise and begin to condense in the fluid. The presence of noncondensables dissolved in the liquid reduces the collapse rate of the vapor bubbles, but the noncondensables can be removed at the submerged condenser surface by slightly pitching the surface ($\sim 5°$) towards the expansion chamber inlet. The small gas bubbles impinging on the surface slide along the surface and are vented into the expansion chamber. As a result, noncondensables do not substantially affect heat transfer at the submerged condenser surface. This is in sharp distinction with the vapor space condenser in which the noncondensables accumulate in the vapor space and impede the flow of vapor toward the condenser surface. The elimination of the vapor space thus significantly reduces the effect of noncondensables on the thermal performance of the system and, in addition, results in considerable economics in volume and weight [8, 9]. Similar advantages can often be realized by utilizing the side walls of the container as the primary cooling surfaces, as shown in Fig. 3, or as secondary cooling surfaces in conjunction with the horizontal submerged condenser.

As in other boiling systems, the dissipative elements in the submerged condenser system experience only moderate increases in temperature as a result of large increases in their dissipated power. Furthermore, low dissipation or thermally passive components immersed in the bulk fluid undergo only slight changes in temperature for large variations in the total system power dissipated. The major obstacle to widespread use of this technique has been the absence of explicit information on significant design parameters and on the rate of heat transfer at the submerged condenser surface.

Fairbanks et al. [10] have provided a basis for research in this field. Their investigation of a finned condenser submerged in water, FC-75, or a mixture of water and ethylene glycol and placed above boiling surfaces,

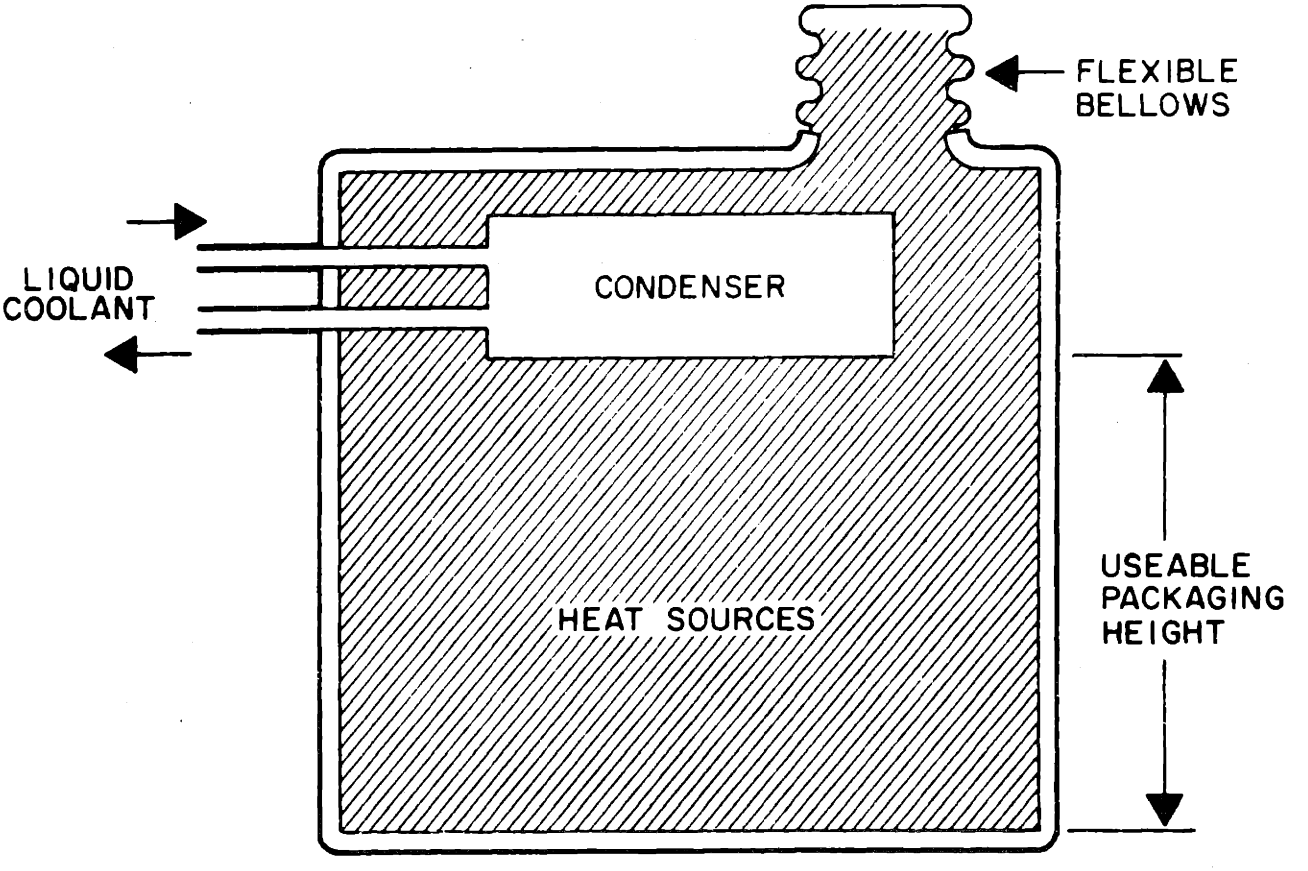

Fig. 2 - Completely Filled Container with Submerged Heat Exchanger

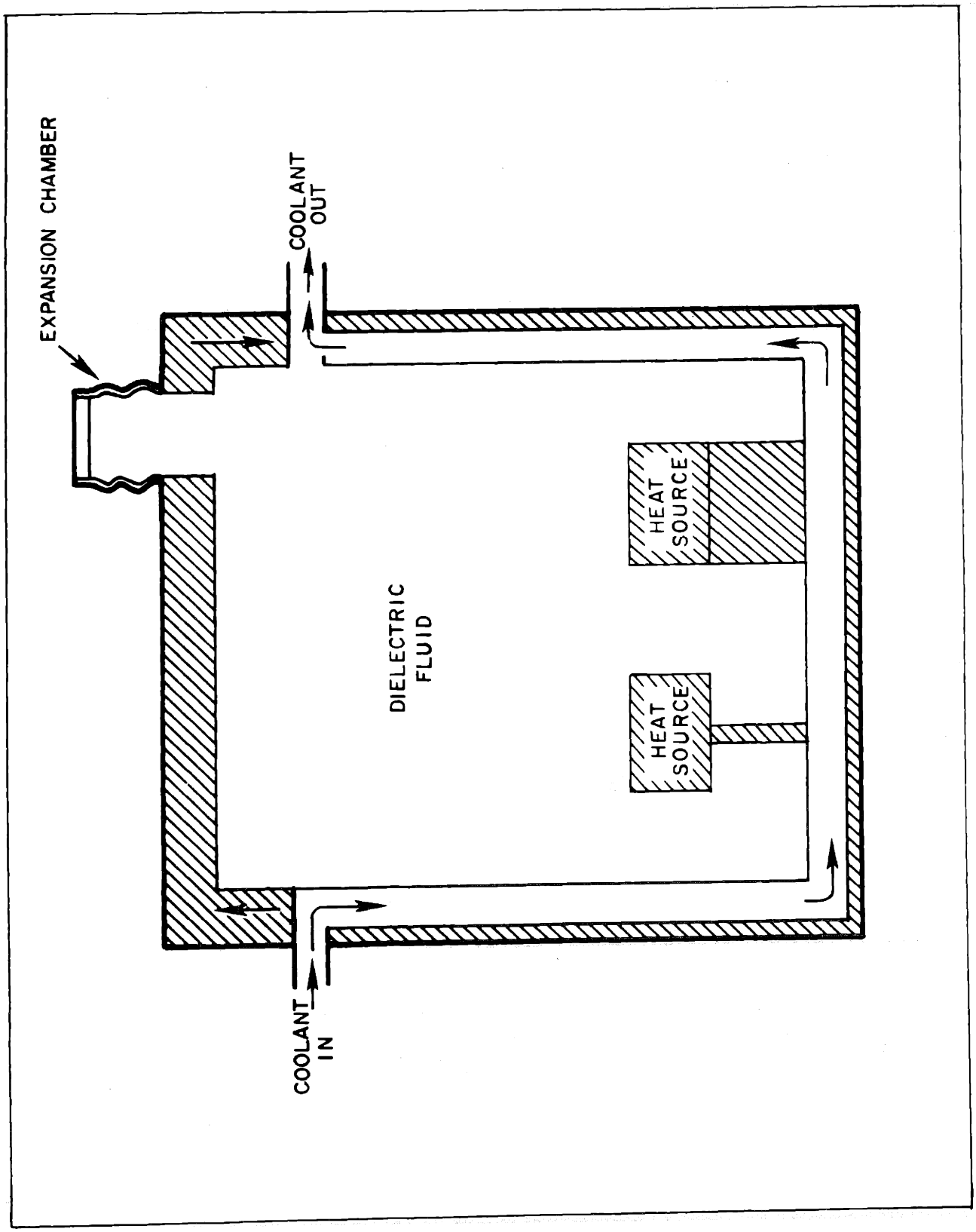

Fig. 3 - Pool Boiler for Electronic Components with Side Wall Cooling

revealed that in the absence of a vapor space the heat transfer coefficients at the condenser surface could attain "50% of the values that would be computed for normal filmwise condensation in a vapor space" [10]. A finned copper plate with 0.25 in. deep and 0.125 in. wide fins spaced 0.125 in. apart with the principal area on the vertical surface of the fins served as the condenser surface. The system was vented to atmospheric pressure and the heat input at the boiling surfaces varied between 0.5 and 1.0 kilowatts, yielding a maximum condenser heat flux based on projected area of approximately 1.9×10^4 Btu/hr-ft^2. Utilizing a trial-and-error dimensionless parameter approach, Fairbanks et al. found that data for all three fluids could be correlated in terms of 3 dimensionless parameters:

$$\phi_1 = \frac{h}{h_{nc}} \quad , \quad \phi_2 = \frac{\rho_v h_{fg}}{\rho c\,(T_s - T_c)} \quad , \quad \phi_3 = \frac{\rho q_c}{\rho_v h_{fg} \mu L}$$

with

$$\phi_1 = c(\phi_2 \cdot \phi_3{}^x)^y$$

to generally within 20 percent. However, the values of x, y, and c were found to vary with the number of heat sources. This latter dependence seriously constrained the usefulness of their correlation and suggested the need for a more fundamental exploration of the thermal mechanisms active in the system.

Simons and Seely [6] investigated the relative performance of several electronic cooling systems, including a submerged condenser system, for a particular electronic packaging configuration. Their results indicate that at a given condenser surface temperature more vapor can be condensed in a system employing a vapor-space condenser than in a system relying on a submerged condenser. The difference in performance between the two systems was small and possible vapor channeling due to the particular packaging configuration substantially reduces the generality of their results.

Despite the absence of a rational design procedure, the inherent advantanges of submerged condenser systems have been recognized and are being presently utilized in the appropriate industrial applications. Raytheon

Company, in particular, has designed a number of submerged condenser systems for cooling high-power radar components [1, 11], as shown in Fig. 4, and continues to specify submerged condenser systems for future applications. However, a fundamental understanding of the thermal mechanism active in submerged condenser systems is necessary if optimum size, cost and efficiency are to be achieved.

1.4 Present Investigation

The aim of this investigation is, then, to conduct a combined analytical and experimental study of the thermal mechanisms active in a submerged condenser system, to define its operational limits and gain explicit information on significant design parameters.

In Chapter 2 the overall operating characteristics of an experimental submerged condenser system utilizing water and Freon-113 as the working fluids are discussed and illustrated with photographs, sketches, and graphs. The relevant thermal mechanisms are examined in detail in Chapter 3. These mechanisms are related to specific operational modes and shown to accurately define the upper and lower bounds of operation. Chapter 4 examines a possible technique for improving the upper bound of operation, and Chapter 5 incorporates the experimental and analytical results in a design procedure for submerged condenser systems.

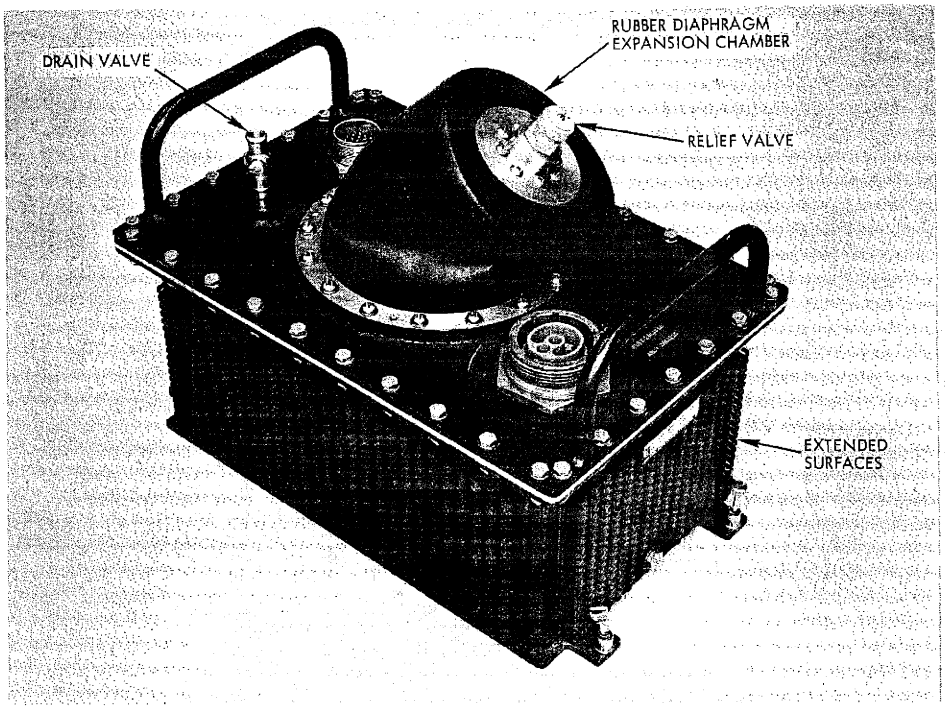

67—38280

Fig. 4A - Side-Wall, Air-Cooled Power Supply Module (1)

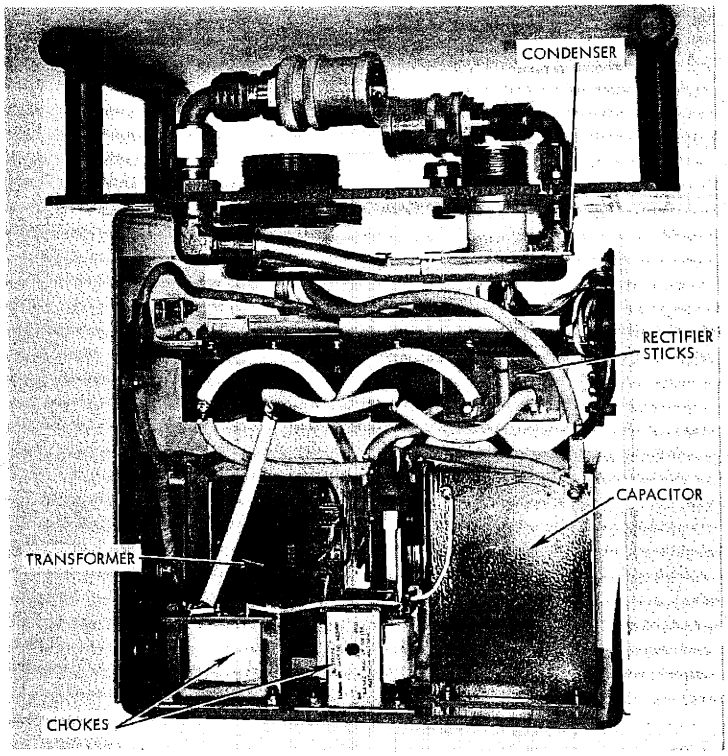

66—35190

Fig. 4B - Submerged Condenser System (1)

2. OPERATING CHARACTERISTICS OF EXPERIMENTAL APPARATUS

2.1 Apparatus and Procedure

The preceeding chapter has briefly reviewed the cooling requirements of electronic devices and components and shown that a particular need exists for submerged condenser cooling systems. However, no analytic or comprehensive design procedure is as yet available. In the present investigation the operating characteristics of a submerged condenser were obtained with the aid of the apparatus shown in Figs. 5 and 6.

The apparatus consisted of five cylindrical heaters, 0.25 inch in diameter, electrically powered and oriented horizontally in an insulated Plexiglas and brass container 6 inches on a side. Degassed water and Freon-113 were chosen as the working fluids. The flat, horizontal condensing surface was at the top of the container, approximately 4.5 inches from the heaters, and incorporated a cooling coil through which city water at nearly 60°F inlet temperature was circulated. A liquid reservoir located on top of the container served to maintain a nearly constant average system pressure of 14.9 psi. The ratio of total heated to condenser surface area varied from 0.14 to 0.71 depending on the number of heaters activated. Flow meters, voltmeters, ammeters, and a stripchart recorder were used as required.

The average condenser surface temperature was determined with thermocouples located 0.030 inch below the surface. The average heated surface temperature was determined by the use of an especially prepared, hollow, thin-walled heater with thermocouples in the center. The appropriate extrapolations based on thermal conductivity and heat flux were made in each case to obtain the average surface temperatures. The bulk temperature of the working fluid was measured by sheathed thermocouples inserted through the base of the container into the fluid.

The operating characteristics and other data were obtained in a series of data runs for each working fluid and heater configuration. Prior to each series of runs the working fluid was carefully degassed. For each run the

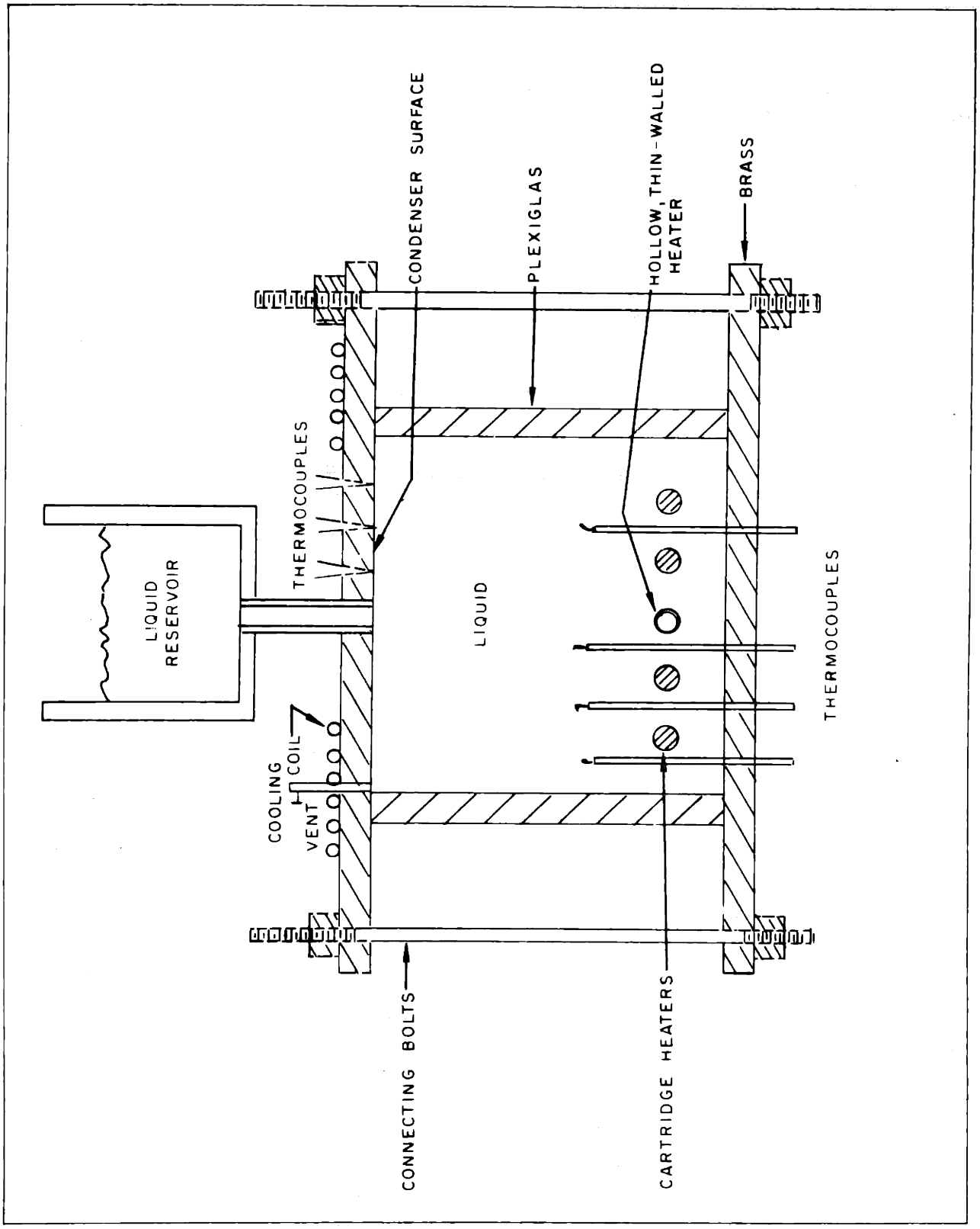

Fig. 5 - Schematic of Experimental Submerged Condenser Apparatus

(U)

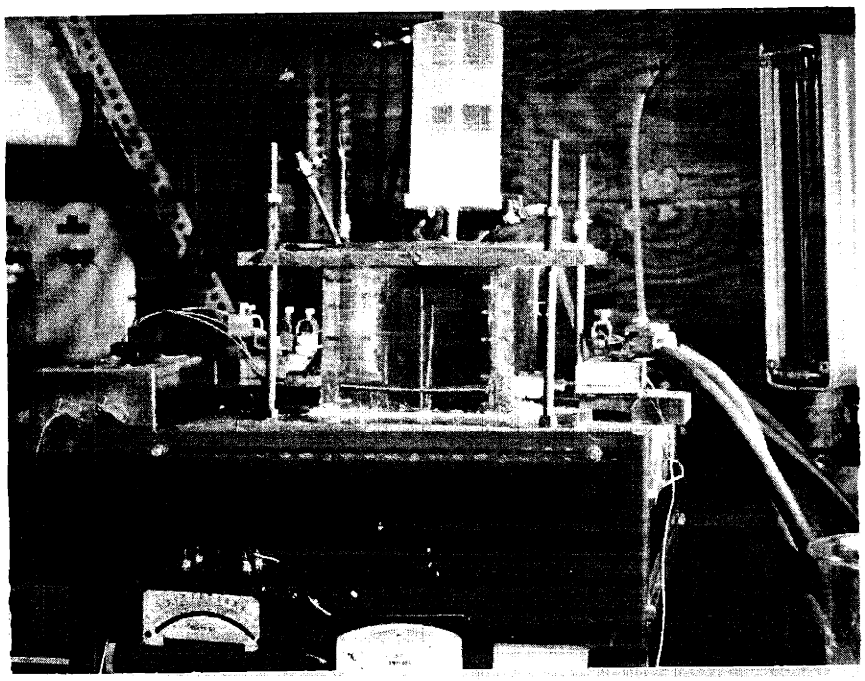

Fig. 6 - Photograph of Experimental Submerged Condenser Apparatus

heat input at the heaters and, hence, the condenser and heated surface heat flux, was maintained constant while the average condenser surface temperature was varied by varying the flow of city water through the condenser cooling coil. Further details on the experimental apparatus and procedure can be found in the Appendix. These experiments served to establish the sequence of thermal transport mechanisms active in the submerged condenser system and defined its operational limits.

2.2 Operating Characteristics

The results of this investigation can be best understood by reference to families of operating curves relating the condenser heat flux, q''_c, to the temperature difference, $T_h - T_c$, between the heater and condenser surfaces. Such operating curves for water and F-113 and 1 and 2 heaters are presented in Figs. 7, 8, 9, and 10. The four figures are seen to be essentially similar differing only in the magnitude of the parameters.

Examing Fig. 7, which is for 1 heater in water, in greater detail, it is apparent that the thermal behavior of a submerged condenser system can be bounded by a proper choice of the limiting heat transfer mechanisms in an enclosed and nearly isobaric liquid. The lower bound of operation (Mode I) corresponds to heat transfer by natural convection at both the heated and condenser surfaces and is associated with relatively low condenser heat flux, q''_c. As q''_c increases, while the condenser surface temperature T_c is held constant, T_h increases past the incipience temperature and subcooled boiling is initiated at the heated surface. For further increases in q''_c, fully developed boiling is achieved at the heater while natural convection augmented by bubble pumping occurs at the condenser surface (Mode IIa). As q''_c is increased still further, the generated vapor bubbles impinge and condense on the condenser surface (Mode IIb) and heat transfer at the surface is achieved primarily by condensation.

The locus of Mode II for T_c = constant essentially follows a boiling curve but its exact shape in the isolated bubble as well as in the fully-developed boiling regions is sensitive to the degree of bulk liquid subcooling. The variation of bulk temperature with q''_c is examined in Subsection 2.3.

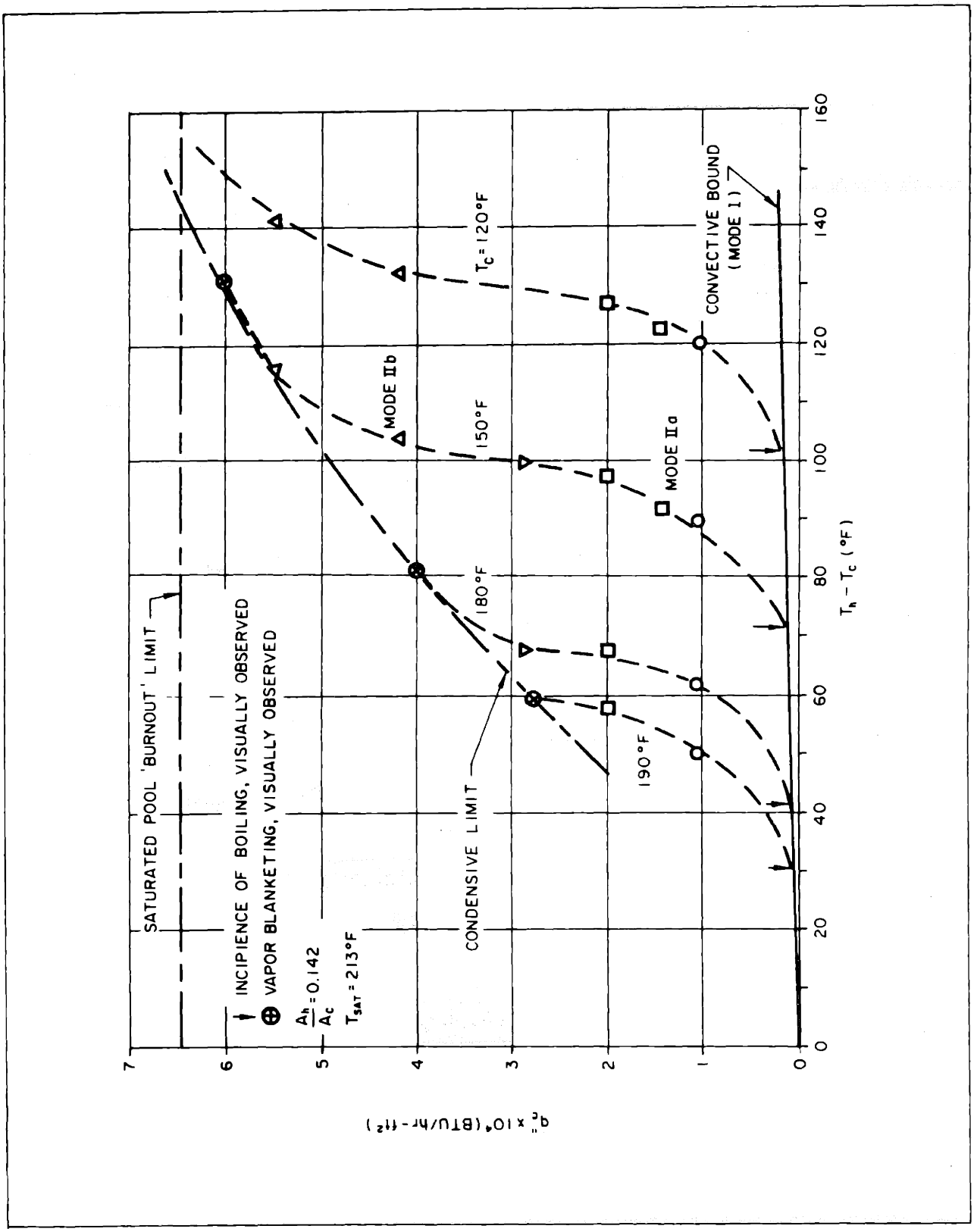

Fig. 7 - Operating Characteristics of a Submerged Condenser System - Water, One Heater

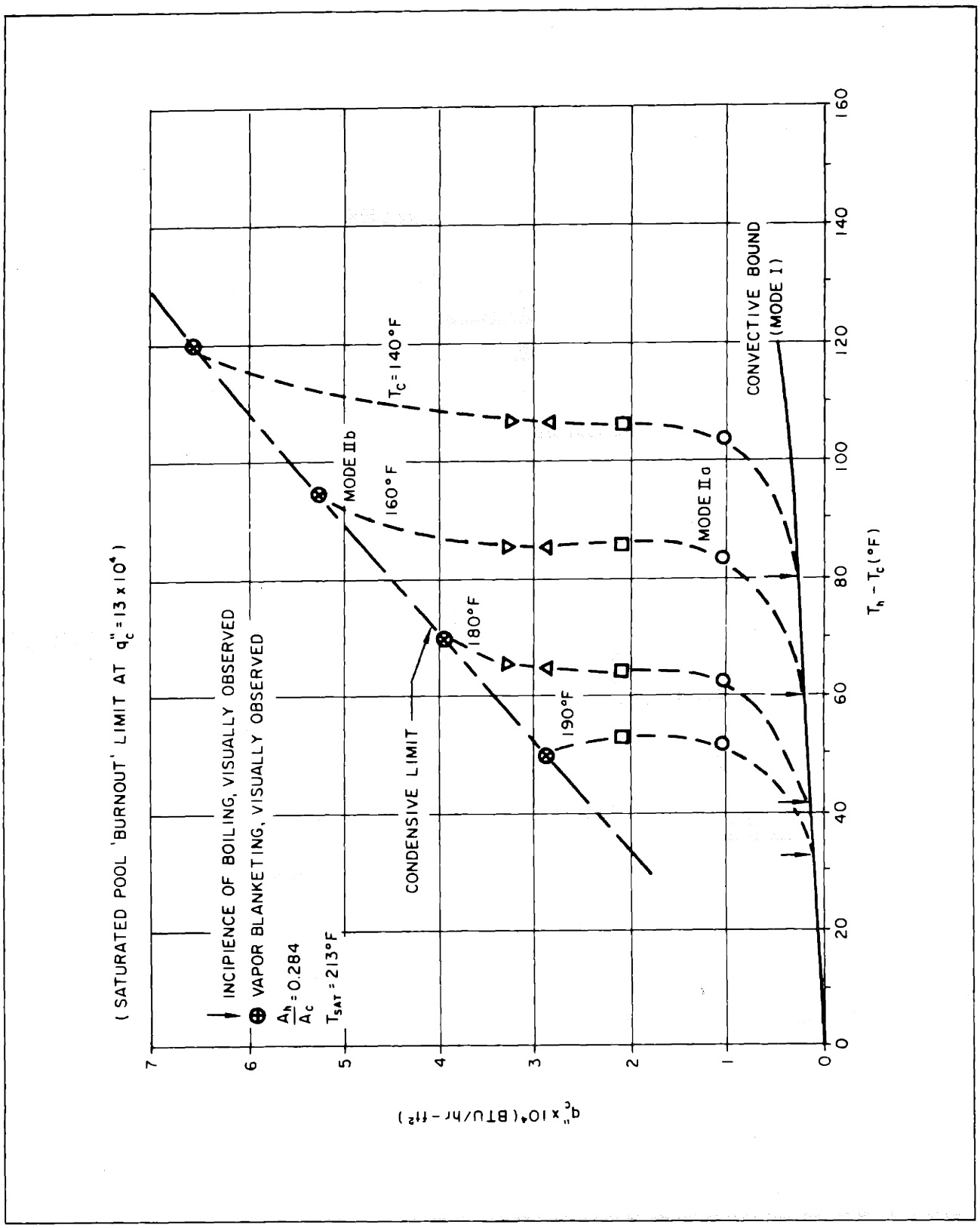

Fig. 8 - Operating Characteristics of a Submerged Condenser System - Water, Two Heaters

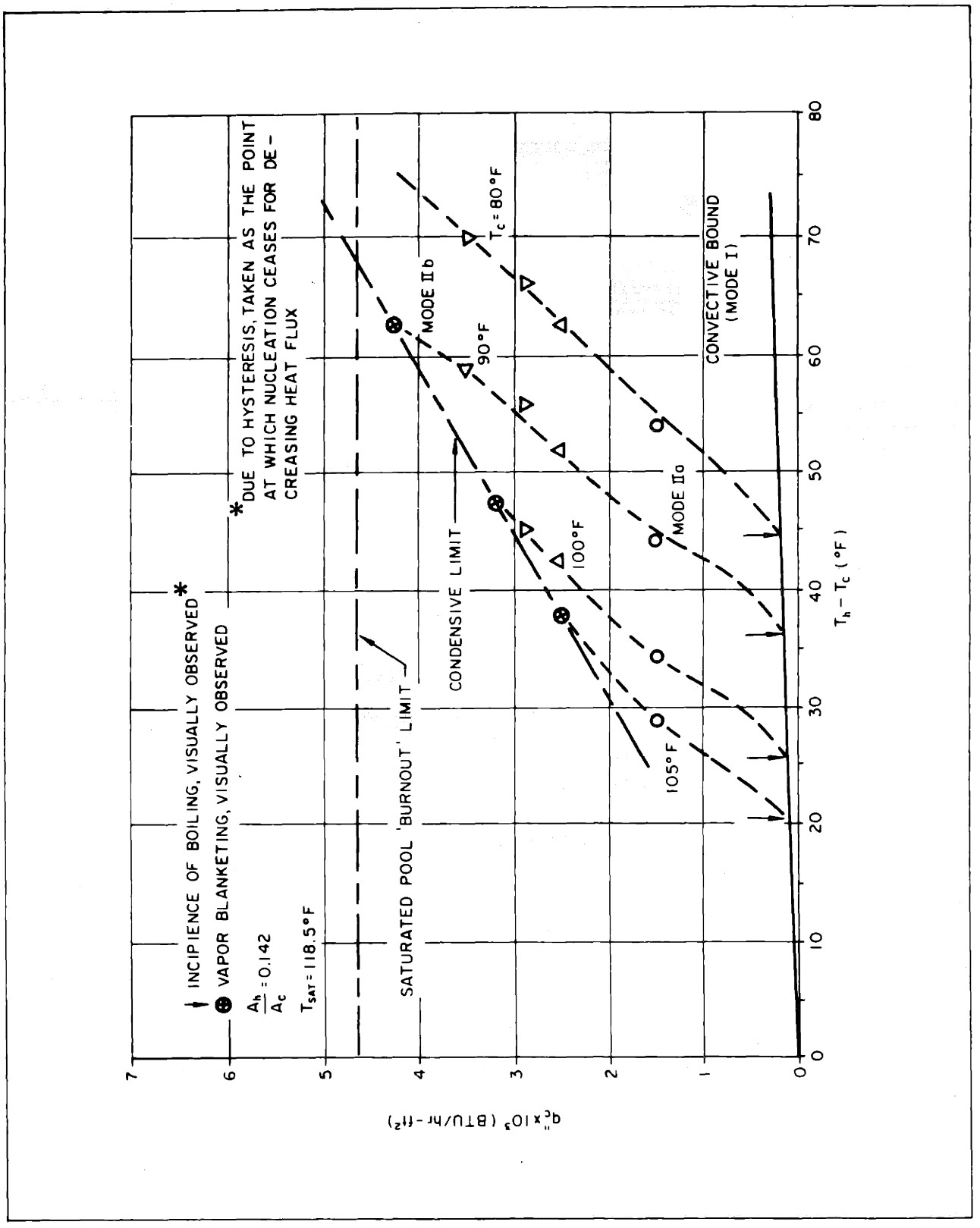

Fig. 9 - Operating Characteristics of a Submerged Condenser System - Freon-113, One Heater

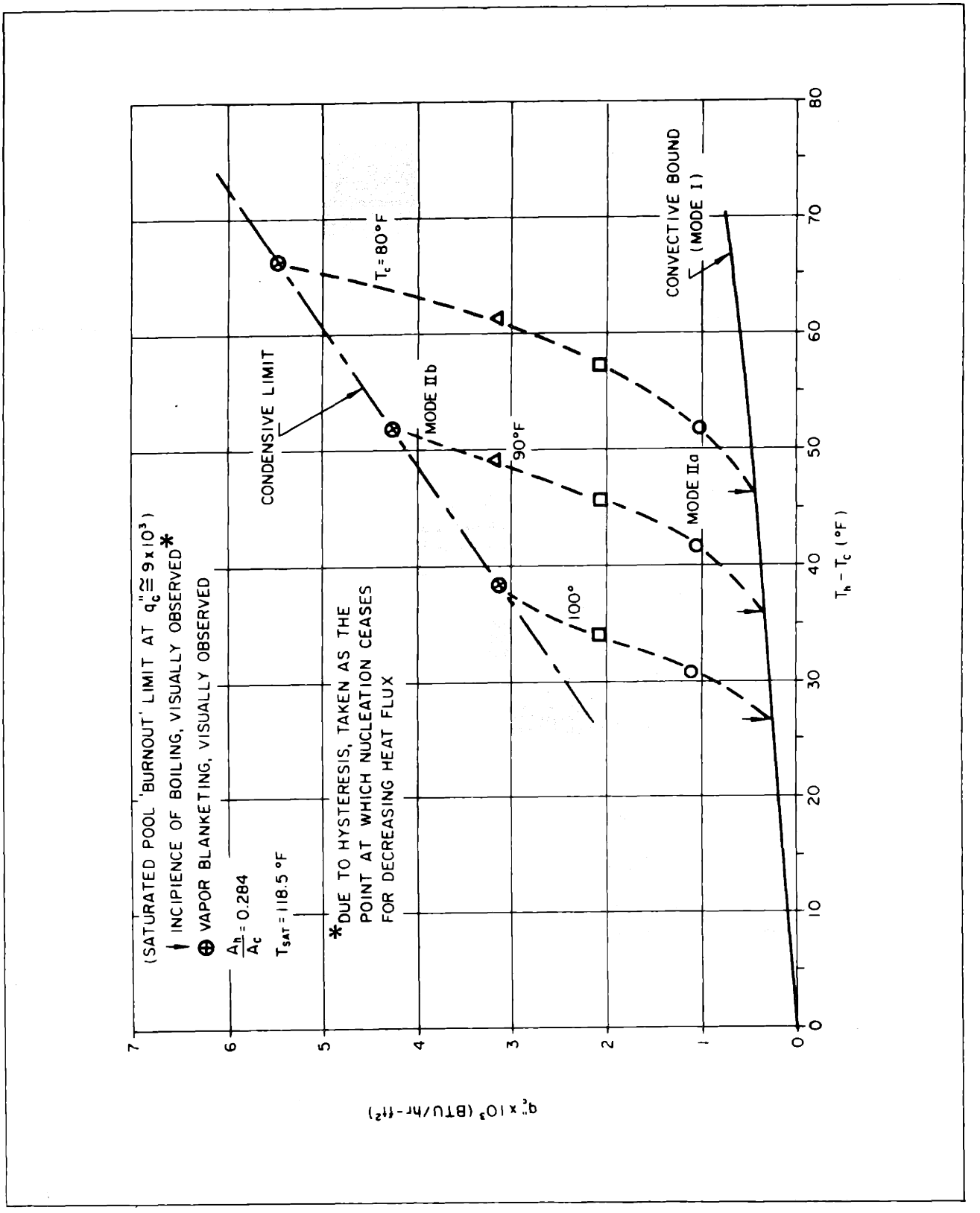

Fig. 10 - Operating Characteristics of a Submerged Condenser System - Freon-113, Two Heaters

The thermal behavior of a submerged condenser system is subject to one of two possible upper bounds depending on the range of system operation. For low values of T_c and/or low heater to condenser surface area ratios, the upper bound is established by the critical or "burnout" heat flux at the heated surface. Alternatively, high values of T_c and/or area ratios approaching unity, result in an experimentally observed upper bound which is significantly below the critical heat flux and apparently due to a condensation limit associated with vapor blanketing at the condenser surface. This sequence of heat transfer mechanisms is illustrated in the series of photographs and accompanying sketches shown in Figs. 11 and 12.

Doubling the heater to condenser surface area ratio by using two heaters rather than one affects the operating characteristics only slightly as can be verified by comparing the two-heater, water data of Fig. 8 with the one-heater, water data shown in Fig. 7. The behavior of the system is again seen to be bounded by a lower convective bound from which distinct T_c = constant curves emerge as q''_c increases. However, at a given value of q''_c, along a T_c = constant curve, T_h is necessarily somewhat lower and slight alterations in the locus of Mode II are also apparent due to the lower heat flux, q''_h, at each heater.

For area ratios much greater than 1, the condensive limit dominates the entire range of operation. The maximum q''_h decreases to a small fraction of the critical heat flux and may, in fact, fall below the flux level necessary to initiate even saturated pool boiling. The operating characteristics shown in Figs. 7 through 10 can not be expected to represent thermal behavior in such systems. But for typically encountered area ratios, the essential operating characteristics are as shown in the above figures and are nearly independent of heater configuration.

Submerged condenser operation in Freon-113 with one and two heaters, represented in Figs. 9 and 10, was similarly found to follow the same modes and be bounded by the same operating limits but necessarily at a q''_c magnitude appropriate to that fluid.

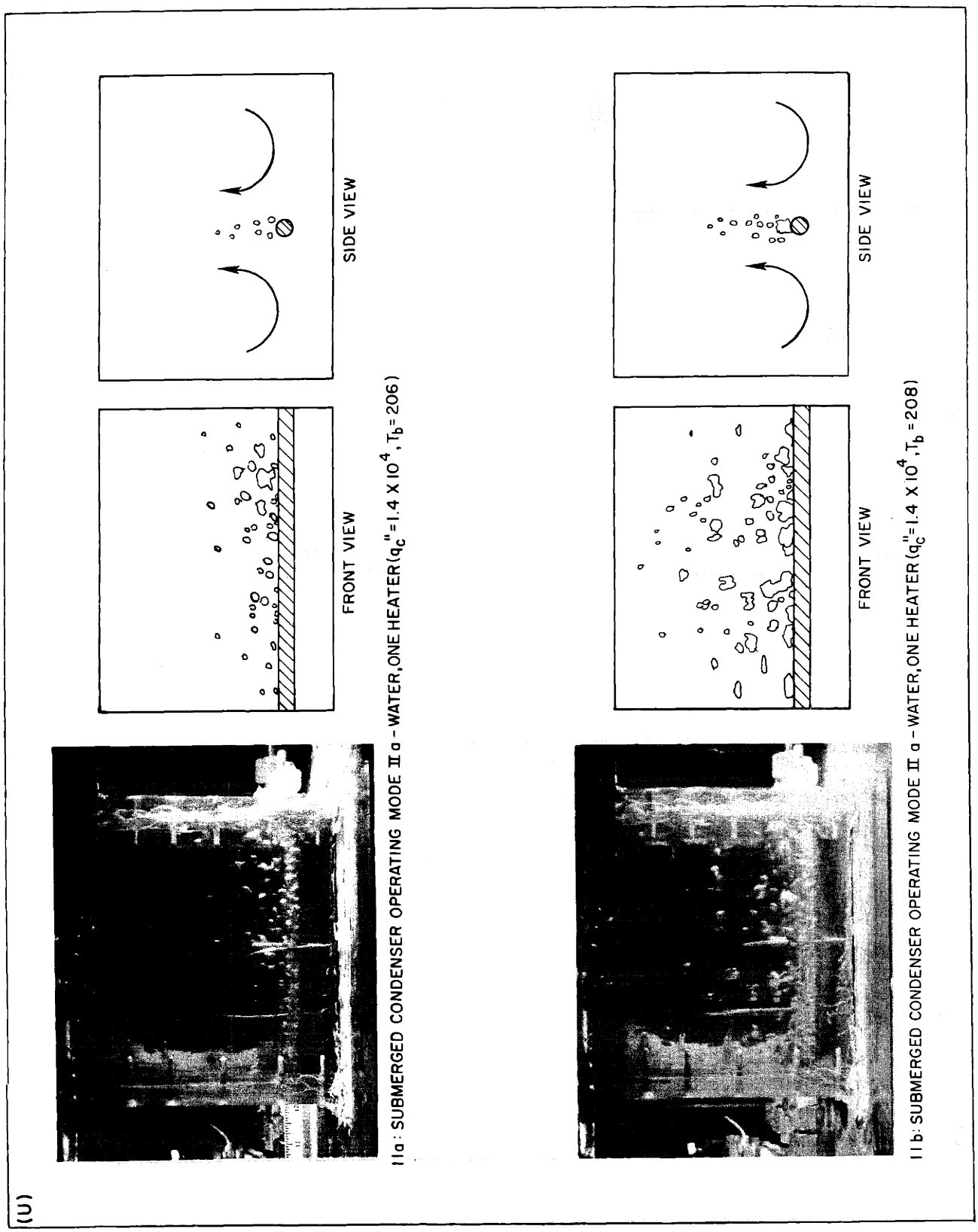
(U)
SIDE VIEW
FRONT VIEW
11a: SUBMERGED CONDENSER OPERATING MODE II a - WATER, ONE HEATER (q_c''=1.4 X 10^4, T_b=206)
SIDE VIEW
FRONT VIEW
11b: SUBMERGED CONDENSER OPERATING MODE II a - WATER, ONE HEATER (q_c''=1.4 X 10^4, T_b=208)

Figure 11

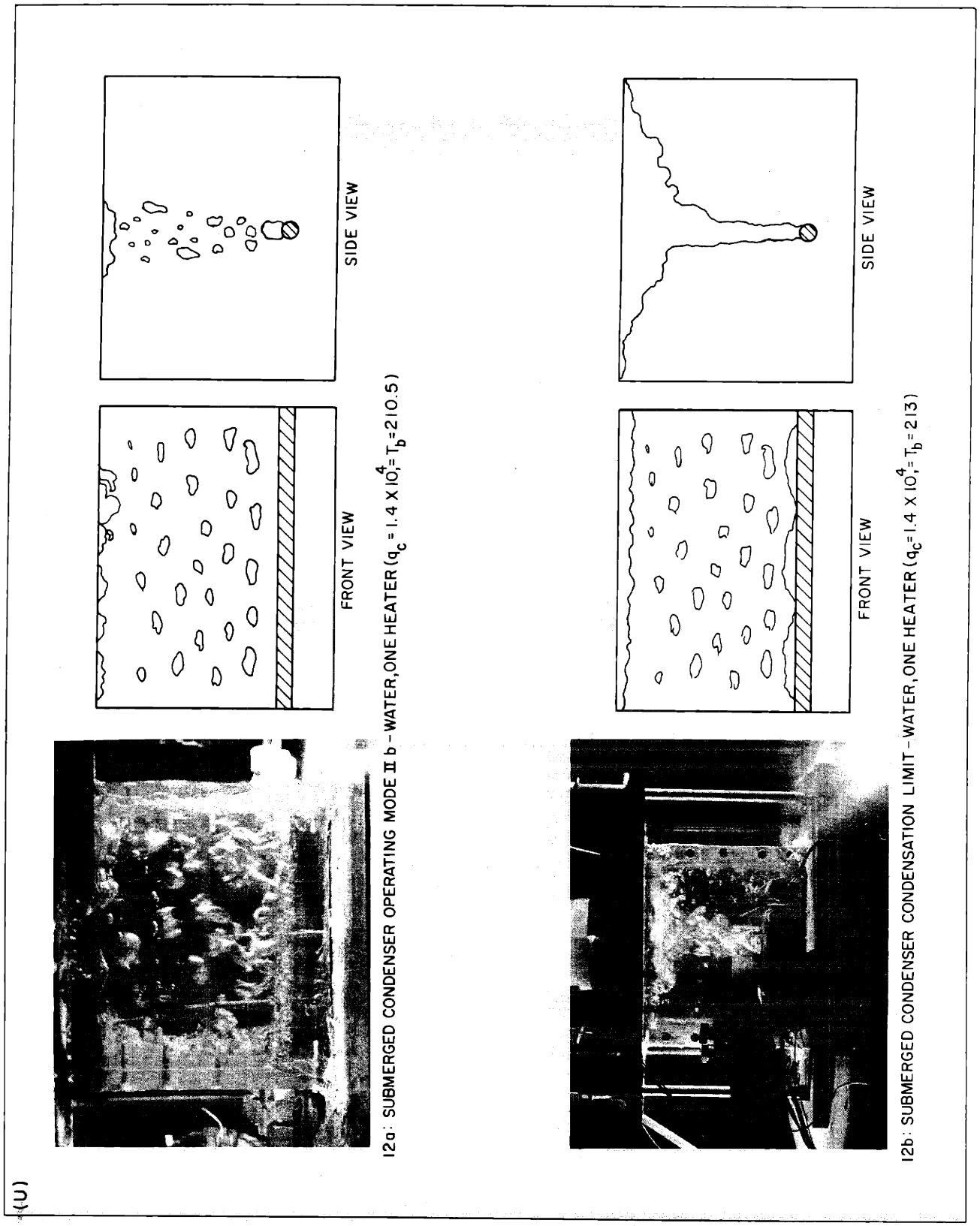
(U)
SIDE VIEW
FRONT VIEW
12a: SUBMERGED CONDENSER OPERATING MODE II b - WATER, ONE HEATER (q_c = 1.4 X 10^4; T_b = 210.5)
SIDE VIEW
FRONT VIEW
12b: SUBMERGED CONDENSER CONDENSATION LIMIT - WATER, ONE HEATER (q_c = 1.4 X 10^4; T_b = 213)

Figure 12

2.3 Bulk Temperature

The temperature of the bulk fluid essentially determines the temperature of the low dissipation and thermally passive elements in the system. While the operating curves relating q''_c to $T_h - T_c$ discussed above contain the basic system information, the bulk subcooling is only implicitly presented through its effect on the boiling curves of Mode II. More precise information on the bulk temperature is presented in Figs. 13 through 16 where T_b and T_h are related to q''_c at constant condenser surface temperature, T_c, for one and two heaters in water and Freon-113. Obviously, some care must be taken in defining the bulk temperature as significant differences exist between the temperature of the heated and condenser surface boundary layers. However, experimental measurements have shown that in the region between the boundary layers the liquid temperature is nearly uniform ($\pm$ 0.5°F) due to convective circulation and bubble-pumping effects. It was this nearly uniform temperature that was defined as the appropriate bulk temperature. The curves thus obtained are again seen to be essentially similar to each other despite differences in working fluid and heater configuration.

Examining Fig. 13 for one heater in water, in greater detail, reveals that the bulk temperature increases asymptotically towards the saturation temperature which is attained at the condensation limit. At the left of the figure is the bulk temperature profile that would result from pure natural convection heat transfer at the condenser surface. The experimentally determined bulk temperature profile thus gives clear evidence of augmented heat transfer at the condenser resulting from bubble pumping and condensation effects.

Fig. 14 for two heaters in water indicates that at the same heat flux through the condenser the value of T_b is slightly higher than for one heater but the difference is greatest in the midrange of q''_c and decreases as the natural connection bound on the one hand and condensive limit on the other are approached. As expected, the analogous curves for Freon-113 are similar.

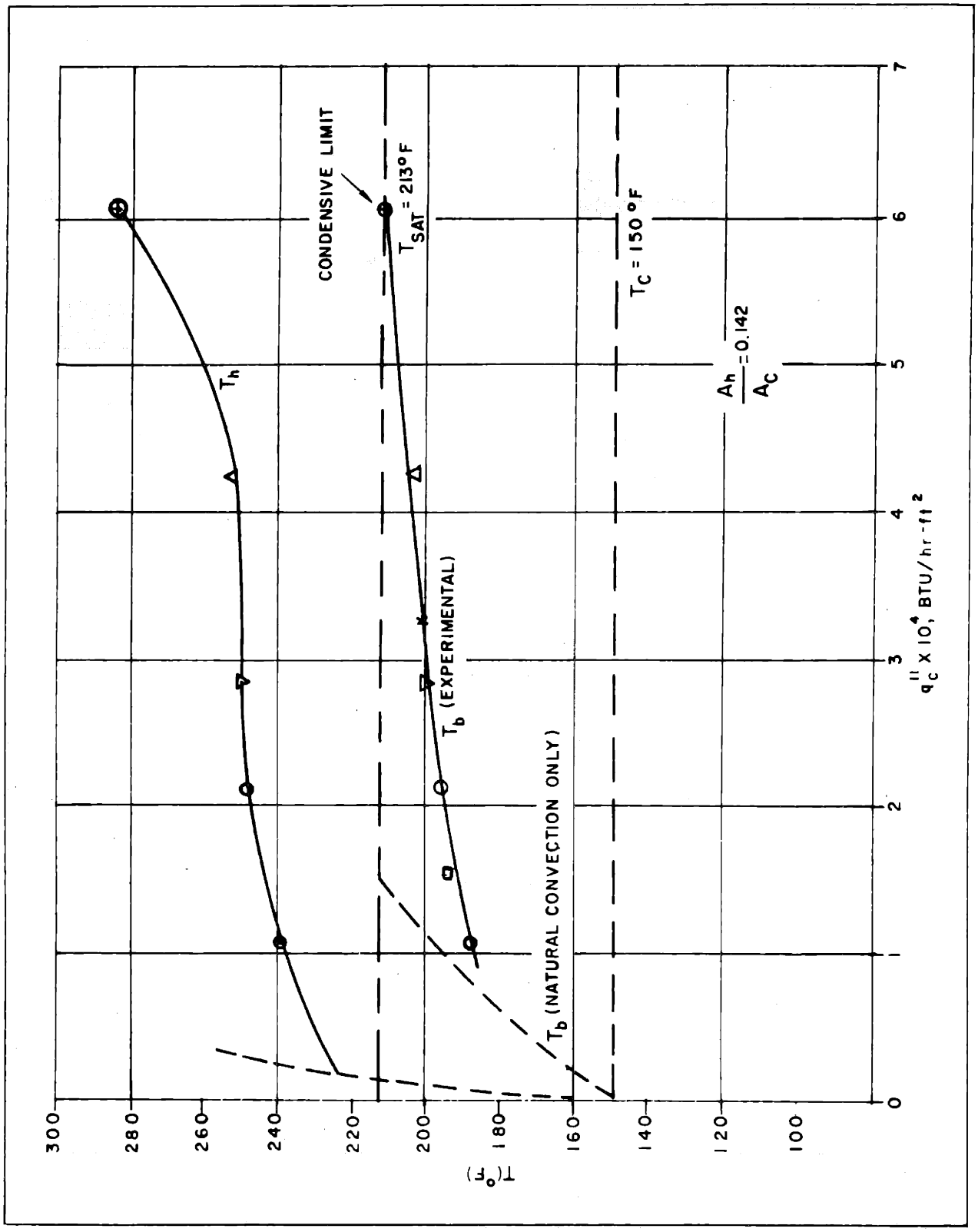

Fig. 13 - Bulk and Heated Surface Temperature Variation with Condenser Heat Flux - Water, One Heater

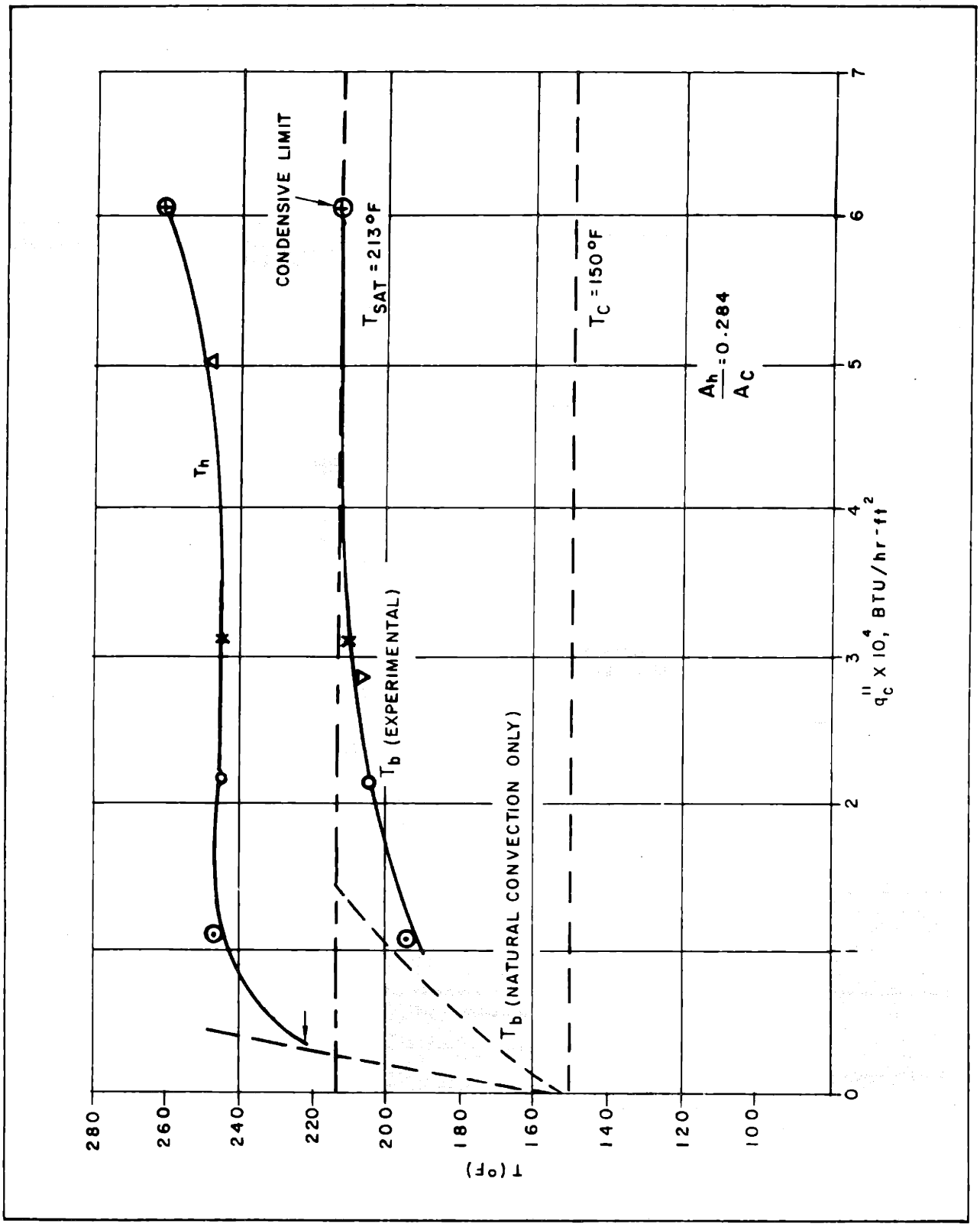

Fig. 14 - Bulk and Heated Surface Temperature Variation with Condenser Heat Flux - Water, Two Heaters

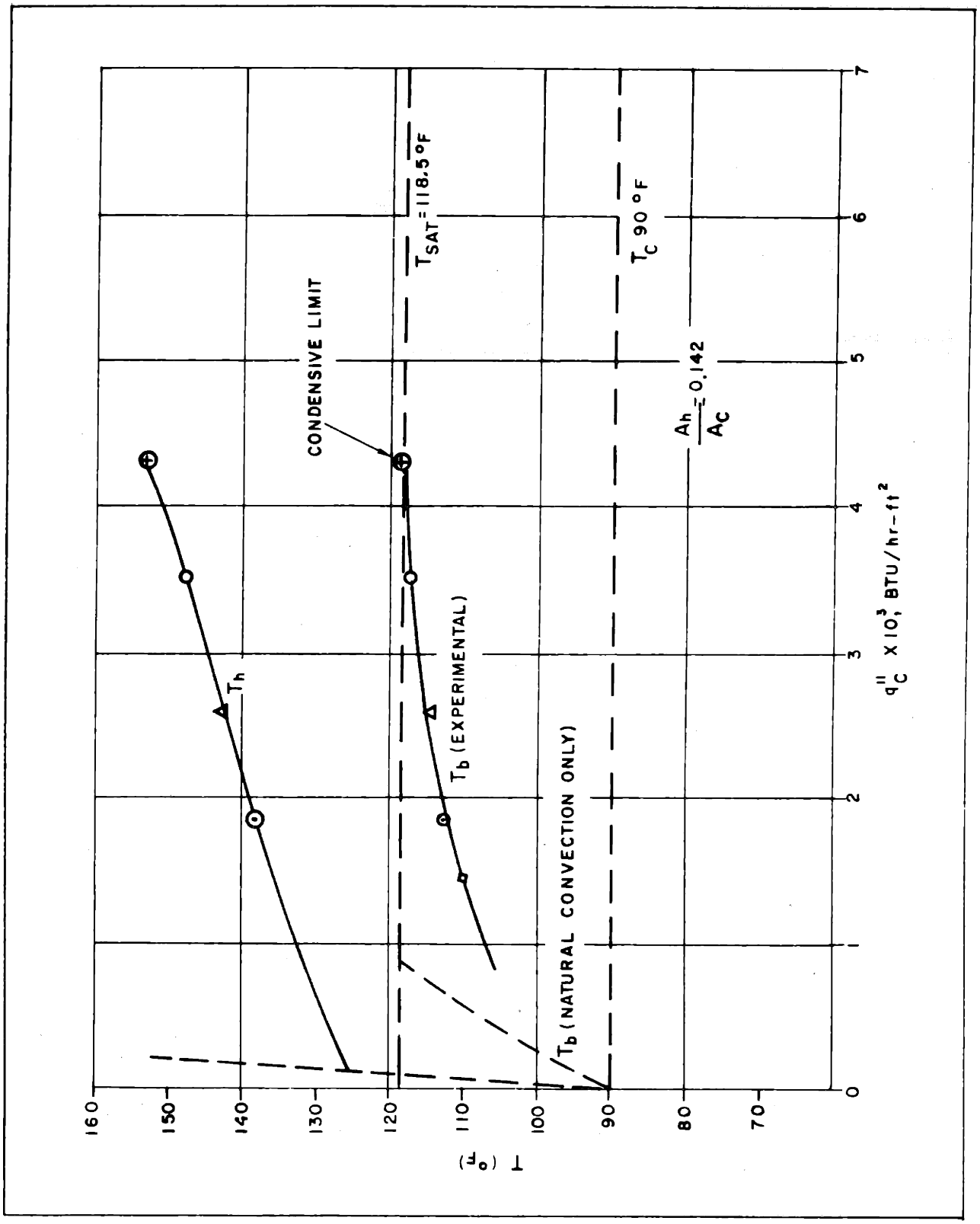

Fig. 15 - Bulk and Heated Surface Temperature Variation with Condenser Heat Flux - Freon-113, One Heater

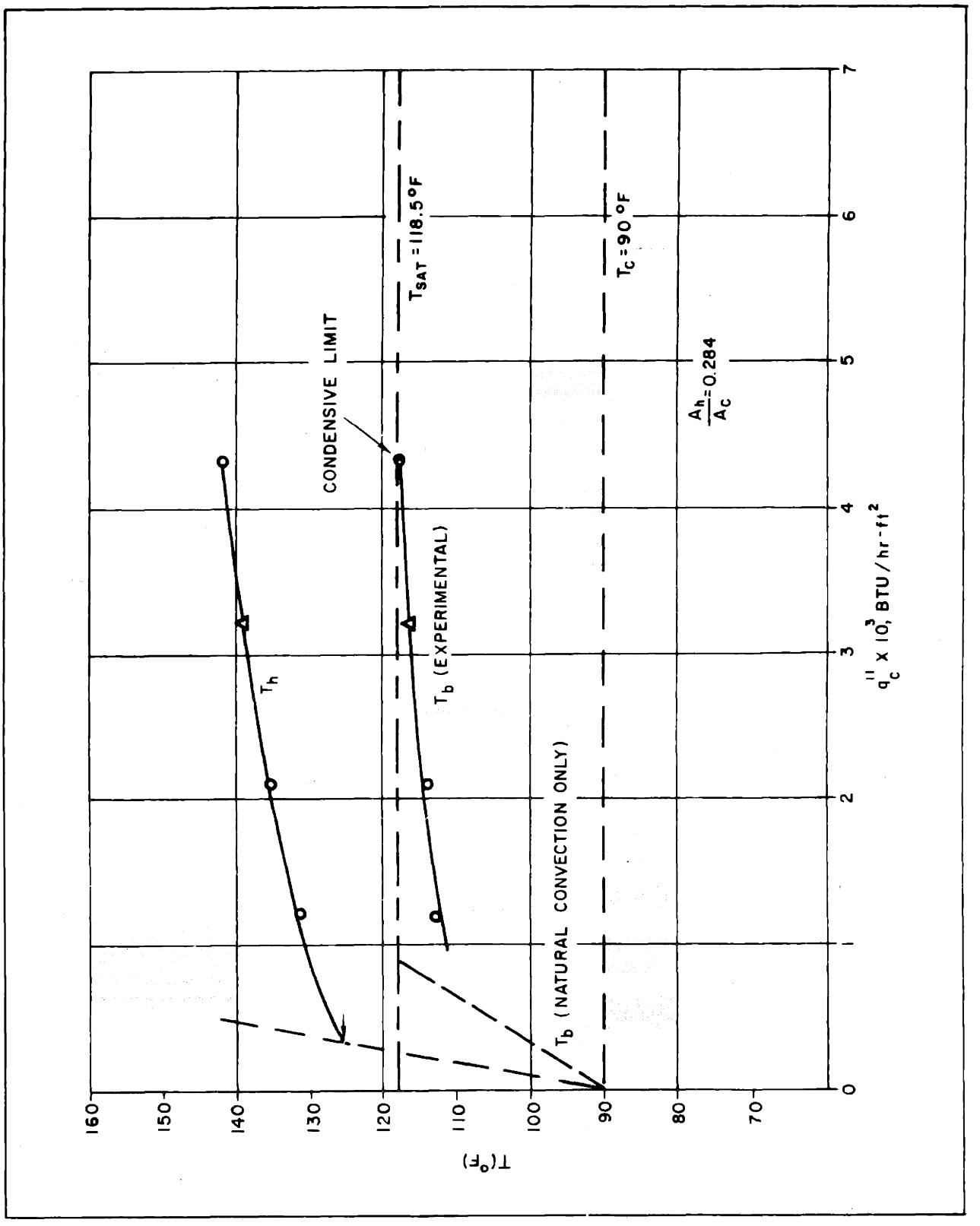

Fig. 16 - Bulk and Heated Surface Temperature Variation with Condenser Heat Flux - Freon-113, Two Heaters

The foregoing has identified the thermal mechanisms active in a submerged condenser system, but considerable analytic and empirical data is necessary before a design procedure can be specified. In subsequent sections, the controlling mechanisms will be examined in detail and, where possible, related to existing models and correlations.

3. OPERATIONAL MODES

The operational limits and thermal performance of an experimental submerged condenser system were outlined in Chapter 2. However, a thorough knowledge of the specific thermal mechanisms active in the system and their possible interactions is required if the experimental results are to be used in evolving a rational design procedure. As shown in Figs. 7 through 10, a lower bound of operation (Mode I) corresponding to natural convection heat transfer at both the heated and condenser surfaces can be defined. Similarly, one of two possible upper bounds, corresponding to a condensive limit at the condenser surface or burnout at the heater, can be shown to exist in submerged condenser systems. For values of q''_c within the envelope of operation (Mode II), lines of constant T_c are found to correspond to pool boiling curves modified by subcooling effects, while pool subcooling is determined by the heat transfer rate at the condenser surface. In the following sections the controlling mechanisms in the operational modes will be explored and, where possible, related to existing correlations. The results will then be combined to yield a prediction of the performance characteristics of submerged condenser systems.

3.1 Mode I - Natural Convection

At low heat flux through the heated surface, thermal transport by natural convection is sufficient to maintain the surface temperature below that required to nucleate vapor bubbles in surface cavities. The fluid in the enclosure circulates under the influence of a thermally induced density gradient and boundary layers are formed at the heated and cooled surfaces. The rate of heat transfer is determined by conduction through the boundary layers at the surfaces of interest and has been studied extensively for various geometries and fluids as summarized in [12, 13]. Assuming side-wall effects to be negligible, it is possible to determine the rate of heat transfer through the enclosure by appropriately combining heat transfer coefficients based on

the average bulk temperature at the hot and cold surfaces. For the present configuration, heat transfer by natural convection from horizontal plates and cylinders must be examined.

Natural convection data for heat transfer from horizontal plates (hot facing up or cold facing down) can be represented as a continuous function of $Gr_L Pr$, for which the power dependence of Nu on $Gr_L Pr$ increases with increasing $Gr_L Pr$. To facilitate computation, this function is often separated into a laminar and a turbulent range. For Pr between 1 and 10

$$Nu = 0.56 \, (Gr_L Pr)^{1/4} \tag{1}$$

in the laminar flow range, $10^4 < Gr\ Pr < 10^9$

and

$$Nu = 0.13 \, (Gr_L Pr)^{1/3} \tag{2}$$

in the turbulent flow range, $10^9 < Gr\ Pr < 10^{12}$. Data for horizontal cylinders with $10^3 < Gr\ Pr < 10^9$ have, similarly, been found to be adequately correlated by Eq. (1) if $\frac{\pi D}{2}$ is substituted for the length L in the dimensionless groups [7].

Solving the above equations for the appropriate heat transfer coefficients, h_{heater} and $h_{condenser}$, combining these as

$$\frac{1}{h_T} = \left(\frac{A_c}{A_h} \right) \frac{1}{h_h} + \frac{1}{h_c} \tag{3}$$

to yield the overall heat transfer coefficient, h_{total}, based on the condenser area and substituting in the thermal transport relation results in:

$$q_c'' = h_T \, (T_h - T_c) \tag{4}$$

Eq. (4) is plotted in Fig. 17 for $T_c = 70°F$ in water and found to compare favorably with data for water which were visually determined to be in the convection mode (Mode I).

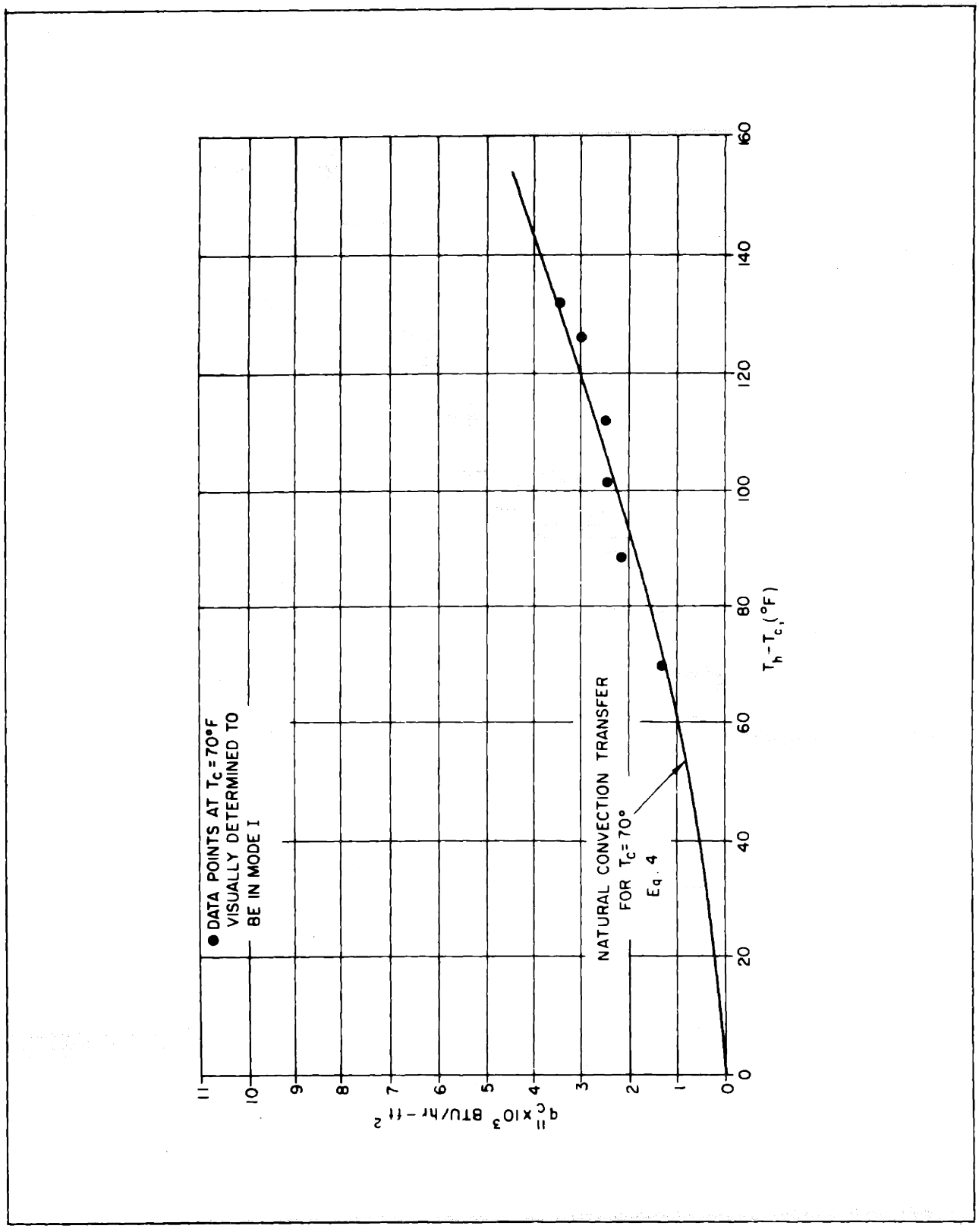

Fig. 17 - Mode I - Convection in Submerged Condenser System - Water, One Heater

3.2 Mode II - Subcooled Boiling

3.2.1 At the Heated Surface

As the heater heat flux increases beyond q''_{incip}, thermal transport by natural convection is no longer sufficient to maintain the surface temperature below that required to nucleate vapor bubbles in surface cavities. Consequently, despite subcooling in the bulk liquid vapor bubbles begin to grow in the superheated layer adjacent to the surface. The relation between heat flux and wall superheat is subcooled nucleate boiling is discussed in great detail in [7, 14, 15] and may be visualized as a perturbation of the saturated pool boiling curve. The saturated and subcooled boiling data for water obtained in this investigation are shown in Fig. 18.

It is important to note at this point that typical design criteria for submerged condenser systems, including available heat sink temperatures and the need to reduce condenser surface area, usually operate to restrict liquid subcooling, and, hence, the magnitude of the perturbation on the saturated pool boiling curve is generally small.

The initial portion of the saturated boiling curve is associated with natural convection and can be successfully correlated as:

$$q''_h = h\,(T_h - T_s) \tag{5}$$

where the heat transfer coefficient is evaluated from the natural convection data. The presence of pool subcooling can be simply accounted for by an additional temperature driving force as:

$$q''_h = h\,[(T_h - T_s) + (T_s - T_b)] \tag{6}$$

where h is evaluated from natural convection data [15] . For some geometries it may be necessary to include a cross flow velocity, due to additional fluid circulation effects, in the determination of the heat transfer coefficient [4] .

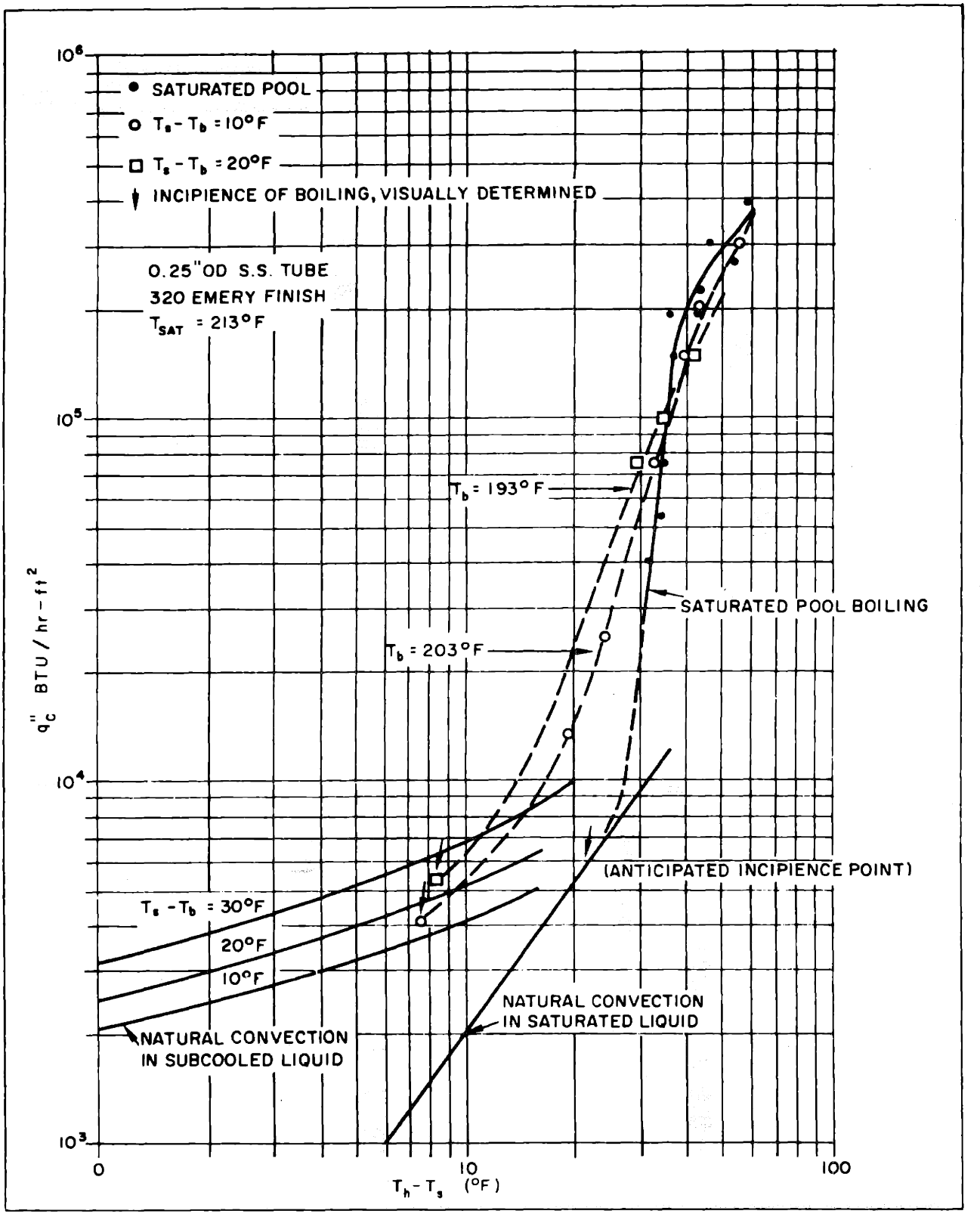

Fig. 18 - Pool Boiling of Water

The wall superheat required to initiate the growth of vapor bubbles in degassed liquids is dependent on the heater surface characteristics, fluid properties and pool subcooling. A precise determination of the nucleation superheat or of the heat flux required to initiate bubble growth on an arbitrary surface is not yet possible. Alternately, it is possible to locate the nucleation point, with reasonable accuracy by smoothly joining the natural convection curve and the full-developed boiling curve, as shown in Fig. 18. The visually determined boiling incipience points are seen to lie above the convective curves, suggesting the presence of some additional circulation effects previously neglected. It must be noted, moreover, that visual incipience, cannot generally be expected to correspond to true incipience, but may be found to lie somewhat further along the boiling curve.

While the water data shown in Fig. 18 does not evidence any temperature discontinuities, the phenomenon of temperature hysterisis is a major concern in the boiling of many fluids including Freon-113 [4]. When temperature overshoot hysterisis is present, convective heat transfer persists past the intersection of the convective and fully-developed boiling curves and suddenly reverts to fully-developed boiling along the entire surface. This behavior is thought to result from the existence of metastable vapor bubbles and the quenching of large cavities during subcooling [4]. The likelihood of boiling hysterisis in some surface-fluid combinations, necessitates the use of the decreasing-heat-flux boiling curves in discussing their boiling characteristics.

Heat transfer in saturated pool nucleate boiling has been correlated by several investigators. One of the more widely used correlation was developed by Rohsenow [7] and based on a bubble-pumping mechanism. The correlation, shown below, utilizes one empirical constant, C_{sf}, evaluated for each surface-fluid combination.

$$q'' = \frac{1}{C_{sf}^{3}} \frac{\mu_\ell C_p^{3}}{h_{fg} Pr^{5.4}} \sqrt{\frac{g(\rho_\ell - \rho_v)}{g_o \sigma}} (T_w - T_s)^3 \qquad (7)$$

A considerable number of values C_{sf} have been determined and tabulated by investigators of boiling phenomena. However, for many surface-fluid combinations of interest, C_{sf} must be determined experimentally, if an accurate prediction of boiling transfer is desired. Hence, the correlation is of limited utility unless used to extrapolate experimental results to other pressure levels.

While some success has thus been achieved in correlating and describing saturated pool boiling, a description of the precise effects of subcooling has so far eluded investigators. As shown in Fig. 18, the data for moderately subcooled pools deviate to some extent from the saturated pool data. However, the direction and magnitude of this shift appears to depend strongly on heater geometry and pool convective conditions [15] . For tubular heaters the subcooled boiling curves cross the saturated curve and in the fully-developed region yield higher wall superheats than the saturated curve. This trend is apparent in Fig. 18 and is in agreement with earlier investigations [16, 17] . Subcooled boiling curves for horizontal flat plates, on the other hand, do not cross the saturated curve and yield wall superheats which are lower than the saturated wall superheats over the entire range of nucleate boiling [18] . Due to a scarcity of data and the inability to precisely identify induced circulation effects, it is thus essential that an experimental determination of the subcooling effects be made for each geometry of interest.

The peak, critical or burnout heat flux marks the end of the nucleate boiling regime. In spite of substantial research there is still no universal explanation for the phenomenon, as even carefully controlled experimental data show considerable scatter. The critical heat flux is known to depend on many factors including the pressure, induced convection effects, diameter and orientation of the heater, but it is especially sensitive to the degree of bulk subcooling.

Zuber's [19] assumption that the critical heat flux results when sufficient liquid can no longer flow past the vapor columns to the heated surface due to the hydrodynamic instability of the liquid-vapor interface, suggests that q''_{crit} can be set equal to:

$$q''_{crit} = 0.18\,\rho_v\,h_{fg}\left[\frac{g g_o\,\sigma(\rho - \rho_v)}{\rho_v^2}\right]^{1/4}\left[\frac{\rho + \rho_v}{\rho}\right]^{1/2} \quad (8)$$

Experimental results for many fluids are close to the range of magnitude indicated by this relation [14] . In the present investigation saturated pool burnout for a 0.25 inch OD, horizontal cylindrical heater in water was achieved at approximately 4.3×10^5 Btu/hr-ft^2 versus 4.9×10^5 predicted by Eq. (8).

For the boiling of subcooled liquids, Ivey and Morris [20] proposed the simple expression:

$$\frac{q''_{crit,\,sub}}{q''_{crit,\,sat}} = \left(1 + 0.1\left(\frac{\rho_v}{\rho_\ell}\right)^{1/4}\left[\frac{c_\ell \rho_\ell\,(T_s - T_b)}{h_{fg}\rho_v}\right]\right)\left(\frac{a}{g}\right)^{0.273} \quad (9)$$

Heat transfer in the isolated bubble regime for moderate subcooling, as well as saturated pool conditions, results primarily enthalpy transport by vapor bubbles departing from the surface [15, 21]. For heater heat flux, q''_h, slightly greater than the incipience flux, q''_{incip}, and for moderately subcooled pools, vapor bubbles formed in isolated surface cavities, depart from the surface individually. However, as the flux increases and more surface cavities are activated, the process of vapor removal from the surface changes from an intermittent to a continuous one and vapor columns form [22] . The stages of transitions are illustrated in Fig. 19, and have been related by Moissis and Berenson [22] to the decreasing bubble separation with increasing vapor flow. Utilizing expressions derived by Moissis and Griffith [23] for consecutive bubble agglomeration, it was shown [22] that, for typical surface finishes, the transition heat flux for saturated pool boiling can be expressed as:

$$q''_{tr} = 0.11\,\rho_v\,h_{fg}\,\beta^{0.5}\left[\frac{g_o g \sigma}{\rho - \rho_v}\right]^{1/4} \quad (10)$$

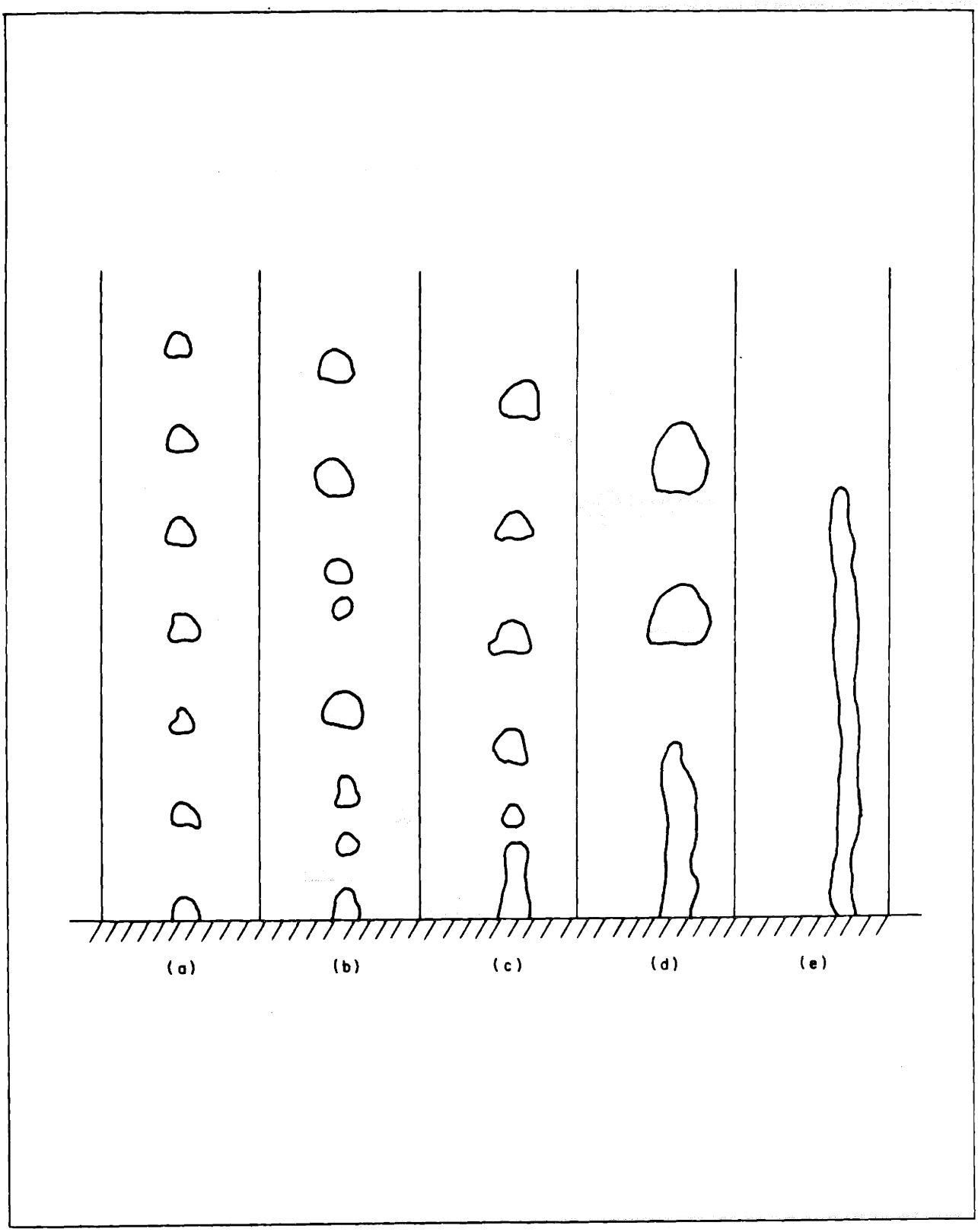

Fig. 19 - Stages in the Transition from the Region of Isolated Bubbles to the Region of Continuous Vapor Columns (vapors flow increasing from a to e) [22]

The transition flux for a subcooled pool can be expected to differ from this result, but for moderate subcooling the difference should not be substantial.

Bubble departure in isolated bubble boiling is governed by bouyant, dynamic and surface tension forces. Fritz [24] , on the basis of earlier work, equated surface tension and bouyancy forces at departure, and obtained relation for the departing bubble diameter as:

$$D_o = c_d \beta \sqrt{2} \left[\frac{g_o \sigma}{g (\rho - \rho_v)} \right]^{1/2} \tag{11}$$

where c_d was found to be 0.0148 for H_2 and H_2O [13].

Eq. (11) provided an adequate departure criteria, but more recent efforts have further refined the correlation by accounting for dynamic effects. In particular, Cole and Rohsenow [25] have included data with substantial pressure variation and proposed that the departure diameter for saturated pools be expressed as:

$$D_o = c \left[\frac{g_o \sigma}{g (\rho - \rho_v)} \right]^{1/2} \left[\frac{\rho c_p T_s}{\rho_v h_{fg}} \right]^{5/4} \tag{12}$$

where

$$c = 1.5 \times 10^{-4} \text{ for water}$$
$$c = 4.65 \times 10^{-4} \text{ for other liquids}$$

and showed Eq. (12) to be in good agreement with available data.

In subcooled pools, the reduction in bubble growth rate and the consequent decrease in the inertia of the surrounding liquid acts to increase the departure diameter. However, the increased pool circulation and greater buoyant force acting on the departing bubble can be expected to lead to somewhat smaller departure diameters. These possible effects have not been fully studied and no correlation for the influence of subcooling on the bubble departure diameter exists at this time.

The total number of bubbles generated at a particular heat flux, q''_h, is far more difficult to determine. While departure frequency and nucleation site density data can be combined to yield an approximate result, the departure frequency is not constant [26] and, as yet, no practical method exists for predicting the nucleation site density. Alternately, it is possible to estimate the rate of vapor generation as some fraction of the heat flux, according to:

$$\frac{Q_v}{A} = \eta \frac{q''_h}{p_v h_{fg}} \tag{13}$$

where $\eta \rightarrow 0$ for high subcooling and low heat flux but for q''_h greater than 20 percent of the critical heat flux $\eta > 0.5$ [27] and increases to $\eta = 1$ at the critical flux.

For heat flux, q''_h, greater than q''_{tr}, vapor columns rooted in the boiling surface appear. Initially, the diameter of the columns is equal to the departure diameter of the bubbles, but with increasing heat flux the column diameter increases to accommodate vapor flow [22] . In a recent study, Gaertner [28] found that in post transition ($q''_h > q''_{tr}$) saturated pool boiling, vapor "mushrooms" each fed by several vapor columns appeared above the boiling surface. Observations in this investigation showed a similar trend and the cylindrical heaters used appeared to be nearly vapor blanketed on the upper surface for high flux rates. The vapor bubbles thus formed were substantially larger than pre-transition bubbles and appeared similar to bubbles formed in film boiling. Studies by Zuber [19, 29] and Berenson [30] indicate that in film boiling the diameter of vapor bubbles formed at the liquid-vapor interface is within the range:

$$3.14 \left[\frac{g_o \sigma}{g (\rho_\ell - \rho_v)} \right]^{1/2} \leq D_o \leq 5.45 \left[\frac{g_o \sigma}{g (\rho_\ell - \rho_v)} \right]^{1/2} \tag{14}$$

The average diameter is thus approximately four times the departure diameter in the isolated bubble region (Eq. (12)) and is in qualitative agreement with the observations.

3.2.2 In the Bulk

In the subcooled boiling mode (Mode II) the vapor bubbles generated at the heater surface rise and condense in the bulk liquid. Their height of penetration into the liquid, and consequently their effect on heat transfer at the condenser surface, is directly related to their initial diameter, rise velocity, and the prevalent collapse mechanism.

3.2.2.1 Departure Diameter

As noted above, the available correlations indicate that the departure diameter varies from approximately

$$1.1 \sqrt{\frac{g_o \sigma}{g\,(\rho_\ell - \rho_v)}}$$

in isolated bubble boiling from typical surfaces, to perhaps four time that value in columar boiling when vapor "mushrooms" cover the surface.

3.2.2.2 Rise Velocity

The rise of vapor bubbles is, as all else in boiling transfer, difficult to evaluate. The rise velocity of an undisturbed bubble in the diameter range of interest can be approximated [31] as:

$$V_b = 1/3 \sqrt{2gD} \tag{15}$$

However, the presence of neighboring bubbles, fluid circulation, and slide walls can exert a profound influence on the rise velocity. These and other influences have been qualitatively and sometimes quantitatively evaluated, but their combined effect on bubble rise velocity can not yet be predicted.

3.2.2.3 Collapse Mechanism

The mechanics of vapor bubble collapse under spherically symmetrical conditions have received extensive attention. Recent investigations [32, 33, 34] have shown that the collapse mode was controlled alternately

by liquid inertia, heat transfer or both, depending on system conditions. The effects of noncondensable gas and translatory bubble motion have also been recently incorporated into the appropriate bubble collapse relations [32].

A dimensionless parameter, B,

$$B = Ja^2 \frac{K}{R_o} \sqrt{\frac{\rho}{\Delta p}} \tag{16}$$

where

$$Ja = \frac{c\rho\,(T_s - T_b)}{h_{fg}\,\rho_v}$$

representing the ratio of the time duration of inertia effects to that of heat transfer effects in the collapse process has been defined [34] and found to characterize the prime mode of collapse. For $B < 0.05$ heat transfer dominates the collapse process while a value of $B > 10$ indicates the predominance of inertia effects.

Inertia controlled collapse is governed by the classical Rayleigh solution [34]:

$$\tau_I = \int_{\gamma}^{1} \frac{x^{3/2}}{(1 - x^3)^{1/2}}\, dx \tag{17}$$

where

$$\tau_I = \frac{t}{R_o} \left(\frac{2}{3} \frac{\Delta p}{\rho} \right)^{1/2}$$

$$\gamma = \frac{R}{R_o}$$

The collapse rate is high and continues to increase as the collapse proceeds. Translatory motion does not materially affect the collapse rate in this mode, but the presence of a noncondensable gas can substantially reduce the rate of collapse. Cavitation bubbles and vapor bubbles collapsing in highly subcooled liquids appear to be primarily inertial controlled.

Heat transfer controlled collapse is governed by:

$$1 = \frac{1}{\pi^{1/2} Ja} \int_0^{\tau} \frac{\gamma^2(z)\,\dot{\gamma}(z)}{\left[\int_z^{\tau} \gamma^4(y)dy\right]^{1/2}} dz \qquad (18)$$

$$\tau = \frac{Kt}{R_o^2}, \quad \gamma = R/R_o$$

An exact solution for Eq. (18) can be obtained by direct numerical integration [32] . Alternately, it is possible to obtain an upper bound on the collapse rate by assuming the existence of a thin thermal boundary layer and utilizing the Plesset-Zwick temperature integral [35] . The latter approach [34] yields a manageable expression for γ as:

$$\tau_h = \frac{1}{3}\left(\frac{2}{\gamma} + \gamma^2 - 3\right) \qquad (19)$$

where

$$\tau_h = \frac{4}{\pi} Ja^2 \frac{Kt}{R_o^2}$$

In this mode, the collapse rate is relatively slow and decreases further as collapse proceeds. Translatory motion of the bubble, such as usually results from buoyancy, increases the collapse rate, especially when the liquid subcooling is small and the collapse rate slow [32] . The presence of noncondensables always retards the collapse, but its effect is manifested earlier when the translatory velocity is high and is, in any event, a highly nonlinear influence on the collapse rate [32] . Bubbles collapsing in moderately subcooled liquid ($Ja \leq 50$) are predominantly heat transfer controlled and it is, hence, this mode which is of prime importance in submerged condenser systems.

Due to the asymptotic nature of heat transfer controlled collapse, no precise criteria exists for the definition of a collapse period. However, since it is the bubble volume which is of prime interest, and at $\gamma = 0.2$ the bubble volume is only one percent of its departure volume, the collapse period τ_c can be defined as:

$$\tau_c = \frac{1}{3}\left(\frac{2}{\gamma} + \gamma^2 - 3\right)\Bigg|_{\gamma = 0.2} \cong 2.3 \tag{20}$$

and

$$t_c = \frac{2.3}{4}\,\frac{\pi R_o^2}{Ja^2 K}$$

It must be further noted that the use of Eq. (19) and the neglect of translational velocity effects have yielded a strictly conservative collapse criteria (in the absence of noncondensables).

3.2.2.4 Height of Penetration

Utilizing the above relations for bubble departure diameter, rise velocity and rate of collapse, it is now possible to determine approximately the height of penetration of the vapor bubbles and the approximate vapor fraction in a moderately subcooled liquid-filled enclosure free of noncondensable gas.

The collapse length L_c equals:

$$L_c = \int_o^{t_c} v_b \, dt \tag{21}$$

Substituting

$$\tau = \frac{4}{\pi}\, Ja^2\, \frac{K}{R_o^2}\, t \tag{22}$$

into Eq. (21)

$$L_c = \frac{R_o \pi}{4\, Ja^2\, K} \int_o^{\tau_c} v_b \, d\tau \tag{23}$$

Introducing Eq. (15)

$$L_c = \frac{R_o^2 \pi}{4\, Ja^2 K} \int_o^{\tau_c} \frac{1}{3} \sqrt{2\, gD} \; d\tau \tag{24}$$

or

$$L_c = \frac{\pi}{12} \frac{R_o^2 \sqrt{2g}}{Ja^2 K} \int_o^{\tau_c} \sqrt{D} \; d\tau \tag{25}$$

and with

$$\gamma = D/D_o$$

$$L_c = \frac{\pi}{12} \frac{R_o^2}{Ja^2 K} \sqrt{2\, gD_o} \int_o^{\tau_c} \sqrt{\gamma} \; d\tau \tag{26}$$

or

$$L_c = \frac{\pi}{48} \frac{D_o^{5/2} \sqrt{2g}}{Ja^2 K} \int_o^{\tau_c} \sqrt{\gamma} \; d\tau \tag{27}$$

Numerical integration of the integral yields:

$$\int_o^{\tau_c = 2.3} \sqrt{\gamma} \; d\tau = 1.38 \tag{28}$$

And, therefore

$$L_c \cong 1.4 \left(\frac{D_o^{5/2} \sqrt{2g}}{Ja^2 K} \frac{\pi}{48} \right) \tag{29}$$

In the isolated bubble regime D_o is calculated from Eq. (12) while in the vapor column regime Eq. (14) can be utilized. The collapse length L_c as a function of bulk subcooling is plotted in Fig. 20 for both bubble generation regimes.

3.2.3 At the Condenser Surface

The rate of heat transfer at the condenser surface determines the bulk temperature and, hence, the degree to which the boiling curves of Mode II deviate from the saturated pool boiling curve. In Subsection 2.2, heat transfer at the condenser was shown to proceed through a series of transport mechanisms. In Mode I natural convection was sufficient to accomplish the necessary thermal transport. In Mode II, however, the presence of collapsing vapor bubbles in the bulk fluid leads to heat transfer rates substantially greater than those associated with natural convection.

The bubble collapse length, determined approximately in Eq. (29), and more specifically the ratio of collapse length to the distance separating the heated and condenser surfaces, L_c/W, plays a crucial role in determining the rate and mechanism of condenser surface heat transfer. For $L_c/W << 1$, all the generated vapor bubbles collapse near the heated surface. Consequently, the bubbles have only a negligible effect on heat transfer at the condenser surface and the observed transfer rate should correspond approximately to those associated with natural convection. For $L_c/W \leq 1$, the vapor bubbles collapse at or near the condenser surface, but a substantial vapor fraction exists in the bulk fluid which induces augmented convection at the condenser surface. In this range, the condenser heat transfer coefficient could be expected to lie above the natural convection coefficient and to increase with increasing values of L_c/W. As L_c/W increases past unity, the vapor bubbles begin to impinge on the form vapor pockets at the submerged condenser surface. The heat transfer coefficient on that fraction of the surface covered with vapor can be determined from existing vapor space condensation correlations. At values of L_c/W only slightly greater than unity, the vapor pockets occupy only a very small fraction of the surface. As a result, heat transfer in this region is still accomplished primarily by

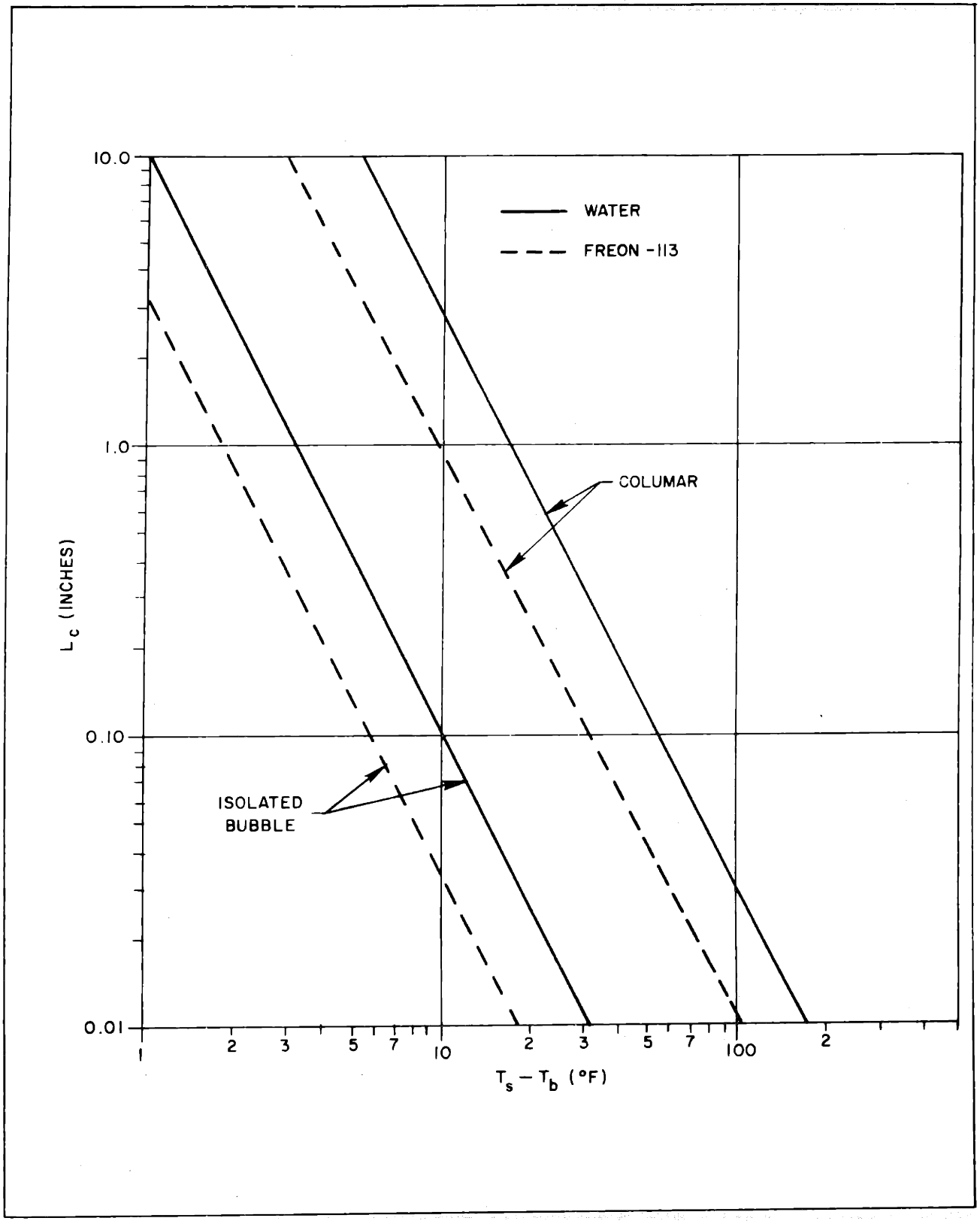

Fig. 20 - Collapse Distance of Bubbles for Varying Bulk Subcooling - Water, Freon-113

augmented convection. However, as L_c/W increases, the vapor pockets grow and for $L_c/W >> 1$ condensation would dominate thermal transport at the condenser surface and high transfer coefficients should be expected. Finally, as $L_c/W \rightarrow \infty$, nearly the entire condenser surface is blanketed by vapor and the heat transfer coefficient should correspond to that associated with vapor space condensation.

In Fig. 21 the experimentally determined variation of the condenser heat transfer coefficient, h_c, is related to the approximately calculated L_c/W for one heater in water and for $q''_h > q''_{tr}$. It should be noted that in the experimental apparatus the natural convection heat transfer coefficient for water at the condenser was typically 220 Btu/hr-ft^2 while the vapor space condensation heat transfer coefficient was approximately 1500. It would, consequently, appear that for values of $L_c/W < 0.15$ heat transfer at the condenser was achieved almost exclusively by natural convection. The region $0.15 < L_c/W < 6$ appears to correspond to the region of bubble-pumped augmented convection, while values of $L_c/W > 6$ would seem to lie in the condensation region. Considering the many assumptions inherent in the calculation of the collapse length and in particular the failure to include the pool circulation effects on the rise velocity, the results are very good and clearly support the general model. A definite progression from the natural convection of Mode I to augmented convection and then to condensation at or near the surface in Mode II can be seen in Fig. 21. These two regions of Mode II are examined in detail below.

3.2.3.1 Mode IIa - Augmented Convection

The rate of heat transfer in free convection at the cold surface is governed by the height of the thermal boundary layer which is determined by the rate of fluid circulation in the liquid-filled enclosure. This circulation is induced by an unstable density gradient and its equivalent buoyant force which normally results from a temperature gradient in the fluid. However, the presence of a vapor fraction in the fluid introduces an additional buoyant force which can dramatically increase the rate of fluid circulation and, hence, the rate of heat transfer at the cold surface.

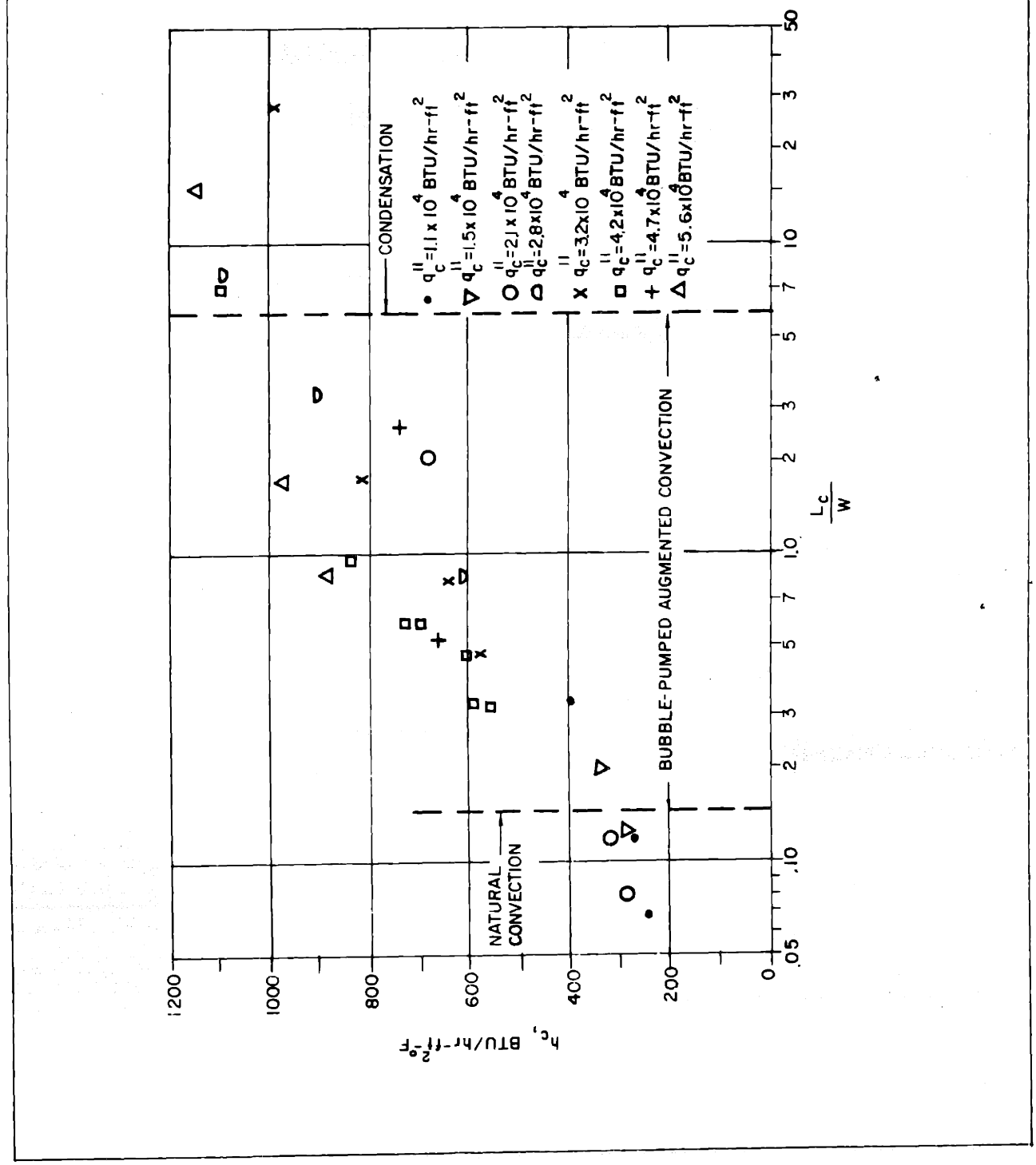

Fig. 21 - Variation of Condenser Heat Transfer Coefficient with Dimensionless Collapse Length - Water, One Heater

As discussed earlier, the rate of heat transfer in natural convection has been correlated by relating the Nusselt Number, Nu_{nc}, to the Rayleigh Number, Ra = GrPr, according to:

$$Nu_{nc} = c\,(Ra)^{n} \tag{30}$$

where

n = 1/4 for laminar flow

n = 1/3 for turbulent flow

c is a geometric constant different for laminar and turbulent flow

It is, consequently, reasonable to expect that the augmented transfer can be expressed as:

$$Nu_{aug} = c\,(Ra_{aug})^{n} \tag{31}$$

or

$$\frac{Nu_{aug}}{Nu_{nc}} = Nu^{*} = \left(\frac{Ra_{aug}}{Ra}\right)^{n} \tag{32}$$

For thermally induced natural convection, the circulation driving force, expressed within the Ra, can be defined as a buoyant force per unit volume, F'_t, equal to:

$$F'_t = g\Delta\rho = g\rho\beta\,(T_b - T_c) \tag{33}$$

For natural convection induced only by the presence of a vapor fraction, the buoyant force per unit volume, F'_v, would equal:

$$F'_v = g\,(\rho_\ell - \rho_v)\,\frac{V_v}{V_e} \tag{34}$$

Summing for the presence of both driving forces and substituting $\alpha = V_v/V_e$ to account for the volumetric vapor fraction

$$F'_{aug} = [g\rho\,\beta\,(T_b - T_c) + \theta g\,(\rho_\ell - \rho_v)\alpha] \tag{35}$$

where θ is a configuration factor allowing for the variable location of the vapor fraction relative to the convective cells.

Substituting the above expression in Eq. (32), the ratio of augmented to natural convection heat transfer rate is found to equal:

$$Nu^* = \left[1 + \theta\,\frac{(\rho_\ell - \rho_v)\alpha}{\rho\beta\,(T_b - T_c)}\right]^n \tag{36}$$

While Eq. (36) expresses Nu^* in an apparently straightforward manner, the determination of α and θ requires considerable effort. The steady-state volumetric fraction of vapor in the liquid-filled enclosure, α, is dependent on the rate of vapor generation at the heater and the rate of vapor condensation in the subcooled liquid. The evaluation of θ is, on the other hand, best left to empirical methods.

3.2.3.2 Evaluating the Vapor Fraction

Utilizing expressions derived above, it is possible to approximately determine the volumetric vapor fraction α as:

$$\alpha = \frac{V_v}{V_e} = \frac{1}{V_e}\,[\text{(bubble generation rate) x (bubble residence time) x (average bubble volume)}] \tag{37}$$

$$\alpha = \frac{1}{V_e}\left[\frac{\text{(vapor generation rate)}}{\text{(bubble departure volume)}}\ \text{x}\ t_c\ (\bar{\gamma}^3 \cdot \text{bubble departure volume})\right] \tag{38}$$

Introducing Eqs. (13), (20)

$$\alpha = \frac{1}{V_e}\left[\frac{\eta q}{\rho_v h_{fg}} \times \frac{\pi R_o^2}{4\,Ja^2 K}\,\tau_c \times\left(\frac{1}{\tau_c}\int_o^{\tau_c}\gamma\,d\tau\right)^3\right] \tag{39}$$

$$\bar{\gamma} = \frac{1}{\tau_c}\int_o^{\tau_c}\gamma\,d\tau \cong 0.36 \tag{40}$$

and, therefore,

$$\alpha = \left[\left(\frac{0.36^3\,\pi\,(2.3)}{4}\right)\left(\frac{R_o^2}{V_e\,\rho_v h_{fg} K}\right)\left(\frac{q}{Ja^2}\right)\right]\eta \tag{41}$$

It is, consequently, possible to approximately determine α to within one constant.

3.2.3.3 Evaluating Nu^*

Substituting α from Eq. (41) into Eq. (36):

$$Nu^* = \left[1 + 0.084\,\theta\eta\left(\frac{R_o^2}{V_e\rho_v h_{fg} K}\right)\left(\frac{q}{Ja^2}\right)\left(\frac{\rho_\ell - \rho_v}{\rho_\ell}\right)\frac{1}{\beta(T_b - T_c)}\right]^n \tag{42}$$

Or, separating the fluid parameters from the system parameters and letting $\lambda = 0.084\,(\theta\eta)$:

$$Nu^* = \left[1 + \lambda\left(\frac{[\rho_\ell - \rho_v]/\rho_\ell}{V_e\rho_v h_{fg} K\beta}\right)\left(\frac{qR_o^2}{Ja^2\,(T_b - T_c)}\right)\right]^n \tag{43}$$

Due to the nature of θ and η, it is not possible to completely determine λ. However, the experimental data for the augmented convective mode, Mode II, should be correlatable in terms of one constant λ for each geometry, where λ is evaluated so as to provide the best fit to the data.

The results of this approach are shown in Fig. 22 where it is seen that, considering the complexity of the model and the assumption made, adequate agreement is obtained between the experimental and calculated values of Nu^* when distinct values of λ are used for one, two and three heaters.

The presence of distinct constants for different heater geometries recalls the results obtained by Fairbanks et al. [10] for a finned submerged condenser surface. This similarity suggests that the prediction of convective augmentation, whether by the dimensionless parameter approach of Fairbanks [10] or the bubble buoyant force model of this investigation, suffers from an inability to determine a priori the relevant configurational factor. It is conceivable that further testing will establish guidelines for evaluating this factor, but for the present, λ must be evaluated experimentally for each configuration of interest.

3.2.3.4 Mode IIb - Condensation

As the bulk subcooling decreases and the collapse length increases beyond the distance of separation between the heated and condenser surfaces, $L_c/W > 1$, vapor bubbles begin to impinge on the form vapor pockets at the submerged condenser surface. This is at once the most prevalent region of submerged condenser operation and the least susceptible to analysis. Heat transfer by condensation initially involves only a small fraction of the condenser surface and must be properly averaged with the augmented convection transfer on the greater part of the surface. However, the high transfer rates associated with condensation soon come to dominate heat transfer in this mode. Experimental results, discussed above, suggest that the condensation region may begin in the vicinity of $L_c/W = 5$.

The need to determine the bulk subcooling is the prime reason for examining the heat transfer coefficient at the condenser surface. However, the interaction of convective and condensive thermal transport in Mode IIb and the dominance of the condensive coefficient at the condenser combine to make this task extremely difficult. The rate of heat transfer on that fraction of the surface covered with vapor can be determined from

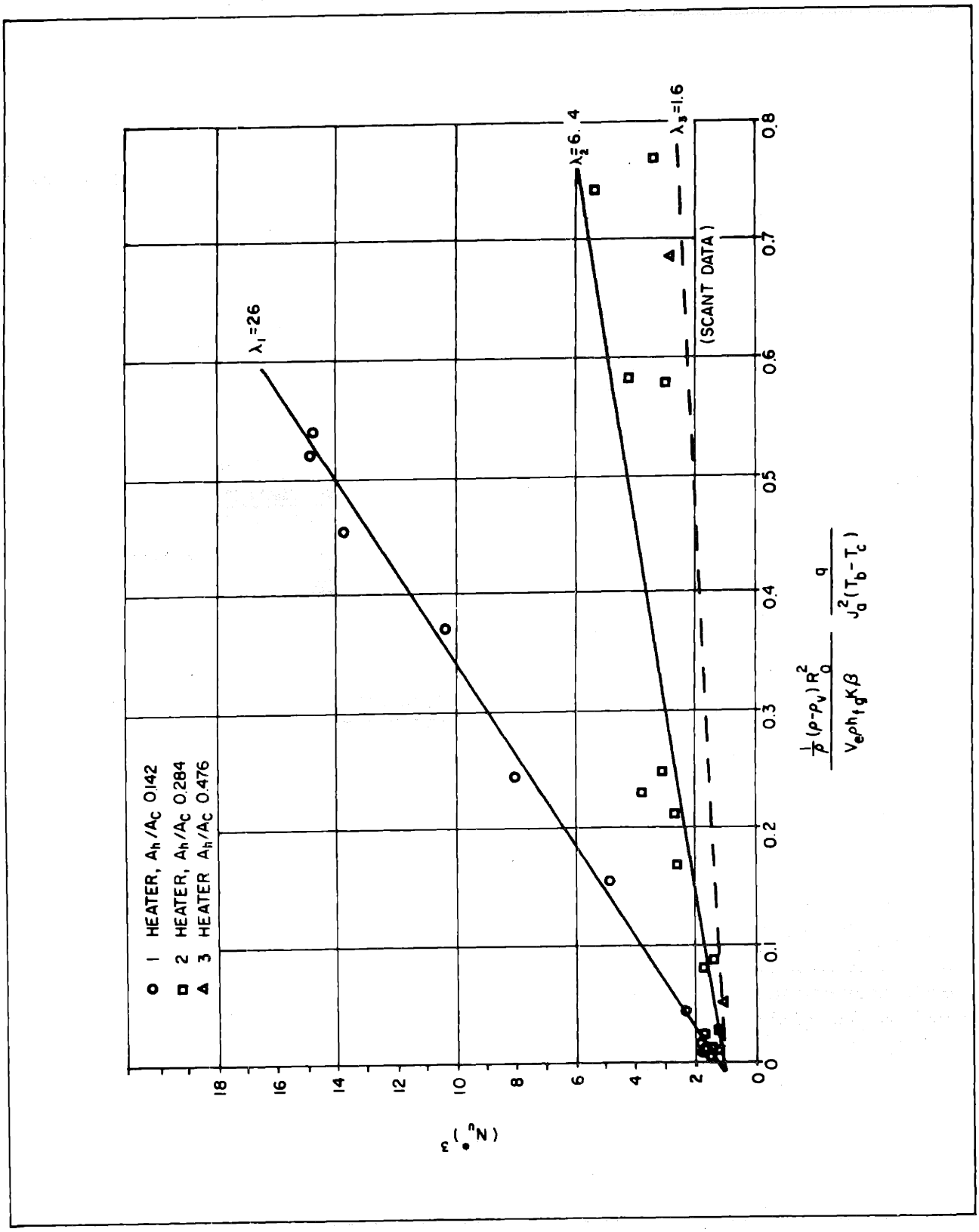

Fig. 22 - Augmented Natural Convection in Water

existing condensation heat transfer correlations while the heat transfer coefficient on the remainder of the surface can be determined as in Subsection 3.2.3.1. Consequently, the overall condenser surface heat transfer coefficient, h_c, can be set equal to:

$$h_c = \frac{1}{A_c} \left[(h_{condensation}) (A_{condensation}) + (h_{aug\ conv}) (A_c - A_{condensation}) \right]$$

However, the surface fraction involved in condensation is not known and is not easily determined. Alternately, since it is the bulk temperature which is being sought, a graphical technique may be used to determine the bulk subcooling in the condensive region (Mode IIb), i.e., in the region where $L_c/W > 5$.

In Figs. 13 through 16, which relate the bulk and heated surface temperature to the condenser heat flux at constant condenser surface temperature, the bulk temperature is seen to vary nearly linearly with q''_c as the condensive limit is approached. The slope of the bulk temperature curve in the linear region varies with the number of heaters and working fluid but the curve can be established by joining T_{sat} at the condensive limit with the bulk temperature at $L_c/W = 5$. Using Eq. (29) for L_c, the appropriate subcooling for $L_c/W = 5$ can be determined. Using that subcooling in Eq. (43) the augmented heat transfer coefficient and, hence, the condenser heat flux at that subcooling can be determined. The procedure is illustrated in Fig. 23.

3.2.3.5 Volumetric Expansion

In a constant pressure system the presence of substantial amounts of vapor in the bulk fluid must result in an increase in system volume or the displacement of fluid. A knowledge of this volumetric expansion is of necessity to the design of optimum submerged condenser systems. However, an approximate or upper limit determination of the volumetric expansion is adequate for this task.

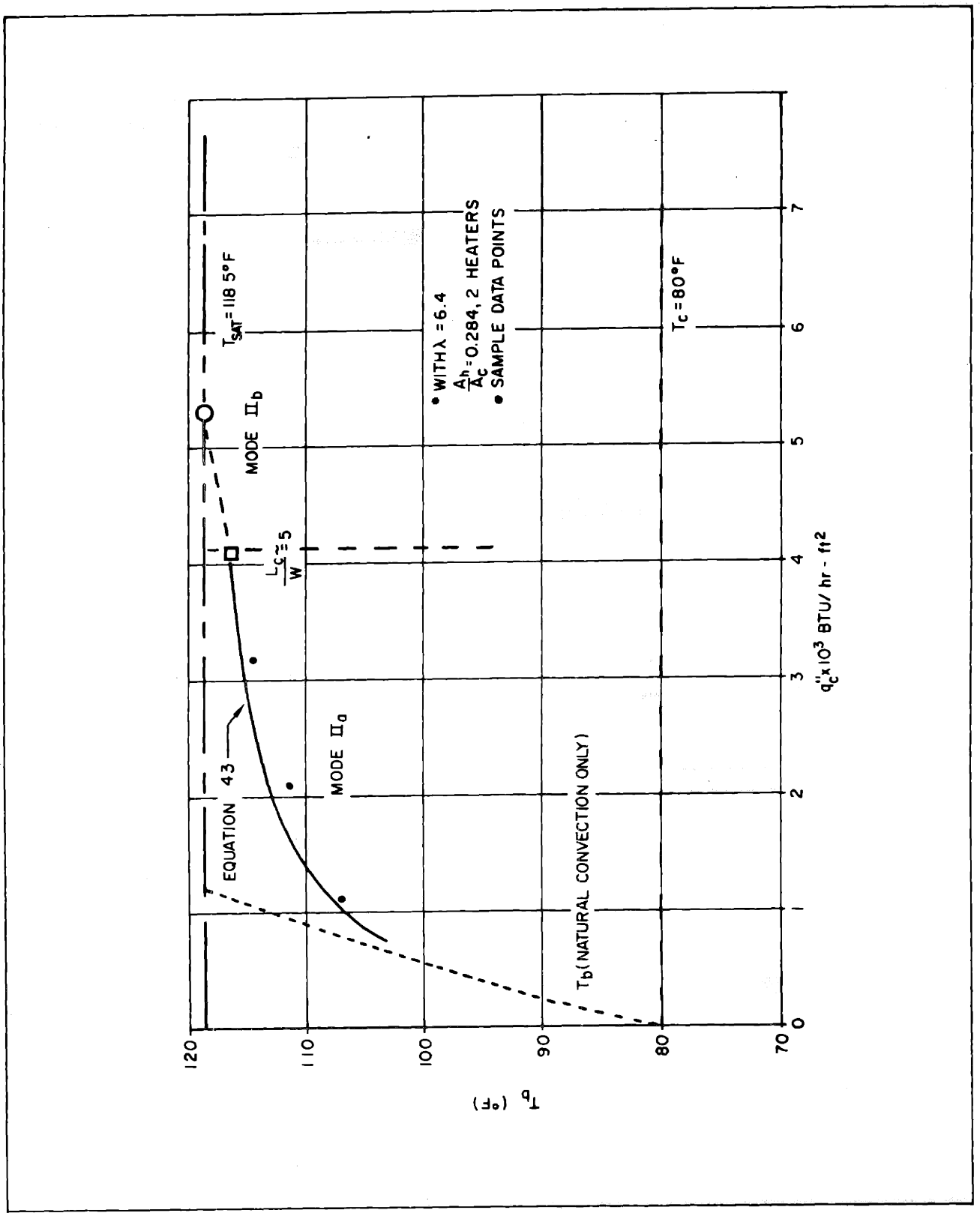

Fig. 23 - Calculated Bulk Temperature Variation with Condenser Heat Flux - Freon-113

The vapor columns and bubbles in the liquid and the vapor pockets at the condenser together comprise the vapor fraction and account for the major part of the volumetric expansion. The thermal expansion of the bulk fluid may also be of consequence in some systems. The difficulties in evaluating the volumetric vapor fraction were discussed earlier in Subsection 3. 2. 3. 1. Nevertheless, an upper limit for the vapor volume in the bulk can be calculated by assuming that no vapor condensation occurs in the bulk. Consequently, the bulk vapor volume can be determined as

$$V_{v,b} = \eta \left(\frac{q}{\rho_v h_{fg}}\right) \left(\frac{v_b}{W}\right) \tag{44}$$

where η is again not precisely known but can be taken to equal one for purposes of this calculation and v_b is calculated by Eq. (15).

The maximum vapor volume at the condenser surface is achieved at the condensive limit when vapor blankets the entire surface. Letting δ equal the depth of the vapor layer, the vapor volume is simply

$$V_{v,c} = \delta A_c \tag{45}$$

where δ is determined in Subsection 3. 2. 4. 2.

Summing all these contributions, the maximum volumetric expansion in a submerged condenser system can be determined as

$$\Delta V = \left(\frac{q}{\rho_v h_{fg}}\right) \left(\frac{v_b}{W}\right) + \delta A_c + \rho\beta \, (T_b - T_{amb}) \tag{46}$$

It is to be anticipated that the volumetric expansion thus calculated will substantially exceed any normal operating volumetric expansion since no system will be designed to operate at the condensive limit. At operating points somewhat below the condensive limit, the vapor fraction in the liquid and at the condenser is dramatically reduced from the maximum value calculated above.

3.2.4 Condensive Limit of Mode II

As the heat flux through the condenser and heated surface increases, the vapor region adjacent to the condenser surface grows and finally blankets the surface, as is shown in Figure 12b. Any further increases in q''_c beyond the vapor blanketing point results in a rapidly thickening vapor layer and the displacement of an increasing volume of fluid. This is the condensive limit apparent in Figs. 7 through 10 and it appears to correspond to the rate of heat transfer associated with film condensation on a downward facing (with respect to gravity) horizontal surface. At the condensive limit the vapor layer blanketing the condenser surface necessarily insulates the bulk liquid from the cold surface and the bulk attains the saturation temperature as is clear in Figs. 13 through 16.

3.2.4.1 Horizontal Surface

Film condensation on the underside of a horizontal surface is governed by thermal conduction through a thin liquid film. An analysis based on the Taylor instability at the liquid-vapor interface performed by Gerstman and Griffith [36] yields an expression for the heat transfer coefficient as:

$$\frac{h}{k}\left(\frac{g_o\sigma}{g(\rho_\ell-\rho_v)}\right)^{1/2} = 0.26\left[\frac{g\rho\,(\rho_\ell-\rho_v)\,h'_{fg}}{k\mu\,(T_s-T_c)}\left(\frac{g_o\sigma}{g(\rho_\ell-\rho_v)}\right)^{3/2}\right]^{1/4} \quad (47)$$

Eq. (47) is plotted in Fig. 24 and compared with the condensive limit data obtained in this investigation. The agreement with both Freon and Water data is excellent, thus leaving no doubt as to the nature of this limit.

3.2.4.2 Determining the Vapor Gap Depth

As discussed above, a knowledge of the depth of the vapor gap at the condensive limit is necessary for the determination of the maximum volumetric expansion in the submerged condenser system. An approximate method for calculating the width of the vapor gap, δ, at the condensive limit is presented below.

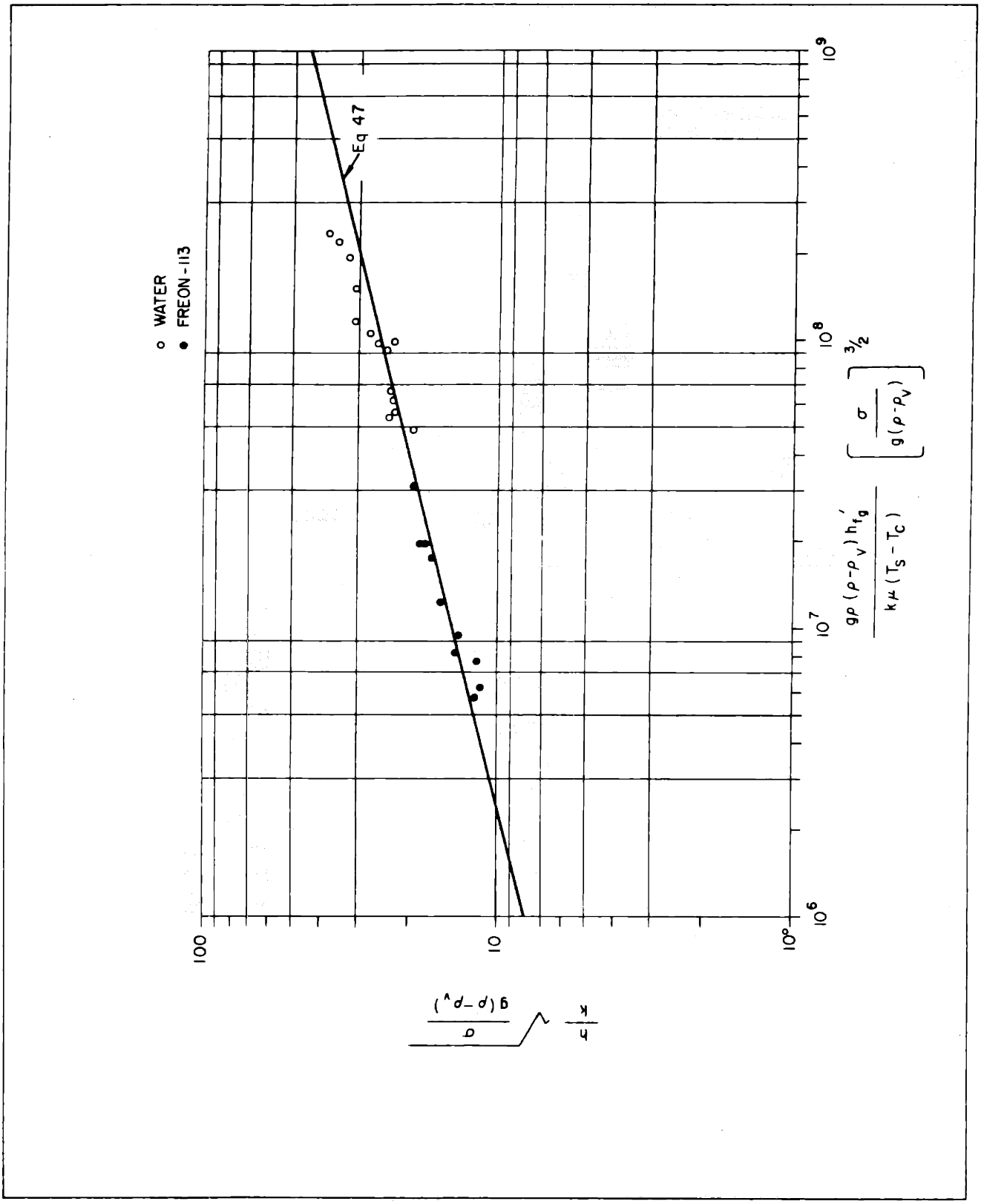

Fig. 24 - Condensive Limit on Horizontal Surface

Assuming that all the vapor is generated in a line source at distance W from the condenser surface and referring to the coordinate system of Fig. 25, it is obvious that, in general, the vapor flow rate, vapor velocity, vapor gap width, and pressure will vary with x along the condenser surface. Due to the existence of a thin liquid film on the condenser, the vapor must flow in a region bounded by liquid. Referring to the control volume in Fig. 25 and establishing a force balance:

$$2\,\tau_o L\,dx = \frac{dp}{dx}\,dx\,L\delta \tag{48}$$

or

$$\tau_o = \frac{\delta}{2}\,\frac{dp}{dx} \tag{49}$$

Assuming a parobolic velocity profile

$$v_x = 1.5\,\overline{v}\left[1 - \left(\frac{y}{\delta/2}\right)^2\right] \tag{50}$$

And substituting

$$\overline{v} = \frac{Q}{\delta L} \tag{51}$$

$$v_x = \frac{1.5Q}{\delta^3 L}\left[\delta^2 - 4y^2\right] \tag{56}$$

Evaluating τ_o,

$$\tau_o = -\frac{\mu}{g_c}\,\frac{dV_x}{dy}\bigg|_{y=\frac{\delta}{2}} = -\frac{1.5Q\mu}{\delta^2 Lg}\left[\delta - 4\right] \tag{53}$$

Equating Eq. (49) with Eq. (53)

$$\frac{\delta^3}{4 - \delta} = \frac{3\,Q\mu}{Lg_c\,\frac{dp}{dx}} \tag{54}$$

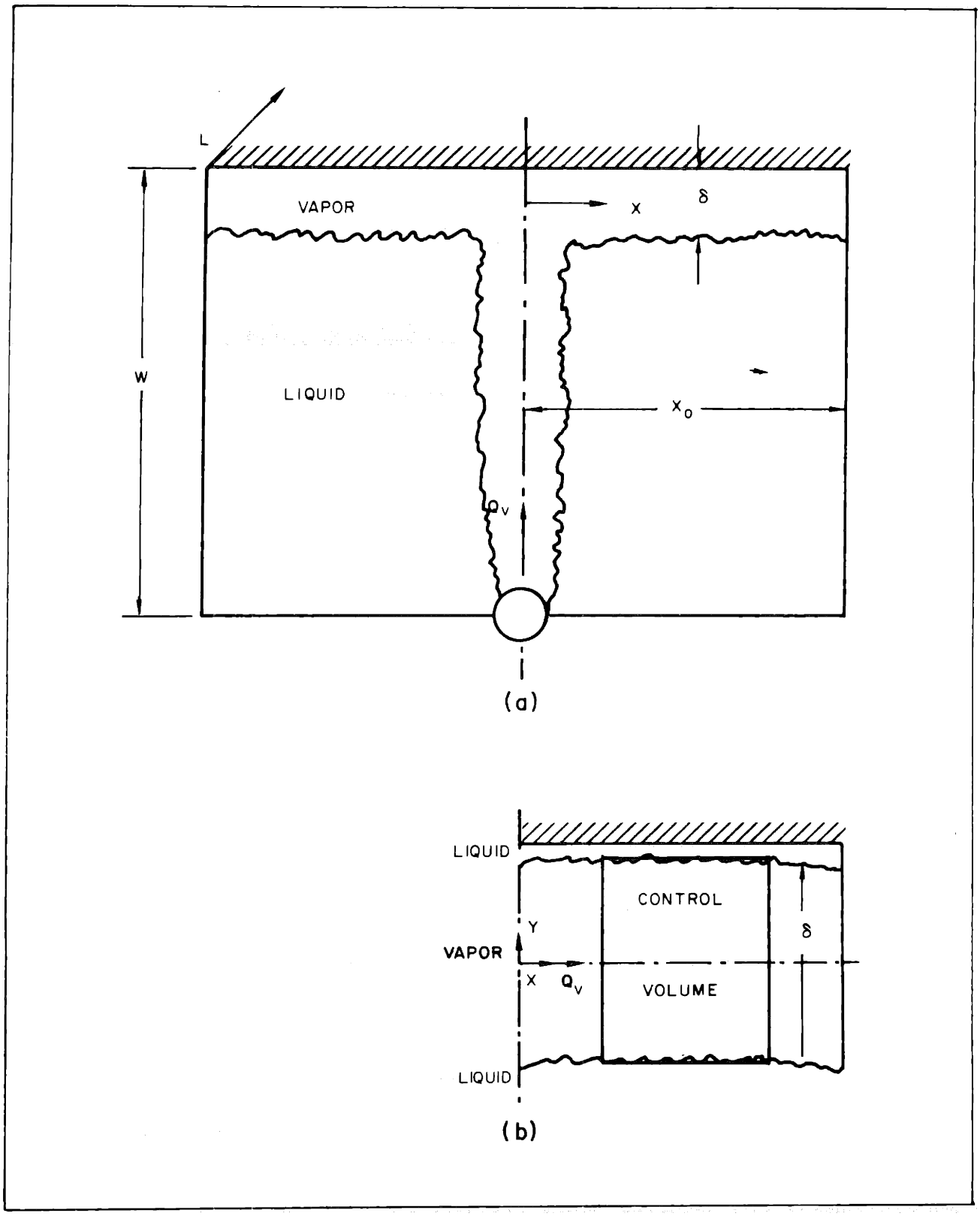

Fig. 25 - Model and Coordinate System for Vapor Gap Analysis

or with

$$\delta << 1$$

$$\delta \cong \left[\frac{12\ Q\mu}{L g_c \frac{dp}{dx}} \right]^{1/3} \tag{55}$$

At the line of vapor impact on the condenser surface the vapor pressure equals the stagnation pressure while at X_o, where the vapor flow rate is zero, it is equal to the system pressure. Consequently:

$$\int_o^{X_o} \frac{dp}{dx}\ dx = p_v = \frac{\rho V_j^2}{2 g_o} \tag{56}$$

A rigorous for δ (x) including the x variation of all parameters is beyond the scope of this investigation and of only limited practical significance.

Alternately, an approximate solution for an average value of δ based on average values of Q and dp/dx is easily obtained and quite sufficient for most practical applications. Assuming:

$$Q\ (x=0) = \frac{1}{2} Q_v$$

$$Q_v = \frac{q_h}{\rho_v h_{fg}} \tag{57}$$

$$\bar{Q}_v = \frac{1}{4} \frac{q_h}{\rho_v h_{fg}}$$

and

$$\overline{\frac{dp}{dx}} = \frac{p_v}{\bar{X}_o} = \frac{\rho v_j^2}{2 g_o \bar{X}_o}$$

Eq. (55) yields:

$$\delta = \left[\frac{12}{4} \frac{q_h}{h_{fg} \rho_v} \frac{\mu}{L g_o} \frac{2 g_o X_o}{\rho_v V_j^2} \right]^{1/3} \tag{58}$$

or

$$\delta = \left[6 \left(\frac{\mu}{h_{fg} \rho_v^2} \right) \left(\frac{q_b}{V_j^2} \right) \left(\frac{X_o}{L} \right) \right]^{1/3} \tag{59}$$

At low heater heat fluxes, $q''_h \leq q''_{tr}$, $V_j \simeq V_b$ and equation (15) can be used. For $q''_{tr} < q''_h \leq q''_{crit}$, by analogy to Zuber's [26] q''_{crit} analysis, V_j can be set equal to

$$V_j = \frac{16 q''_h}{\pi h_{fg} \rho_v} \tag{60}$$

The resulting gap width for typical operating conditions are in qualitative agreement with observations and are of the order of 0.5 inch for water and F-113.

The vapor gap resulting from a point source can be determined in a completely analogous manner and shown to equal:

$$\delta \cong \left[8.5 \left(\frac{\mu}{\rho_v^2 h_{fg}} \right) \left(\frac{q_h}{V_j^2} \right) \right]^{1/3} \tag{61}$$

3.2.4.3 Moderate Inclination

While the submerged condenser system is designed to operate with the condenser surface horizontal, on occassion, as a result of error or structural defect, the surface may be inclined as much as 10 to 15 degrees to the horizontal. The Gerstmann-Griffith [36] model for heat transfer on an inclined surface in a vapor space indicates a rapid deterioration of transfer rate at slight inclination and a later partial recovery due to an initial

thickening of the liquid film, as shown in Fig. 26. The data obtained in the submerged condenser apparatus shown in Fig. 27, however, did not provide evidence of this deterioration. This discrepancy can be explained by the partial submerging of the inclined condenser surface and the sloshing of liquid in the enclosure. The sloshing action alternately washing the surface and exposing it to vapor results in a transient condensation which is not comparable to condensation on an inclined surface in a quiescent vapor space. It is, therefore, not surprising that a deterioration in heat transfer rate did not occur, although a precise analysis of this phenomenon would be required to fully interpret the experimental results.

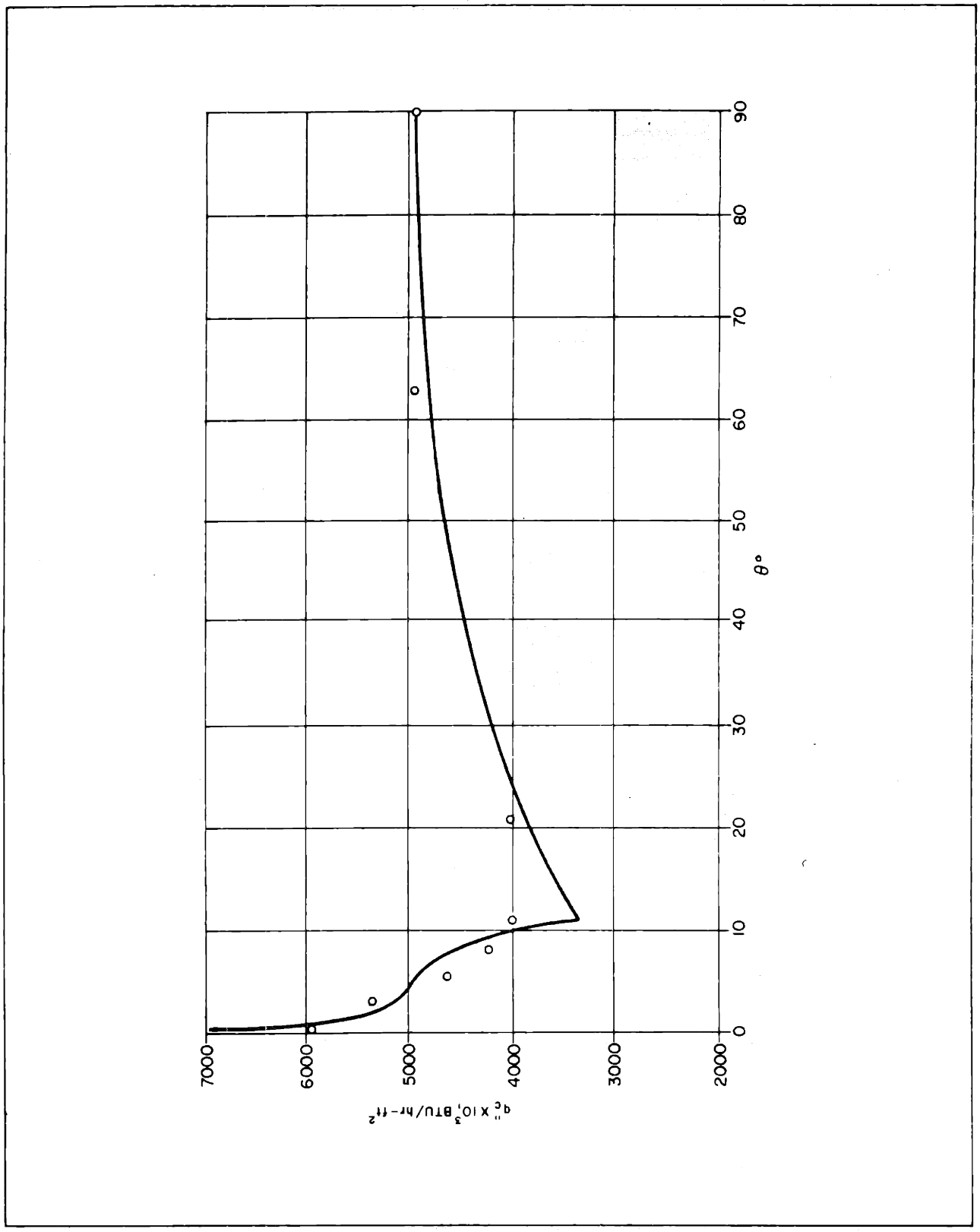

Fig. 26 - Heat Transfer Rate as a Function of Angle at a Temperature Difference of 40°F [36]

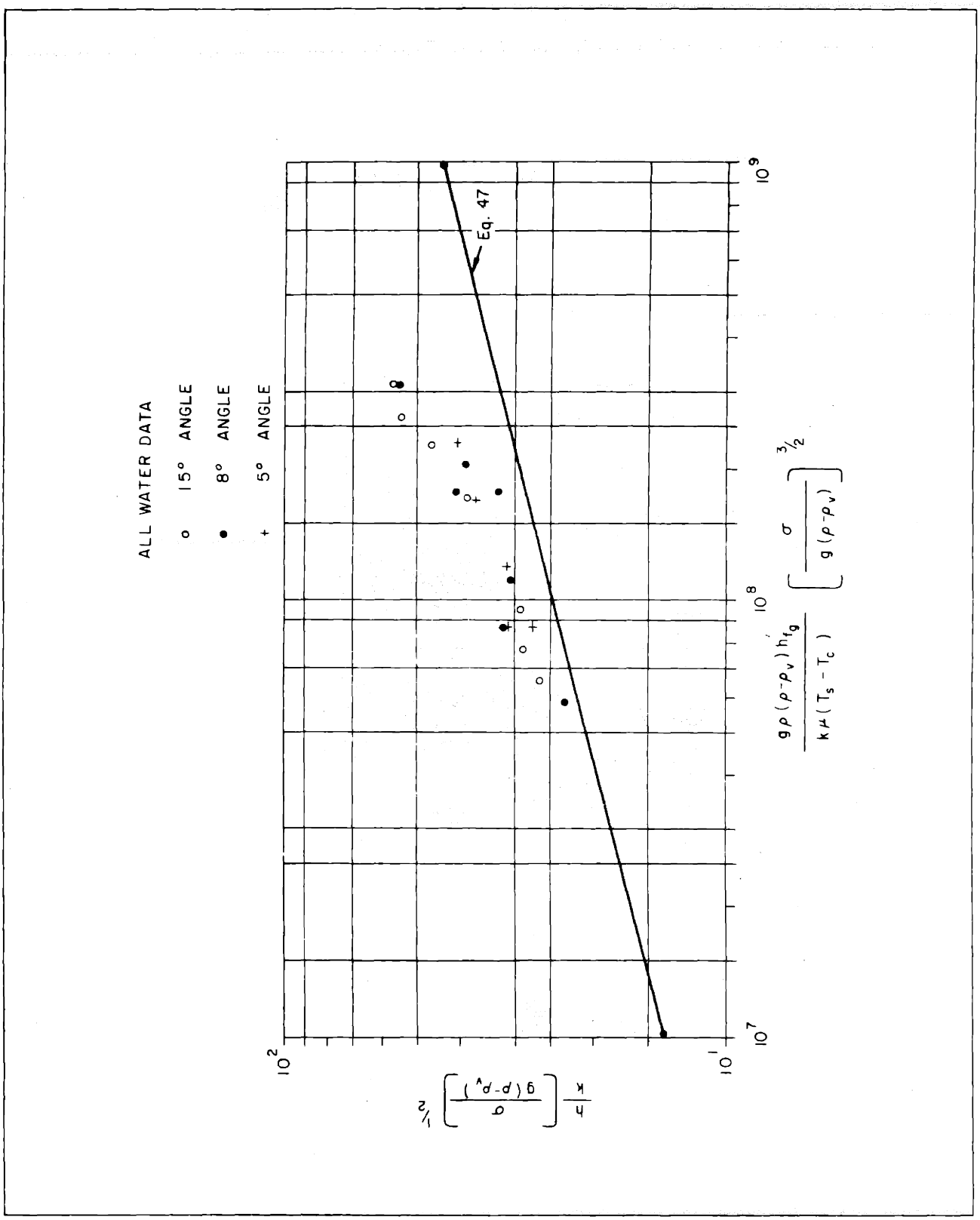

Fig. 27 - Condensive Limit on an Inclined Surface

4. CONDENSATION ON A RIPPLED SURFACE

4.1 Introduction

The operation of submerged condenser systems was examined in detail in Chapters 2 and 3 and shown to possess two possible upper bounds. For large values of condenser surface subcooling and/or low heater to condenser surface area ratios, the upper bound is established by the critical heat flux or "burnout" at the boiling surface. For low values of condenser surface subcooling and/or high area ratios, however, a condensive limit exists which has been found to correspond to the heat flux associated with film condensation on a downward facing horizontal surface. Typical design criteria for submerged condenser systems including available heat sink temperatures and the need to reduce condenser surface area, usually result in system operation in the region bounded by the condensive limit. It is, consequently, significant to examine techniques for augmenting condensation heat transfer on horizontal surfaces.

Condensation occurs when a subcooled surface is exposed to saturated or supersaturated vapor. The liquid condensate formed at the surface normally spreads out and establishes a stable film. Condensation then occurs on the vapor-liquid interface and the heat released is conducted through the liquid film to the condenser surface. However, when the liquid does not wet the surface, individual droplets form, condensation occurs on the drop surface and the released heat is conducted through the liquid drops to the condenser surface. Most of the heat transfer in dropwise condensation occurs through drops in early stages of growth and as a result, heat transfer coefficients in dropwise condensation are typically one to two orders of magnitude higher than in film condensation [38] . Dropwise condensation thus appears to be the obvious technique for increasing the condensive limit. However, in order to maintain this mode of condensation on a condensing surface, the surface must be treated with a so-called promoter which repels the liquid molecules while being strongly attracted to the surface itself. A substantial amount of work has been done in identifying successful promoters, but research

has unfortunately been restricted to dropwise condensation of water vapor. It is, consequently, not yet possible to promote dropwise condensation of the dielectric inert fluids which must be used in electronic cooling and other augmentation techniques must be examined.

In film condensation the rate of heat transfer is governed by thermal conduction through the liquid film adhering to the surface. Consequently, if augmentation of film condensation is to be achieved, some way must be found to thin the liquid film. In 1953, Gregorig [39] while studying condensation on wavy surfaces noted that surface tension could give rise to large pressure gradients in the liquid film due to the varying curvature of the condensate surface. Large pressure gradients necessarily lead to thin films and coefficients of heat transfer several times greater than in normal film condensation were achieved. Gregorig thus proposed that improved vertical condenser tubes could be made by placing grooves of the proper geometric form parallel to the tube axis. The profile suggested by Gregorig [39] utilized a gradually decreasing solid surface curvature to produce a very thin but nearly uniform condensate film. However, the general concept is also valid for a solid surface of constant curvature which is far easier to form in practical applications. This general technique has since been extended to horizontal condenser tubes [40] and other geometries, but can not be directly applied to horizontal surfaces.

In previous applications of this augmentation technique, surface tension forces were used to reduce the film thickness but gravity forces were then used to drain the condensate from the surface. On downward facing horizontal surfaces condensate removal is normally accomplished by drop formation resulting from the growth of disturbances on the liquid-vapor interface. Consequently, it is not sufficient to provide undulations on the condenser surface, but rather a two-dimensional profile as shown in Figs. 28 and 29 would appear to be required if the surface tension forces are to produce the desired result. The doubly-rippled surface of Fig. 28 was prepared and tested to determine whether the heat transfer coefficients for film condensation on a downward facing horizontal surface could be improved by surface tension effects. Though obviously any obtained augmentation of the heat transfer rate must be weighed against the considerable cost of fabricating this surface.

(U)

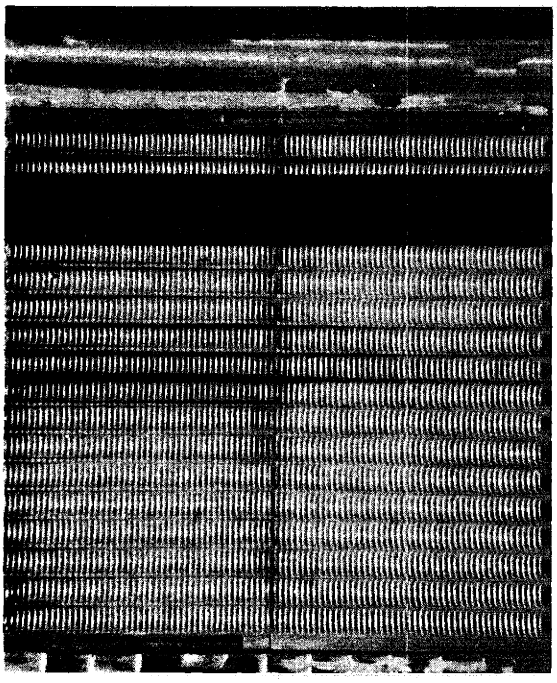

Fig. 28 - Photograph of Doubly-Rippled Surface

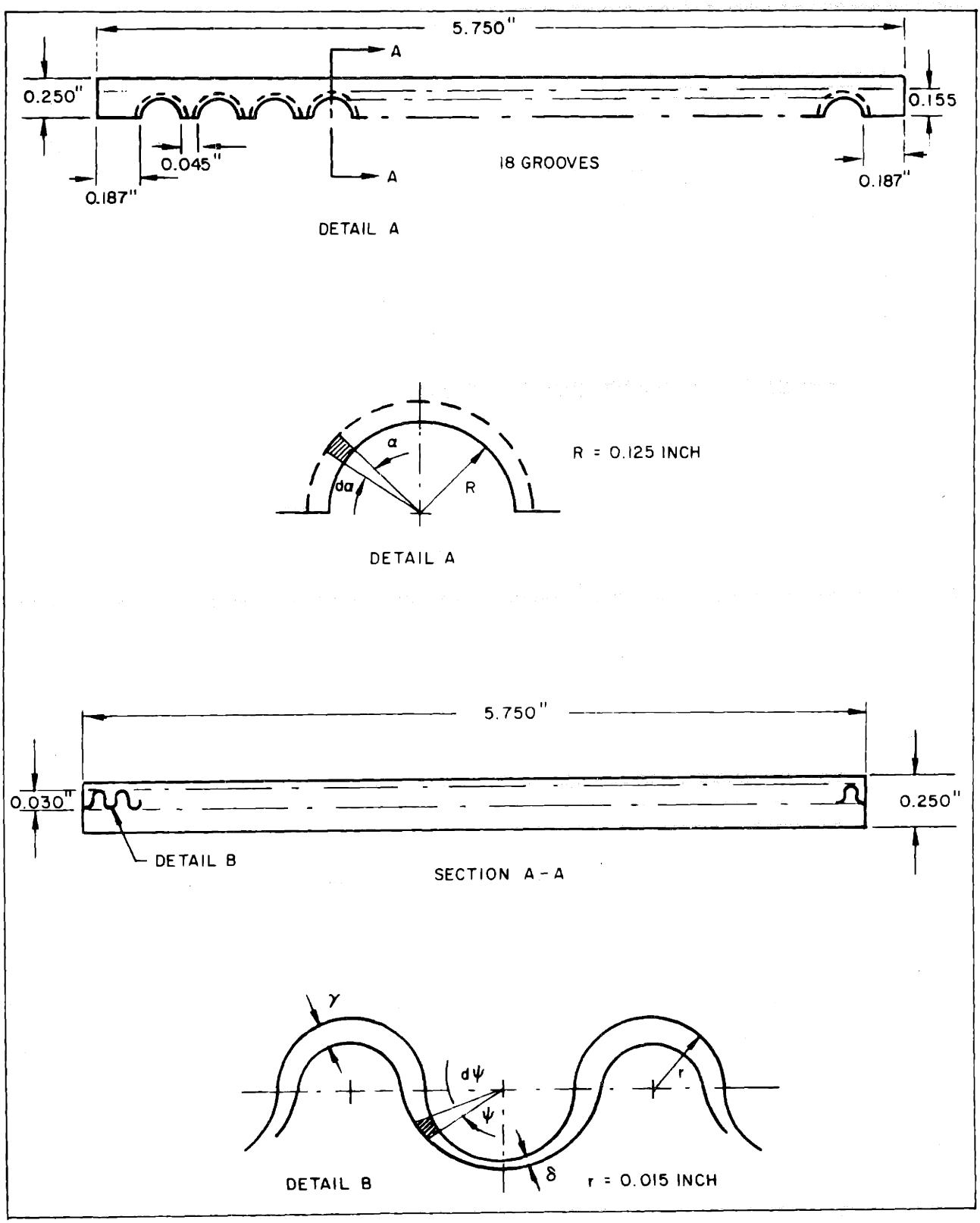

Fig. 29 - Schematic and Coordinate System for Doubly-Rippled Surface

4.2 Experimental Apparatus and Procedure

The doubly-rippled surface shown in Figs. 28 and 29 was used as the test surface. The undulations were of constant curvature with a radius of 0.015 in., while the arches were 0.125 in. in radius. The total area of the surface was 2.38 times its projected area. The test surface was soldered to the water-cooled plate and incorporated into the submerged condenser apparatus shown in Figs. 5 and 6 and described briefly in Subsection 2.1. The apparatus consisted of five cylindrical heaters, 0.25 in. in diameter, electrically powered and oriented horizontally in an insulated Plexiglas and brass container 6 inches on a side. Freon-113 was used as the working fluid. The doubly-rippled surface was at the top of the container, approximately 4.5 in. from the heaters, and incorporated a cooling coil through which city water at nearly 60°F inlet temperature was circulated. A liquid reservoir located on top of the container served to maintain a constant average system pressure of 14.9 psi. The ratio of total heated to condenser surface area varied from 0.14 to 0.71 depending on the number of heaters activated. Flowmeters, voltmeters, ammeters and a stripchart recorder were used as required.

The average condenser surface temperature was determined with thermocouples located 0.005 in. below the root of the surface undulations. The temperatures recorded at these locations were extrapolated to an imaginary plane passing through the root of the undulations at the top of the grooves and a weighted average condenser surface temperature determined. It must be noted that this temperature does not correspond to the true surface temperature along the groove. Rather, it is somewhat lower and encorporates the temperature difference associated with thermal conduction through the 'ribs' separating the grooves.

The average heated surface temperature was determined by the use of an especially prepared, hollow, thin-walled heater in whose center thermocouples were placed. The appropriate extrapolations based on thermal conductivity and heat flux was made to obtain the average surface temperatures. The bulk temperature of the working fluid was measured by sheathed thermocouples inserted through the base of the container into the fluid.

The condensive limit data were obtained in a series of data runs. Prior to each run the working fluid was carefully degassed. For each run, the heat input at the heaters and, hence, the condenser and heated surface heat flux, was maintained constant while the average condenser surface temperature was slowly increased by decreasing the flow of city water through the condenser cooling coil. The condensive limit was attained when the doubly-rippled surface was completely blanketed by vapor and large quantities of vapor were seen to be rising into the liquid reservoir. Further details on the experimental apparatus and procedure can be found in the Appendix.

4.3 Analysis

An investigation by Gregorig [39] in 1953 indicated that film condensation may be augmented by utilizing the powerful surface tension forces which arise during condensation on an undulated surface of varying curvature. In the present investigation an attempt was made to extend this principle to condensation on a downward facing horizontal surface containing undulations of constant curvature.

4.3.1 At the Undulation Crest

The condensate on a surface undulation shown in Fig. 29 forms a laminar film which flows along the surface. Considering a small angular segment $r_o d\psi$ and neglecting ψ-direction momentum changes, a force balance may be written in the ψ-direction as:

$$-\mu \frac{dv}{dx} \cdot r_o d\psi = -g (\rho - \rho_v) \sin \psi (\delta - x) \cdot r_o d\psi + \frac{dp}{d\psi} \cdot d\psi (\delta - x) \tag{62}$$

Assuming that the gravitational force can be neglected relative to the surface tension force and simplifying:

$$\mu \frac{dv}{dx} = - \frac{dp}{d\psi} \frac{(\delta - x)}{r_o} \tag{63}$$

Throughout the analysis the condensate film will be assumed very thin $\delta << r_o$ and, hence, changes in the center of curvature of the interface will be neglected. Furthermore, the analysis will be restricted to $o < \psi < \frac{\pi}{2}$. With these assumptions, the pressure difference across the curvature of the liquid-vapor interface is given by:

$$p - p_v = \frac{\sigma}{r_o + \delta} \tag{64}$$

But p_v is constant and, consequently,

$$\frac{dp}{d\psi} = - \frac{\sigma}{(r_o + \delta)^2} \frac{d\delta}{d\psi} \tag{65}$$

Or, for $\delta << r_o$,

$$\frac{dp}{d\psi} \cong \frac{-\sigma}{r_o^2} \frac{d\delta}{d\psi} \tag{66}$$

And

$$\mu \frac{dv}{dx} = \frac{\sigma}{r_o^3} \frac{d\delta}{d\psi} (\delta - x) \tag{67}$$

Integrating over x to find V_ψ

$$V_\psi = \frac{\sigma}{r_o^3 \mu} \frac{d\delta}{d\psi} \left(\delta x - \frac{x^2}{2}\right) \tag{68}$$

The mean velocity

$$\overline{V}_\psi = \frac{1}{\delta} \int_o^\delta V_\psi \, dx \tag{69}$$

is found to equal:

$$\overline{V}_\psi = \frac{\sigma}{r_o^3 \mu} \frac{d\delta}{d\psi} \frac{\delta^2}{3} \tag{70}$$

By continuity

$$\Gamma = \rho \bar{V}_{\psi} \delta \tag{71}$$

Or, differentiating:

$$d\Gamma = \rho\, d\left[\bar{V}_{\psi} \delta\right] = \frac{\rho\sigma}{r_o^{\,3}\mu}\, d\left[\frac{d\delta}{d\psi}\,\frac{\delta^3}{3}\right] \tag{72}$$

and

$$d\Gamma = \frac{\rho\sigma}{r_o^{\,3}\mu}\,\frac{1}{12}\, d\left[\frac{d\delta}{d\psi}^4\right] \tag{73}$$

Applying the energy equation by equating the heat released at the interface with the heat conducted through the film and assuming a linear temperature profile in the film:

$$d\Gamma = \frac{k\,(T_s - T_c)\, r_o\, d\psi}{\delta\, h'_{fg}} \tag{74}$$

Equating (73) and (74)

$$\delta\left[\frac{d^2\delta}{d\psi^2}^4\right] = \frac{12\,\mu r_o^{\,4} k\,(T_s - T_c)}{\rho\sigma\, h'_{fg}} \tag{75}$$

This second order differential equation for δ, the film thickness, can be solved numerically by finite difference techniques when two boundary conditions, chosen for historical and physical reasons to be δ and its first derivative $\frac{d\delta}{d\psi}$, are specified at $\psi = 0$. By symmetry, at the top of the undulation, $\psi = 0$, the slope of the interface, $\frac{d\delta}{d\psi}$, equals zero. The value of δ_o is not so easily determined, though it can be found by two different approaches.

The first approach utilizes the definition of surface curvature to yield:

$$\frac{d^2\delta}{d\psi^2} = r_o + \delta \cong r_o \tag{76}$$

Returning to Eq. (75) and modifying it slightly

$$\delta \frac{d}{d\psi}\left[\delta^3 \frac{d\delta}{d\psi}\right] = \frac{3\mu r_o^4 k (T_s - T_c)}{\sigma \rho h'_{fg}} \tag{77}$$

But at $\psi = 0$, $\delta = \delta_o$, and $\frac{d\delta}{d\psi} = 0$; therefore,

$$\delta_o^4 \frac{d^2\delta}{d\psi^2} = \frac{3\mu r_o^4 k (T_s - T_c)}{\sigma \rho h'_{fg}} \tag{78}$$

And substituting Eq. (76) into Eq. (78)

$$\delta_o = \left[\frac{3\mu r_o^3 k (T_s - T_c)}{\sigma \rho h'_{fg}}\right]^{1/4} \tag{79}$$

Alternately, it is possible to determine δ_o by analogy to gravity dominated condensation on a cylinder where

$$\delta_o = \left[\frac{3\mu k (T_s - T_c) r_o}{g (\rho - \rho_v) \rho h'_{fg}}\right]^{1/4} \tag{80}$$

In the present investigation, surface tension forces have replaced gravity as the driving force for condensate removal from the surface. It would, therefore, appear appropriate to replace the gravity term in the denominator of Eq. (80) by a surface tension term. Utilizing r_o as the characteristic length and multiplying together the traditional nondimensional groups $Fr \times We^2$,

$$(\rho - \rho_v)\, g = \frac{\sigma}{r_o^2} \tag{81}$$

Inserting Eq. (81) into Eq. (80)

$$\delta_o = \left[\frac{3\,\mu k\,(T_s - T_c)\, r_o^3}{\sigma\, \rho\, h_{fg}'} \right]^{1/4} \tag{82}$$

The alternate derivations for δ_o, Eqs. (82) and (79), are now seen to yield identical results. At atmospheric pressure and 10°F surface subcooling on an undulation or horizontal cylinder with a 2×10^{-2} in. radius of curvature, Eq. (82) yields $\delta_o = 2 \times 10^{-4}$ in.

Returning to the governing equation for δ and nondimensionalizing it with

$$\begin{aligned} \hat{\lambda} &= \left(\frac{\delta}{r_o}\right)^4 \\ \hat{\psi} &= \sqrt{c}\ \psi \end{aligned} \tag{83}$$

where

$$c = \frac{12\,\mu k\,(T_s - T_c)}{\rho\,\sigma\, h_{fg}\, r_o}$$

leads to:

$$(\hat{\lambda})^{1/4}\ \frac{d^2\hat{\lambda}}{d\hat{\psi}^2} = 1 \tag{84}$$

The solution for $(\hat{\lambda})^{1/4}$ as a function of $\hat{\psi}$ obtained by finite difference techniques in the range $0 < \hat{\psi} < \frac{\sqrt{c}\,\pi}{2}$, is shown graphically in Fig. 30 for several values of λ_o.

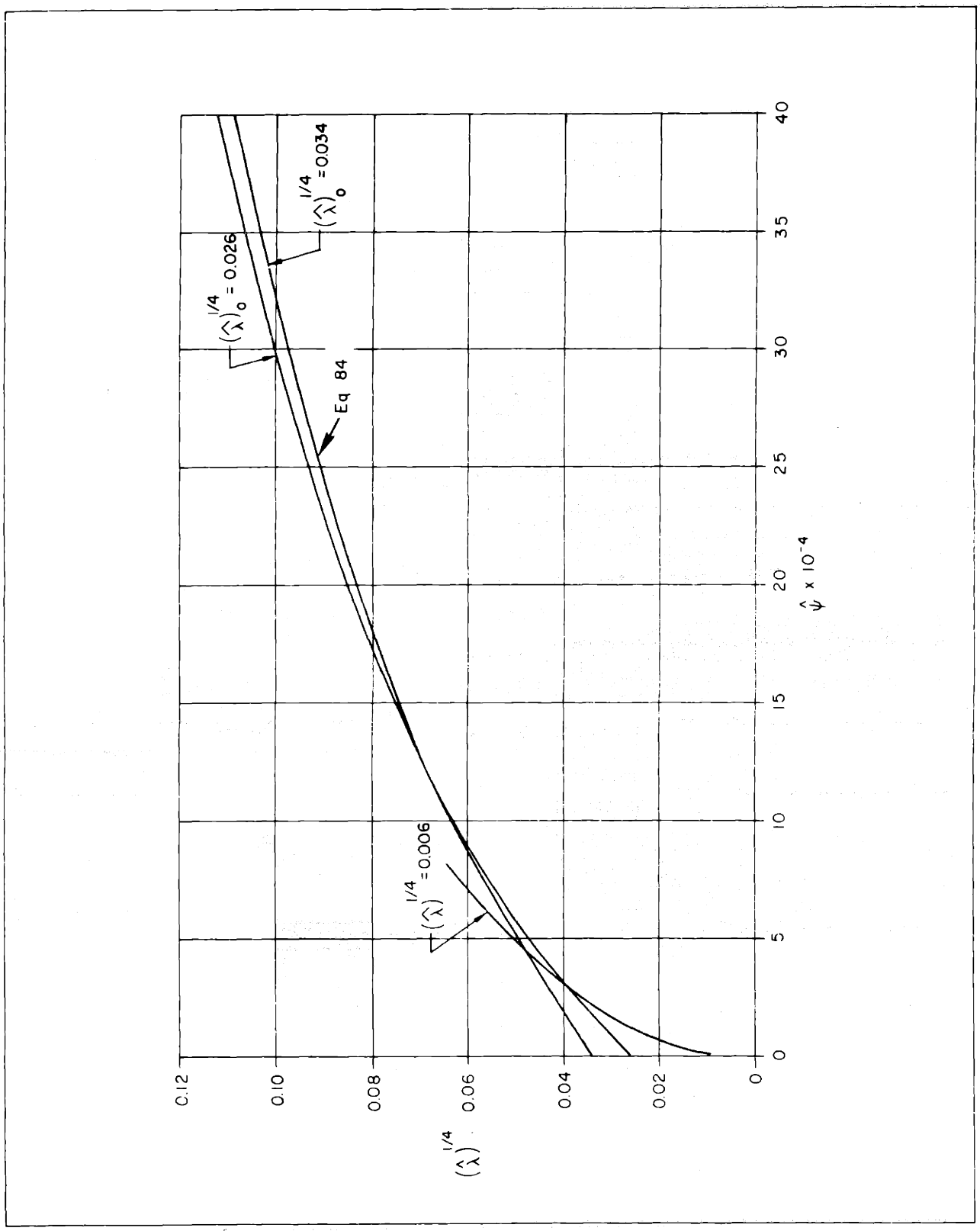

Fig. 30 - Nondimensional Film Thickness Along Crest of Sinusoidal Undulation

The heat transfer coefficient, h_c, in film condensation is equal to:

$$h_c = \frac{k}{\delta} \tag{85}$$

Relating back to the nondimensional film thickness, $\hat{\lambda}$,

$$h_c = \frac{k}{(\hat{\lambda})^{1/4} r_o} \tag{86}$$

Therefore, the average heat transfer coefficient on a segment of the surface $0 < \hat{\psi} < \hat{\psi}_1$, equals:

$$\bar{h}_c = \frac{k}{\left[\hat{\lambda}_m (\hat{\psi}_1)\right]^{1/4} r_o} = \frac{k/r_o}{\left[\frac{1}{\hat{\psi}_1} \int_o^{\psi} (\hat{\lambda})^{1/4} d\hat{\psi}\right]} \tag{87}$$

On the upper part of the undulation, shown in Fig. 29, the pressure gradient resulting from surface tension forces leads to an extremely thin condensate film. However, for $\psi > \frac{\pi}{2}$ the solid surface curvature reverses and the film thickness is substantially increased. In this region, the film thickness, δ, can no longer be considered very small in relation to r_o and, consequently, the above analysis no longer applies. However, little additional condensation occurs in the troughs and heat transfer in this thick film region can be neglected. As a result, it is the thin film region that accounts for most of the heat transfer on this surface, and the analysis presented above can be used to calculate the approximate rate of heat transfer over the entire surface when proper account is taken of the fraction of the area occupied by the undulation crests.

4.3.2 At the Undulation Trough

The vapor condensed on the crest of an undulation is pumped by surface tension into the undulation trough. From the trough the condensate flows by gravity along the specified arch and then drips off the doubly-rippled

surface at the base of the arch. The height of the liquid layer in the trough, γ, increases along the arch and reaches its maximum value at the base of the arch. For values of $\gamma \cong r_o$, the condensate flowing in the trough may wash or "flood" the undulation crest and substantially increase the film thickness on the crest. However, the relatively short path length along the arch suggests that the condensate film remains thin and that flooding is not achieved at commonly employed values of condenser surface subcooling. The condensate film thickness in the trough can be determined approximately in the following manner.

Referring to the differential element in Fig. 29 and assuming the liquid-vapor interface to be at a uniform height above the surface (equivalent to a thin film assumption), a force balance in the α direction yields

$$\mu \frac{dv}{dx} = g (\rho - \rho_v) \cos \alpha (\gamma - x) \tag{88}$$

Integrating across x to find the fluid velocity in the α direction

$$V = \int_o^x \frac{dv}{dx} dx = \frac{g}{\mu} (\rho - \rho_v) \cos \alpha \left(\gamma x - \frac{x^2}{2}\right) \tag{89}$$

The mean fluid velocity can now be found as

$$\bar{V} = \frac{1}{\gamma} \int_o^\gamma v dx = \frac{g}{\mu} (\rho - \rho_v) \cos \alpha \frac{\gamma^2}{3} \tag{90}$$

By continuity

$$\Gamma = \rho \bar{V} \gamma = \frac{\rho g (\rho - \rho_v) \cos \alpha \cdot \gamma^3}{3 \mu} \tag{91}$$

However, if condensation in the trough is neglected the condensate flowing in the trough is equal to the condensate draining off the undulation crests. Consequently,

$$\frac{\bar{h}_c (T_s - T_c) R\alpha}{h'_{fg}} = \frac{\rho g}{3\mu} (\rho - \rho_v) \cos \alpha \cdot \gamma^3 \qquad (92)$$

And simplifying

$$\gamma = \left[\frac{3 \mu \bar{h}_c (T_s - T_c) R \alpha}{h'_{fg} \rho (\rho - \rho_v) g \cos \alpha} \right]^{1/3} \qquad (93)$$

The insertion of numerical values in Eq. (93) reveals that for commonly encountered values of surface subcooling, γ at the base of the arch is still small as compared to r_o. However, γ is somewhat greater than δ at the inflection point in the curvature and an artificial discontinuity thus exists. For the range of r_o likely to be chosen in practical applications, γ is approximately 50 percent greater than δ at that point. The magnitude of this discontinuity suggests that it could be easily smoothed by surface tension forces without substantially effecting δ on the crest of the undulation. The analysis in Subsection 4.3.1 is thus valid for the film thickness on the crest and the rate of heat transfer on the doubly-rippled surface can be approximately determined.

4.4 Results and Discussion

In the preceding sections of Chapter 4, a method was presented for determining the condensate film thickness on a surface with 3-D sinusoidal undulations. The film thickness was found to increase rapidly along the crests of the undulations, suggesting that an approximate rate of heat transfer for the entire surface could be obtained by neglecting condensation in the undulation troughs.

4.4.1 Condensate Film Thickness

Previous attempts to exploit surface tension forces to produce thin condensate films have utilized surfaces of varying radii of curvature. The surfaces were shaped to produce uniform thickness condensate films along

the entire crest surface [39, 40] with δ equal to the value attained at the top of the crest. Due to the difficulties associated with accurately machining such a surface, the use of sinusoidal undulations appeared attractive.

Regardless of the precise surface profile, the evaluation of the film thickness at the top of the undulation crest, δ_o, is central to any determination of heat transfer on the surface. Gregorig [39, 41] specified no direct method for calculating δ_o. The value of δ_o determined by Eq. (79) is compared in Fig. 31 with the value suggested by Gregorig [39, 41] for an undulation with an initial radius of curvature equal to 2.36×10^{-2} in. For steam saturated at 85°F and a surface subcooling of 0.955°F, Eq. (79) yields $\delta_o = 2.3 \times 10^{-4}$ in., while Gregorig determined a value of 1.97×10^{-4} in. Further comparison would be desirable but the literature contains only this one calculated value. Nevertheless, the approach followed in deriving Eq. (79) appears to be valid and yields accurate results.

As is clear from Eqs. (64) and (65), maintaining the surface curvature, r_o, constant requires that δ, the film thickness, increase with ψ to produce the desired pressure gradient in the film. Consequently, the use of a sinusoidal undulation rather than a profile with a variable radius of curvature can be expected to result in a larger mean film thickness. The condensate film thickness on the crest of a sinusoidal and variable radius of curvature undulation with initial radius of 2.36×10^{-2} in. are compared in Fig. 31. For the conditions stated above, the sinusoidal profile yields a film thickness which increases to 4 times the minimum value at the inflection point of the undulation. The mean film thickness for the sinusoidal profile is thus approximately 3 times greater than the comparable film thickness on the Gregorig-type profile [39], but still nearly a factor of 3 less than the average film thickness for the same conditions on a smooth, horizontal surface. It is apparent, then, that the use of a sinusoidal rather than a variable radius of curvature profile does lead to considerably lower rates of heat transfer. However, the results of the analysis are in qualitative agreement with expectation and indicate that sinusoidal undulations of sufficiently small radius can be used to substantially reduce the film thickness and, hence, significantly increase thermal transport in film condensation on horizontal surfaces.

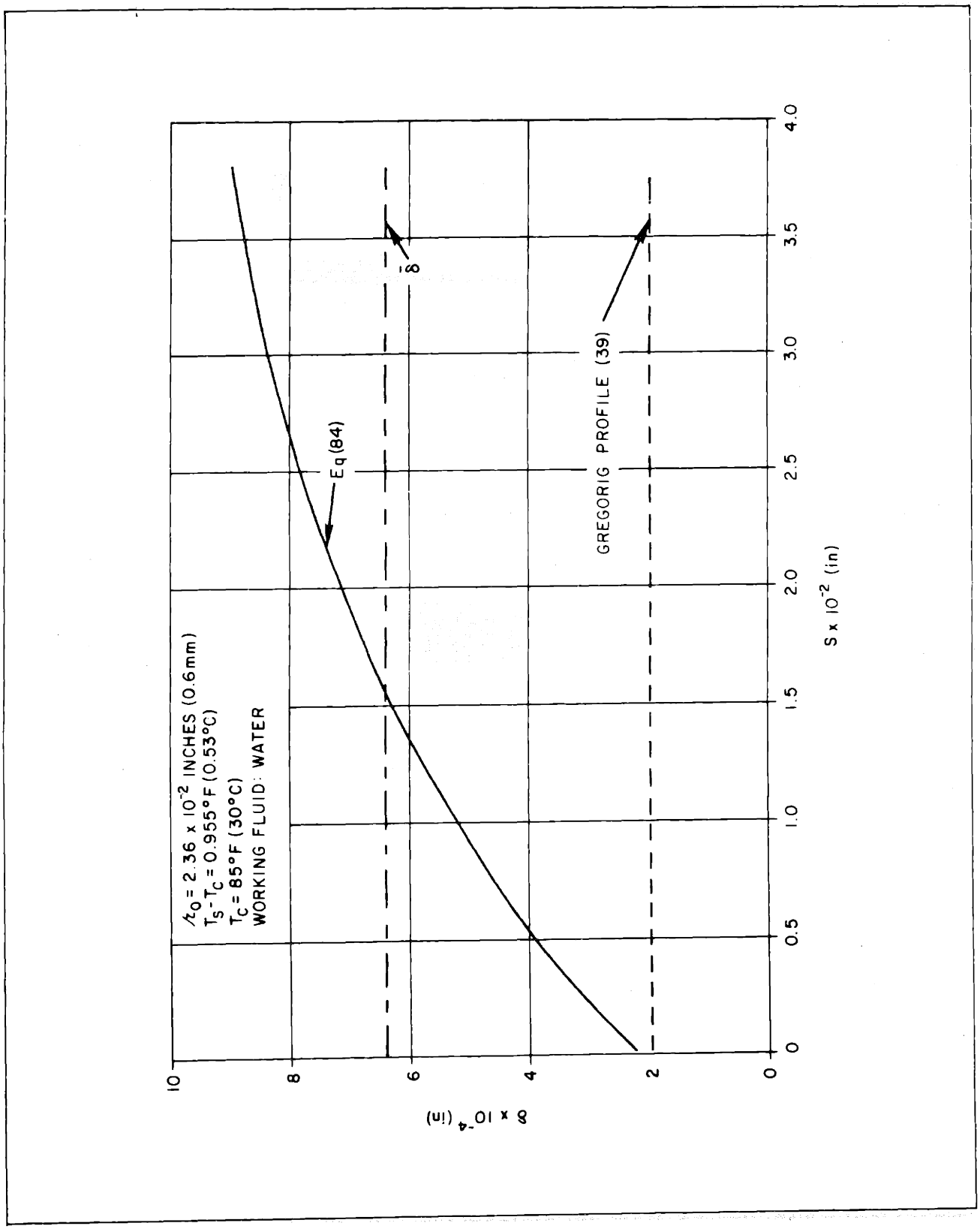

Fig. 31 - Condensate Film Thickness on Crest of Sinusoidal and Gregorig Type Profiles

4.4.2 Condensive Limit

In previous chapters the operation of the submerged condenser system was found to possess a condensive limit in the most significant range of operation. It became essential, therefore, to examine techniques for augmenting condensation heat transfer on horizontal surfaces. Since dropwise condensation is not yet possible with the standard dielectric fluids, a sinusoidally undulated surface was investigated.

The experimental results obtained for the condensive limit of a system employing a doubly-rippled condenser submerged in Freon-113 are presented in Fig. 32. The condenser heat flux based on the projected area of the undulated surface is seen to correspond to nearly twice the heat flux associated with film condensation on a smooth horizontal surface of the same projected area, (Eq. (47)). The condensive limit of the experimental submerged condenser system was, thus, raised by a factor of 2.

However, the augmented performance is almost 40 percent lower than was anticipated on the basis of the analysis in Subsection 4.3. While some "flooding" of the undulation crests may have occurred and while some of the undulations are rendered ineffective by flat regions, it is unlikely that these factors could cause such a dramatic discrepancy between analysis and data. Alternately, the presence of noncondensables, primarily air, could very well have led to the observed deterioration in thermal performance.

As discussed earlier in Subsection 4.2 and in the Appendix, the Freon-113 used as the working fluid was degassed prior to filling the submerged condenser system and then degassed for approximately one hour in the system. This procedure appears to have worked successfully for the smooth condenser surface since, as shown in Fig. 24, the condensive limit data correspond closely to film condensation on that surface. However, the numerous undulations present on the doubly-rippled surface may have trapped a substantial number of small air bubbles during system degassing and led to the observed discrepancy. The presence of small amounts of noncondensables has long been known to cause dramatic degradation in condenser performance [7] , but noncondensables are especially troublesome in condensers with nonuniform heat fluxes. As a result of spatial variations

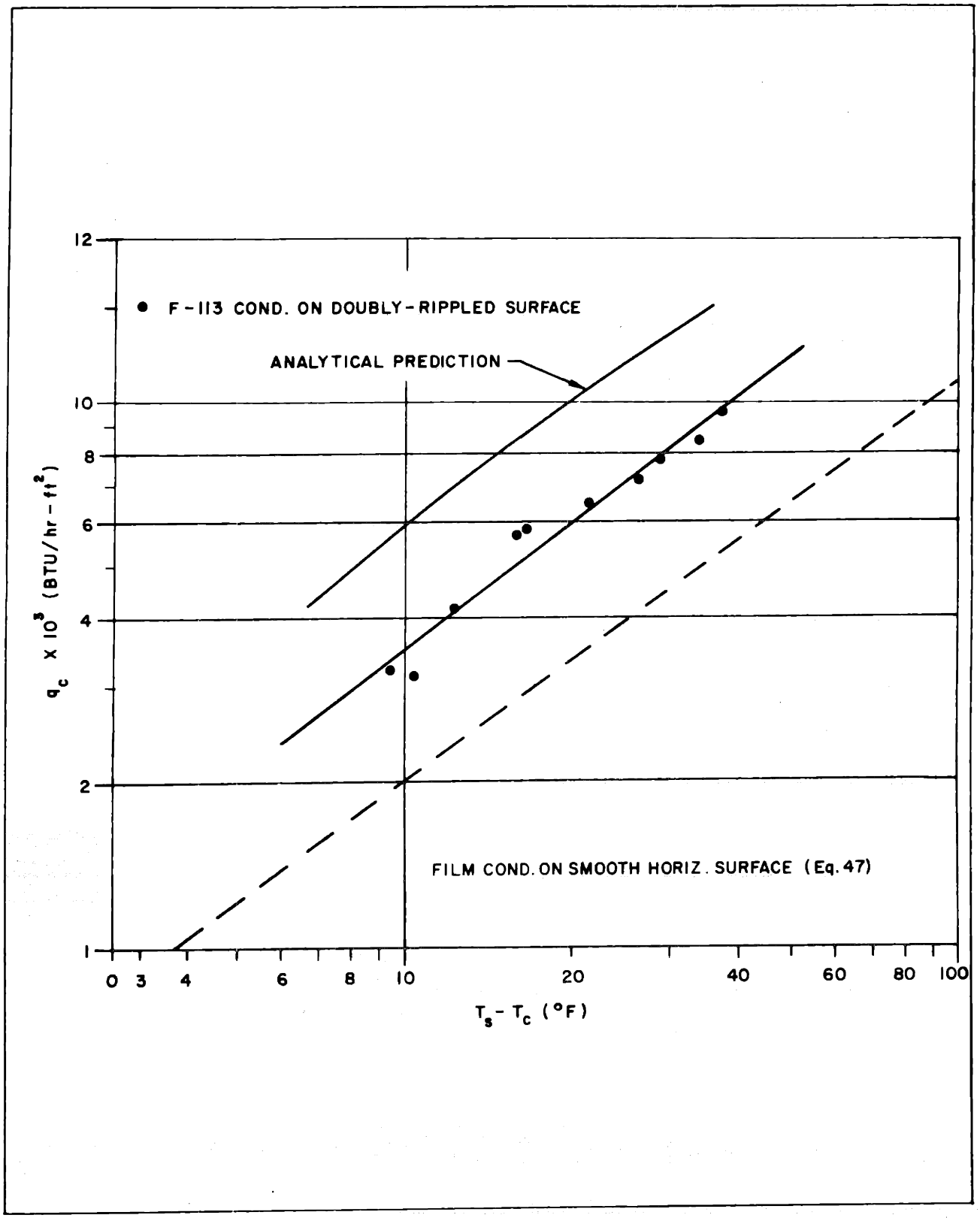

Fig. 32 - Condensive Limit for Doubly-Rippled Horizontal Condenser Surface

in heat flux the noncondensables collect near the regions of initially high heat flux and thus prevent high rates of condensation in those regions [42] . Degradation in thermal performance of 50 to 100 percent are not uncommon . The implications for the doubly-rippled condenser surface which is strongly dependent on nonuniform heat flux are clear and may help explain the observed performance.

If noncondensables are, indeed, the cause of the observed discrepancy between the predicted and observed condensive limit on the sinusoidally undulated surface, then greater success could be achieved by using more sophisticated degassing equipment. However, the experimental apparatus used throughout this investigation attempted to duplicate as closely as possible a practical submerged condenser system for cooling of electronic components. The degassing procedure was again modelled after common techniques utilized by installation and maintenance personnel. It would, consequently, appear that no easily maintained submerged condenser system could operate at peak efficiency with the doubly-rippled condenser surface. Though obviously some improvement over the observed performance could be obtained by judicious redesign of the condenser surface, operation at 50 to 60 percent of the theoretical limit may well be typical of practically attainable performance levels for condenser surfaces of this type.

5. DESIGNING A SUBMERGED CONDENSER SYSTEM

5.1 Introduction

The rapidly increasing use of high speed, high power electronic components has necessitated the development of electronic cooling systems which employ boiling heat transfer to dielectric fluids. While initially pool boilers were designed to operate with remote condensers, as shown in Fig. 1, difficulties with noncondensables and varying liquid level have led to the use of condensers submerged in the liquid. In a submerged condenser system, shown in Fig. 2, the condenser surface serves primarily to subcool the liquid in the pool boiler and vapor bubbles generated at the surfaces of the dissipative electronic components rise and begin to condense in the fluid. Due to the elimination of a vapor space, considerable economics in volume and weight can be realized [8, 9] and the presence of noncondensables is of significantly less consequence.

As in other boiling systems, the dissipative elements in the submerged condenser system experience only moderate increases in temperature as a result of large increases in their dissipated power. Furthermore, low dissipation or thermally passive components immersed in the bulk fluid undergo only slight changes in temperature for large variations in the total power dissipated. The operation of the submerged condenser system has been found to possess two possible upper bounds. For large values of condenser surface subcooling and/or low heater-to-condensersurface area ratios, the upper bound is established by the critical heat flux or "burnout" at the boiling surface. For low values of condenser surface subcooling and/or high area ratios, however, a condensive limit exists which has been found to correspond to the heat flux associated with film condensation on a downward facing horizontal surface. Typical design criteria for submerged condenser systems including available heat sink temperatures and the need to reduce condenser surface area, usually result in system operation in the region bounded by the condensive limit.

The preceding chapters have presented in detail the operating characteristics of an experimental submerged condenser system, shown in Figs. 5 and 6. The thermal mechanisms active in the system, its operational limits and significant design parameters have been identified, explored and, where possible, related to available heat transfer correlations. The working fluids, water and Freon-113, were chosen to span the range of fluid and thermal properties and the similarity in the operating characteristics for the two fluids enhances the generality of the obtained results. Utilizing the proposed models and correlations, it is now possible to establish a systematic design procedure for electronic pool boilers, of the type shown in Figs. 2 and 4b, employing horizontal condensers submerged in dielectric fluids. Although, it must be noted that some allowance should be made in Modes I and IIa for heater geometry and orientation.

5.2 Design Considerations

The heat transfer or packaging engineer called upon to design a submerged condenser system for the cooling of electronic components and/or devices by boiling transfer, is generally required to operate within a closely constrained environment. The heat dissipation of the components to be cooled, their target temperatures, and the operating environment are all specified. In addition, the system must be easy to maintain, transport and operate while its weight and physical dimensions must be compatible with adjacent and interrelated systems. It is the task of the design engineer to develop or choose hardware to meet these specifications.

In describing the operational behavior of the components and/or devices to be cooled, several aspects are of prime interest. The component or device geometry including the dimensions and physical structure, as well as mounting method and mounting density, establishes the physical size of the cooling system. The rate of heat dissipation by the components and/or devices and level of heat flux including time-averaged and peak values, as well as the time history or duty cycle, establishes the range of required heat removal capability.

The target component temperatures are the crux of the design. For most electronic components and/or devices several temperature constraints must be satisfied. First, an absolute maximum temperature, which if exceeded will result in the destruction of the element, is specified. Next, a desirable maximum temperature corresponding to the peaks in dissipation rate and a desirable average or base temperature are specified or implied through an element temperature - element reliability relation. Finally, reliability arguments are again invoked to limit the maximum spatial and temporal temperature variations within devices and components. These temperature considerations as well as the heat flux levels specified earlier help determine the thermal properties of the fluid in which the elements are to be submerged.

However, the operating environment of the submerged condenser system and electrical considerations also exert a profound influence on the choice of primary coolant. The range of pressures in which the system must operate, the nature of the secondary coolant available to cool the condenser, as well as the temperature and flow rate of this coolant must all enter into consideration. In addition, the dielectric constant of the primary coolant must be sufficiently high to prevent electrical arcing between the container wall and electrical elements or adjacent elements under the highest voltage differences to be encountered.

It is important to note that this design process, as most others, does not progress in a linear fashion. Some of the imposed constraints can be relaxed or altered if necessary to facilitate a practical thermal design. It will, therefore, be generally necessary to perform several cycles of calculations for slightly varying constraints, before the final design will emerge. Nevertheless, the procedure to be followed in each cycle will be similar to that indicated below.

5.3 Design Procedure

The submerged condenser system to be designed is of the type shown in Fig. 2 and is most appropriate for the cooling of power supplies and associated equipment. Judging from present submerged condenser systems it is anticipated that the mean distance of separation between the dissipative elements

and the condenser surface will be of the order of 4-6 inches and that a bellows type expansion chamber will be provided above the condenser. The system will be filled initially with a dielectric fluid which has been degassed by boiling at the ambient pressure and sealed.

Special note must be made of the significant role played by the ambient pressure in determining the operation of the submerged condenser system. Substantial reductions in ambient pressure, such as could be encountered in airborne applications, will influence both boiling and condensation in the system. With decreasing pressure the boiling curve of Fig. 18 shifts to the right, while the critical heat flux decreases slightly, but more importantly the reduction in T_{sat} leads to considerably lower surface temperatures. On the other hand, for a given condenser surface temperature the thermal driving force for condensation, $T_{sat} - T_c$, will be significantly reduced at lower ambient pressures and the condensive limit will be encountered at lower values of condenser heat flux. Furthermore, at reduced ambient pressure the lower vapor density will result in greater volumetric expansion in the condensive region of Mode II and at the condensive limit. Consequently, the range of environments within which the designed submerged condenser system must operate should be carefully studied and the most severe environment for each aspect of submerged condenser operation should be identified.

1. Choosing a Primary Coolant

Examine the design constraints and choose a dielectric coolant for which, at the highest pressure to be encountered, the maximum component heat flux does not exceed the critical heat flux, $q''_{h,\,max} < q''$ crit, and for which the incipence heat flux is below the minimum component heat flux, $q''_{incip} < q''_{h,\,min}$. In addition, determine that for the fluid chosen, the boiling surface temperature at $q''_{h,\,max}$ is at an acceptable level and the surface temperature difference between the minimum and maximum heat flux levels is within acceptable bounds.

2. Determining Condenser Surface Temperature

Use available information on the secondary coolant temperature, flow rate, and thermal properties as well as the dimensions of the coolant

passages in the condenser plate, in Eq. (94) below, to determine the heat transfer coefficient on the coolant side of the condenser. Eq. (94) is typical of the available forced convection correlations. For a particular geometry, other more accurate correlations may be available.

$$\frac{hD_e}{k} = 0.023 \left(\frac{\rho V D_e}{\mu}\right)^{.8} \left(\frac{\mu C_p}{k}\right)^{.4} \tag{94}$$

Add the film resistance, thus determined, to the conduction resistance through the condenser plate to establish the overall thermal resistance, R_t, between the condenser surface and the secondary coolant.

Using the total maximum power dissipation rate in the system and the average secondary coolant temperature in Eq. (95), determine the maximum average condenser surface temperature as a function of condenser surface area.

$$\overline{T_c} = \overline{T_f} + \frac{q_t R_t}{A_c} \tag{95}$$

3. Determining Flat Horizontal Condenser Area

Using Eq. (47) calculate the condensation heat transfer coefficient as a function of surface subcooling at the lowest ambient pressure to be encountered. The minimum condenser surface area, as a function of $\overline{T_c}$, is thus equal to:

$$A_c = \frac{q_t}{h_c(T_s - T_c)} = \frac{q_t}{C_2(T_s - T_c)^{3/4}} \tag{96}$$

Eqs. (95) and (96) can now be solved simultaneously to yield the minimum condenser surface area. To allow for the inevitable presence of some non-condensables and for possible error in the estimation of dissipation rates, increase the calculated condenser area by 15-25 percent.

4. Determining Volumetric Expansion

The maximum volumetric expansion in the submerged condenser system occurs at the condensive limit. Use Eq. (59) or (61) to determine the vapor gap depth, δ, at the condenser surface. Introduce this value into Eq. (46) along with the total dissipated power, the physical dimensions of the system, and the fluid properties to determine the maximum volumetric expansion.

5. Determining Heater Surface Temperature

Tabulate the peak and average heat flux level for all surfaces of interest and, if possible, use Eq. (7) for saturated pool boiling to determine the appropriate surface temperatures. However, as discussed in Subsection 3.2.1, for many surface-fluid combinations the value of C_{sf}, the constant required for Eq. (7), and the effects of subcooling on wall superheats are unknown. Consequently, if accuracy is required it may be necessary to experimentally determine the boiling curve and subcooling effects for the fluid and component geometries utilized in the designed submerged condenser system.

To determine the surface temperature of low dissipation components, a natural convection correlation such as Eqs. (1) and (2) is required. However, the actual heat transfer coefficients are likely to be considerably higher than calculated due to bubble-pumped augmentation resulting from vapor bubbles generated at the high dissipation components.

Steps 1-5 have served to establish the heater and condenser surface temperatures and the minimum area for a horizontal submerged condenser completely blanketed by vapor. However, as mentioned earlier, a prudent design should include a safety margin of 15-25 percent. With this margin, at the maximum design dissipation rates, the condenser will be only partially blanketed by vapor and the bulk temperature of the primary coolant will be below the saturation temperature. Furthermore, at off-design points resulting from average dissipation rates (as opposed to the maximum rates), operation in improved external environments or device and component startup, the condenser may be substantially free of vapor and rely primarily

on bubble-pumped convection to transport the dissipated heat. Under these conditions, an accurate knowledge of the bulk temperature is essential to the determination of the surface temperatures of the dissipative elements and the temperature of low dissipation control devices often present in the system.

The subcooling of the primary coolant at one off-design condition can be determined in the following manner:

a) Repeat Step 2 utilizing the off-design dissipation rates to calculate the condenser surface temperature.

b) Follow the procedure outlined in Subsection 3.2.3.2 and illustrated in Fig. 23, to determine the required bulk temperature.

If a more precise knowledge of the bulk subcooling for a range of total dissipation rates is required, the above procedure can be repeated several times and a family of constant condenser temperature curves relating condenser heat flux to $T_b - T_c$ can be generated as shown in Fig. 33 for 1 heater in water. As discussed in Chapters 2 and 3, at low condenser heat flux, heat transfer at the condenser is achieved exclusively by natural convection. Hence, the heat transfer coefficient at this lower bound can be determined from Eqs. (1) and (2) and $T_b - T_c$ calculated. At the condensive limit the bulk is at the saturation temperature and $T_{sat} - T_c$ is known from Eq. (47). As q''_c increases, T_b obviously increases towards T_{sat} and the bulk temperatures calculated in Step 7 can be used to establish the necessary curves.

5.4 Additional Considerations

5.4.1 Increasing Effective Condenser Area

Due to the many geometric constraints that must be satisfied in the design of a submerged condenser system, it may not always be possible to provide the required horizontal condenser area. Alternately, more compact packaging of the dissipative components could be realized if the condenser area could be reduced. A number of distinct approaches can be used to achieve this goal. Vertical fins can be added to or used to replace the horizontal surface. A doubly-rippled horizontal surface can be designed. The side walls of the submerged condenser container can be used as additional cooling surfaces.

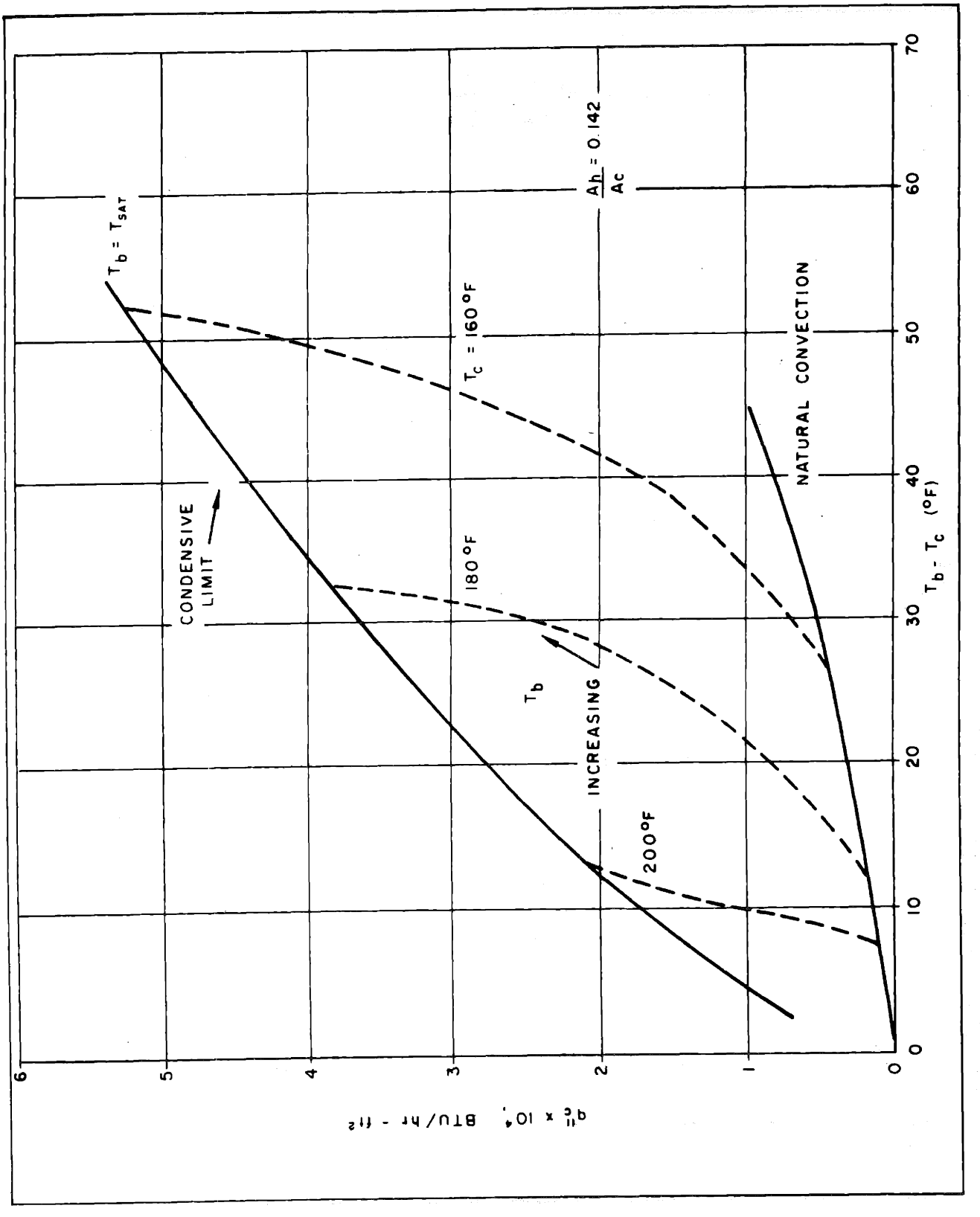

Fig. 33 - Bulk Temperature Variation with Condenser Heat Flux - Water

Fairbanks et al. [10] utilized a vertically finned condenser in their study of submerged condenser operation. Vertical fins can be used in a straightforward manner to increase the condenser area. However, the benefits gained may be outweighed by the substantial increase in the vapor volume as the condensive limit is approached and the loss of volumetric compactness.

The doubly-rippled surface discussed in Chapter 4, utilizes surface tension forces to improve the rate of condensation on a horizontal surface. The particular surface tested, described in detail in Subsection 4. 2 and the Appendix, led to a factor of two improvement in the condenser heat flux based on the projected surface area. The observed performance was, however, only 60 percent of the anticipated values due apparently to non-condensable gas difficulties. Thus, while Eq. (84) can be used to determine the theoretical performance characteristics of the doubly-rippled surface, the actual performance in a submerged condenser system is not likely to exceed 60 percent of that value.

The use of the side walls of the submerged condenser container as additional transfer surfaces can often be an extremely attractive solution. This approach was not explored in the present investigation, but it may be possible to establish an upper bound on the augmented coefficient by analogy to the present investigation. As discussed in Subsection 3. 1, the rate of convective transfer increases with the increase in buoyant force per unit volume resulting from the presence of a vapor fraction. The data available on the horizontal surface for the experimental submerged condenser system indicate that the highest augmented coefficient in the so-called convective mode was 2. 5 times the natural convection coefficient. The mechanism of augmentation on a vertical surface appears similar to that on a horizontal surface in the convective mode and, hence, the augmented convection coefficient can possibly be expected to approach 2. 5 times the natural convection coefficient in a system of similar dimensions.

5.4.2 Presence of Noncondensables

While all possible measures are to be taken to remove air and other noncondensables, it must be anticipated that some noncondensables will be present in the system. The design of the submerged condenser has, however, severely reduced the impact of noncondensables on the performance characteristics. When operating below the condensive limit the presence of noncondensables dissolved in the liquid reduces the collapse rate of the bubbles and small bubbles, containing primarily noncondensables, impinge on the condenser surface. If the condenser surface is pitched slightly ($\sim$ 5 degrees) towards the expansion chamber inlet, the gas bubbles slide along the surface and are vented into the expansion chamber. As a result, noncondensables do not substantially affect heat transfer at the submerged condenser surface. This is in sharp distinction with the vapor space condenser in which the noncondensables accumulate in the vapor space and impede the flow of vapor toward the condenser surface.

As the condensive limit is approached, a vapor gap does form at the condenser surface and some deterioration due to noncondensables may occur. However, most of the noncondensables will have been removed in the earlier stages of operation. Consequently, when noncondensables are present, the performance of the submerged condenser system can be expected to exceed that of a vapor space system even near the condensive limit.

While the effect of noncondensables on the performance characteristics has, thus, been minimized, the dissolved gases will substantially increase the system volumetric expansion as degassing of the coolant occurs. Due to the high gas solubility of many commercially used dielectric fluids, the resulting volumetric expansion might well be an order of magnitude higher than obtained from Eq. (46). It is, hence, essential that every reasonable effort be made to degas the working fluid prior to the commencement of submerged condenser operation.

5.4.3 Changing the Physical Scale

The physical scale of the submerged condenser system including the heater to condenser surface area ratio and separation distance can affect its range of thermal operation but the mechanisms described and operational limits defined are obviously independent of scale. Furthermore, small changes in the distance of separation between the heater and condenser surfaces are not expected to significantly affect the heat transfer coefficient at the condenser surface, although further research will be required to firmly support this concept.

5.4.4 Heater Configuration

The heater geometry and configuration used in the experimental apparatus were generally similar to the orientation and distribution of the dissipative electronic components typically found in submerged condenser systems. Nevertheless, locally dense and vertical packaging of components could lead to vapor channeling and slight alterations in the operational modes of the system. Of greater importance, however, is the effect of stacking one component above another on the boiling surface temperature. A recent study by Plevyak [43] , revealed that improved boiling transfer could be obtained on a surface placed above a bubble-generating source. The surface superheats in the nucleate boiling region were found to be significantly lower when the bubble source was activated. While these results are not surprising, they do point to a possible benefit to be derived from the judicious location in the submerged condenser system of critical components.

5.4.5 Two-Fluid Submerged Condenser System

While the use of a submerged condenser in pool boilers for electronic cooling has been found to possess many advantages, the high density of most commercially available dielectric fluids may impose a weight penalty in specific applications. It has, consequently, been proposed that two immissible

fluids be used jointly in the system and that the electronic components be immersed in the dense, dielectric fluid, while the condenser would be submerged in a low density, high saturation temperature fluid.

The condensive limit of such a system using Freon-113 and water was obtained in the present investigation. At the limit, the Freon vapor bubbles rose through the highly agitated water layer, and a Freon-113 vapor gap was found to form at the condenser surface. The rate of heat transfer was identical to that obtained with the pure Freon-113 submerged condenser system discussed in previous chapters.

This result is at variance with the findings of Simons and Seely [6] that, at a given condenser surface temperature, less vapor could be condensed in a two-fluid system than in a pure system and may suggest that the condensive limit of such a system depends on the choice of fluids. In particular, since some of the secondary fluid vapor mixes with the dielectric fluid vapor in the vapor gap, the vapor pressure of the low density fluid and the diffusivity of the dielectric fluid vapor through vapor of the secondary fluid can be expected to have some effect on the condensive limit.

CONCLUSIONS

The foregoing has presented in detail the results of an experimental and analytical investigation of boiling and condensation in a liquid-filled enclosure. The operating characteristics of an experimental boiling system, utilizing a condenser submerged in the fluid, were obtained and related to specific operational modes and thermal transport mechanisms. The working fluids, water and Freon-113, were chosen to span the range of fluid and thermal properties.

A lower bound of operation, corresponding to natural convection at both the heater and condenser surfaces, was identified. One of two possible upper bounds was similarly shown to govern system behavior. For large values of condenser surface subcooling and/or low heater-to-condenser area ratios, the upper bound was established by the critical or "burnout" heat flux at the heated surface. Alternately, low subcooling and/or area ratios approaching unity, typical of practical systems, resulted in an experimentally observed upper bound which was significantly below the critical heat flux and due to a condensation limit associated with vapor-blanketing of the condenser. Contrary to expectation, the condensive limit was found to be nearly insensitive to moderate inclination of the condenser surface.

A nondimensional vapor bubble collapse length, L_c/W, was found to govern the rate and mechanism of heat transfer at the submerged condenser surface. Values of $\frac{L_c}{W} \ll 1$ were associated with natural convection heat transfer at the submerged condenser. For $\frac{L_c}{W} \sim 1$, the presence of a substantial vapor fraction in the bulk liquid led to augmented convection, while for values of $\frac{L_c}{W} \gg 1$ condensation was found to dominate thermal transport at the condenser surface.

In the augmented convection region it was postulated that the presence of a vapor fraction in the fluid introduces an additional buoyant force which can dramatically increase the rate of heat transfer at the cold surface. Utilizing the appropriate bubble dynamics relations, it was found possible

to correlate the experimental results in terms of a single configuration factor for each geometry. Furthermore, the augmented convection relation was shown to facilitate the semiempirical determination of the bulk temperature variation with condenser heat flux.

It was found possible to increase the condensive upper bound in the submerged condenser system by enlisting surface tension forces to thin the condensate film on the surface. A doubly-rippled surface with small, constant radius of curvature undulations was shown to double the rate of vapor space condensation based on the projected area of the condenser surface.

A systematic design procedure for horizontal submerged condenser systems was presented and related to typical design considerations in the cooling of dissipative electronic components and devices.

REFERENCES

1. Cochran, D. L., "Boiling Heat Transfer in Electronics", presented at NEPCON-East, New York, 4-6 June 1968.

2. Weber, Samuel, et al., "LSI: The Technologies Converge", Electronics, February 20, 1966, p. 123.

3. Tirrell, J. C., "Power Considerations in High Speed TTL Logic", Computer Design, February 1969, pp. 36-47.

4. Bergles, A. E., N. Bakhru, and J. W. Shires Jr., "Cooling of High-Power-Density Computer Components", Tech. Report No. 70712-60, Dept. of Mech. Eng., MIT, 1968.

5. Hughes Aircraft Company, "Environmental Stabilization of Data Processors Program - Final Report", 21 September 1969.

6. Simons, R. E., and J. H. Seely, "A Survey of Vapor Phase Cooling Systems", EDN, January 1, 1969 pp. 53-56.

7. Rohsenow, W. M., and H. Choi, Heat, Mass and Momentum Transfer, Prentice Hall, Inc., New Jersey, 1961.

8. Mark, M., M. Stephenson, and C. E. Goltsos, "An Evaporative-Gravity Technique for Airborne Equipment Cooling", IRE Transactions, Vol. ANE-5, March 1958, pp. 47-52.

9. Goltsos, C. E., and M. Mark, "Packaging with a Flexible Container for Oil-Filled or Evaporative-Cooled Electronic Equipment", IRE Transactions, Vol, PEP-6, September 1962, pp. 44-48.

10. Fairbanks, D. R., C. E. Goltsos and M. Mark, "The Submerged Condenser", ASME Publication 67-HT-15, presented at ASME-AIChE Heat Transfer Conf., Washington, August 6-9, 1967.

11. Paradis, L. R., "Simplified Transmitter Cooling System", presented at 8th Inter. Circuit Packaging Symposium, San Francisco, California, August 21-22, 1967.

12. McAdams, W. H., Heat Transmission, McGraw-Hill Book Company, New York, 1954.

13. Jakob, M., Heat Transfer, Vol. I, Wiley, 1949.

14. Rohsenow, W. M., editor, Developments in Heat Transfer, MIT Press, Cambridge, Massachusetts, 1964.

15. Bergles, A. E., "Pool Boiling", Notes for MIT course, 1966.

16. Bergles, A. E., and W. M. Rohsenow, "The Determination of Forced-Convection Surface-Boiling Heat Transfer", Journal of Heat Transfer, 8, 1964, pp. 365-374.

17. Rallis, C. J., R. V. Greenland, A. Kok, "Stagnant Pool Nucleate Boiling from Horizontal Wires under Saturated and Sub-Cooled Conditons", South African Mechanical Engineer, 1, 1961, pp. 171-187.

18. Duke, E. E., and V. E. Schrock, "Void Volume, Site Density and Bubble Size for Sub-Cooled Nucleate Pool Boiling", Proceedings Heat Transfer and F. M. Instit. 1961, pp. 130-145.

19. Zuber, N., "On the Stability of Boiling Heat Transfer", Trans. of ASME, Vol. 80, No. 3, p. 711, 1958.

20. Ivey, H. J., and D. J. Morris, "On the Relevance of the Vapor-Liquid Exchange Mechanism for Subcooled Boiling Heat Transfer at High Pressure", AEEW-R 137, January 1962.

21. Han, C. Y., "Mechanism of Heat Transfer in Nucleate Pool Boiling", ScD Thesis, Mech. Eng. Dept., MIT (February 1962).

22. Moissis, R., and P. J. Berenson, "On the Hyrodynamic Transitions in Nucleate Boiling", ASME paper 62-HT-8, 1962.

23. Moissis, R., and P. Griffith, "Entrance Effects in a Two-Phase Slug Flow", J. of Heat Transfer, Trans. ASME Series C, Vol. 84, 1962, pp. 29-39.

24. Fritz, W., Phys Zeitschr, 36, 379 (1935).

25. Cole, R., and W. M. Rohsenow, "Correlation of Bubble Departure Diameters for Boiling of Sturated Liquids", AIChE Preprint 25, 10th Nat. Heat Transfer Conf., AIChE-ASME, Phil., Penn., August 1968.

26. Ivey, H. J., "Relationships Between Bubble Frequency, Departure Diameter and Rise Velocity in Nucleate Boiling", Journal of Heat and Mass Transfer, Vol. 10, 1967, pp. 1023-1040.

27. Graham, R. W., and R. C. Hendricks, "Assessment of Convection, Conduction, and Evaporation in Nucleate Boiling", NASA TND-3943, May 1967.

28. Gaertner, R. F., "Photographic Study of Nucleate Pool Boiling on a Horizontal Surface", Journal of Heat Transfer, February 1967, pp. 17-29.

29. Zuber, N., "Hydrodynamic Aspect of Boiling Heat Transfer", AEC Report, AECU-4439, 1966.

30. Berenson, P., "Transition Boiling Heat Transfer from a Horizontal Surface", MIT Report, DSR No. 7-8077, 1960.

31. Zuber, N., M. Tribur, and J. W. Westwater, "The Hydrodynamic Crisis in Pool Boiling of Saturated and Subcooled Liquids", Paper No. 27, Inter Heat Transfer Conference, Boulder, Col., 1961.

32. Wittke, D. D., and B. T. Chao, "Collapse of Vapor Bubbles with Translatory Motion", J. of Heat Transfer, February, pp. 17-24 (1967).

33. Tokuda, N., W. J. Yang and J. A. Clark, "Dynamics of Moving Gas Bubbles in Injection Cooling", J. of Heat Transfer, November 1968, pp. 371-378.

34. Florschuetz, L. W., and B. T. Chao, "On the Mechanics of Vapor Bubble Collapse", Journal of Heat Transfer, May 1965, pp. 209-220.

35. Plesset, M. S., and S. A. Zwick, "A Non-Steady Heat Diffusion Problem with Spherical Symmetry", J. of Applied Physics, Vol. 23, 1952, p. 95.

36. Gerstman, J., and P. Griffith, "The Effects of Surface Instabilities on Laminar Film Condensation", Tech. Report No. 5050-36, Dept. of M. E., MIT, 1965.

37. Jacob, J. D., and A. H. Shade, "Measurement of Temperature Associated with Bubbles in Subcooled Pool Boiling", J. of Heat Transfer, February, 1969, pp. 123-128.

38. Griffith, Peter, "Dropwise Condensation", Notes for Special Summer Course, Developments in Heat Transfer, MIT, 1970.

39. Gregorig, V. R., "Hautkondensation an feingewellten Oberflächen bei Berüchsichtigung der Oberflächenspannungen", Z. agnew, Math. U. Phys. (ZAMP) Vol. 5, 1954, p. 36.

40. Nabavian, K., and L. A. Bromley, "Condensation Coefficient of Water", Chem, Eng. Science, Vol. 18, 1963, pp. 651-660.

41. Gregorig, V. R., Exchangeuri De Chaleur, Librairie Polytechnic Beranger, Paris, France, 1965.

42. Gerstman, J., S. M. Thesis, Dept. of Mech. Eng., MIT, 1964.

43. Plevyak, T. J., "Improved Boiling Heat Transfer with Induced Vapor Bubble Mixing", ASME paper, 68-WA/HT-29, 1968.

44. Gill, D., MS Thesis, Mech. Eng. Dept., MIT, (1967).

APPENDIX
EXPERIMENTAL APPARATUS AND PROCEDURE

A. Apparatus

The apparatus used in the present investigation is shown in Figs. 5 and 6 and was chosen to simulate a practical submerged condenser system. Degassed water and Freon-113 were used as the working fluids. The apparatus consisted of five cylindrical heaters, 0.25 inch in diameter, electrically powered and oriented horizontally in a Plexiglas and brass enclosure 6 inches on a side.

A.1 Construction

The side walls of the container were made of 0.5 inch thick Plexiglas assembled from two 7 in. by 6 in. and two 6 in. by 6 in. plates bonded together with di-ethylene chloride and reinforced with screws. The top and bottom of the container were made of 0.5 in. brass plates, each 12 in. on a side. A groove, 0.25 in. deep and 0.75 in. wide, was machined in the upper plate to form a 5.75 in. square plateau in the center of the plate.

Rubber gaskets were placed between the Plexiglas and brass plates along the surfaces of contact. Four 0.25 in. threaded brass rods and appropriately placed nuts were used to compress the gaskets and insure proper sealing of the liquid-filled enclosure. The space remaining between the upper brass plate plateau and Plexiglas side walls, approximately 0.25 in. deep and 0.25 in. wide, was filled with liquid polyester resin which was allowed to harden.

An open reservoir, consisting of a 3 in. diameter, Plexiglas cylinder 5 in. long, sealed at one end and connected by a short, 0.375 in. diameter brass pipe to the liquid-filled enclosure, was located on top of the container. The reservoir served to maintain a nearly constant average system pressure of 14.9 psi despite fluctuations in the vapor fraction in the liquid. A valved vent tube was also provided in the near, left corner for removal of noncondensables from the system.

The entire apparatus was heavily insulated with glass fiber insulation. The apparatus was then placed on a dexion and asbestos board stand and raised approximately 4.5 ft. above floor level. The asbestos board provided thermal insulation for the lower brass plate and was in turn covered with fiber glass insulation. The dexion stand also provided the submerged condenser apparatus with a slight pitch ($\sim 5°$) towards the corner in which the vent was located to facilitate the removal of noncondensables.

A.2 Condensing Surface

The 0.23 ft.^{2} plateau of the upper brass plate served as the condensing surface. A 10 in. maximum diameter, doubly-wound, helical coil of 0.25 in. copper tubing was soldered to the exterior of the brass plate. City water at approximately 60°F inlet temperature and at a maximum flow rate of 1 gpm was circulated through the cooling coil. The water flow rate was measured with a Fischer-Porter Flowrator having a range of 0-6.8 lb. water/min.

A.3 Heaters

Four of the five heaters used were 0.25 in. in diameter and 8 in. long, 7029 Superwatt, Hotwat cartridge heaters powered by a-c current and rated at 940 watts each. Only the 6.0 in. in the center of the cartridge heaters was heated. The heaters were located 1.5 in. above the bottom of the enclosure and were inserted through Conax adapters in the Plexiglas side walls. The fifth and central heater was an especially prepared, thin-walled, 304 stainless steel tube, 0.212 in. I.D., 0.250 in. O.D., and 6 in. long. The tube was held between two copper rods which were connected to bus cables from a nearby d-c power source. The copper rods were inserted through Conax adapters in the Plexiglas side walls. The power supplied to the heater was determined by measuring the current and the voltage drop across the tube. At the maximum current of 520 amps, 3.74 kilowatts were dissipated in the tube wall.

The surface of all the heaters was finished with 320 emery paper prior to each series of runs. The ratio of total heated to condenser surface area varied from 0.14 to 0.71 depending on the number of heaters activated. The stainless steel tube heater was always one of the activated heaters and was used to determine the heater surface temperature. When necessary the tube heater was moved to alternate locations. When multiple heaters were used they each dissipated the same amount of heat. Properly calibrated ammeters and voltmeters were used to monitor the dissipated power in each heater.

A.4 Temperature Measurement

Two, 30 gauge copper-constantan thermocouples were positioned inside the hollow tube by teflon discs inserted from alternate ends of the tube. The teflon discs electrically insulated the thermocouple beads and insured accurate measurement of the inside tube wall temperature. The average heater surface temperature was, then, determined using Eq. (97), derived in [44] .

$$T_c = T_i - \frac{EI}{k}\left\{\frac{1}{4\pi L} - \frac{\ln (r_e/r_i)}{2\pi\left[\left(\frac{r_e}{r_i}\right)^2 - 1\right] L}\right\} \tag{97}$$

EI is the electrical power supplied to the tube, L the tube length, and k the thermal conductivity.

The thermal conductivity of the 304 stainless steel in Btu units was taken as $k = 8.7\ (1 + 5.25 \times 10^{-4}\ T)$.

The average condenser surface temperature was determined with three, 30 gauge copper-constantan thermocouples located 0.03 in. below the surface and at increasing distances (1.00, 1.625, and 2.50 in.) from the center of the condenser surface along the central plane. The temperatures recorded at these locations were extrapolated to the surface and a weighted average surface temperature determined. As anticipated, the condenser surface was found to be somewhat cooler away from the center, due to non-uniform heat flux near the ends of the plateau. However, the maximum

difference between any measured temperature and the average surface temperature did not exceed 7°F and was then less than 10 percent of the significant temperature driving force, $T_s - T_c$.

The bulk temperature of the working fluid was measured by four, 30 gauge copper-constantan thermocouples sheathed in 0.072 in. O.D. stainless steel tubes. The thermocouple beads were exposed approximately 1/16 in. The sheathed thermocouples were inserted through Conax adapters in the brass plate forming the base of the enclosure. The four bulk temperature thermocouples were free to travel vertically in the enclosure.

In addition to the above measurements, the inlet and outlet temperatures of the circulating city water were obtained by attaching insulated thermocouple beads to the inlet and outlet of the cooling coil. All the thermocouples described above were connected individually to a Brown recording potentiometer which was referenced to an ice junction. Periodic potentiometer tests using a standard cell were made to insure accuracy.

Using the measured coolant flow rate and inlet and outlet temperatures as well as the power dissipation of the heaters, an exact heat balance could be performed on the submerged condenser system. A series of tests indicated that a heat balance to better than 5 percent could be obtained due to the heavy insulation on the apparatus. Consequently, in subsequent data runs the dissipated power in the heaters was taken as the true heat input to the system.

A.5 Doubly-Rippled Condenser Surface

The doubly-rippled brass surface shown in Figs. 28 and 29 was used in the condensation experiments described in Chapter 4. The 0.25 in. thick and 5.75 in. square surface was assembled from 4 smaller squares and contained both undulations and grooves. The undulations were of constant curvature with a radius of 0.015 in. and ran continuously along each groove. The grooves were 0.125 in. in radius and were spaced 0.295 in. from center to center. Two 0.25 in. wide shoulders extended the entire length of the surface, 5.75 in., and ran parallel to the grooves. The surface area of the

doubly-rippled surface, excluding the two smooth shoulders, was approximately 0.51 ft.^{2}, while the total surface area equaled 0.53 ft.^{2} or 2.38 times its projected area.

The doubly-rippled surface was silver-soldered to a 0.5 in. thick brass plate, 12 in. on a side. One side of the brass plate contained a 0.25 in. deep trough, 6.5 in. square. The undulated surface, described above, was centered in the trough and silver-soldered to the brass plate. A 5.75 in. square undulated plateau was thus formed at the center of the plate.

The brass plate containing the undulated surface was now used to replace the upper brass plate in the submerged condenser apparatus. Rubber gaskets were again used along the Plexiglas-brass surfaces of contact and were compressed by tightening the nuts on the connecting rods. Liquid polyester resin was used to fill the gap around the undulated plateau.

The undulated plateau served as the condensing surface in the experiments described in Chapter 4. A doubly-wound helical groove, 0.125 in. deep and 0.25 in. wide was machined in the external side of the brass plate and a 12 in. square, 0.5 in. thick, Plexiglas plate was bolted to the brass plate to form a closed cooling channel. City water at 60°F inlet temperature was circulated through the channel.

The average condenser surface temperature was determined with three, 30 gauge copper-constantan thermocouples located 0.005 in. below the root of the surface undulations at the top of the groove and at increasing distances (0.75, 1.75, and 2.75 in.) from the center of the condenser surface along the central plane. The temperatures recorded at these locations were extrapolated to an imaginary plane passing through the root of the undulations at the top of the grooves and a weighted average condenser surface temperature determined. It must be noted that this temperature does not correspond to the true surface temperature along the groove. Rather, it is somewhat lower and incorporates the temperature difference associated with thermal conduction through the "ribs" separating the grooves. The variation in surface temperature from the top to the bottom of the undulation was calculated to be less than 0.5°F for the maximum heat flux encountered.

All other details of construction and instrumentation were identical to those of the basic submerged condenser apparatus.

B. Procedure

The operating characteristics of the submerged condenser apparatus and other significant data were obtained in a series of data runs for each working fluid and heater configuration. Prior to each series of runs, the working fluid was carefully degassed.

B. 1 Degassing Procedure

Nearly complete degassing of the working fluid was accomplished in a two-step procedure. One gallon of the working fluid was first poured into a large beaker and placed above a gas burner. The fluid was brought up to the saturation temperature and allowed to boil vigorously (for 5 minutes in the case of Freon-113 and approximately 30 minutes for water). The boiling fluid was then poured into the reservoir on top of the submerged condenser apparatus and allowed to fill the enclosure. The air formerly occupying the enclosure was allowed to escape through the open vent. Small additional quantities of fluid were boiled in a similar manner and added to the reservoir until all the air was driven out of the enclosure and the reservoir was half filled with liquid. The vent was now closed.

Next, the four cartridge heaters were activated and the power increased until boiling had commenced at each one. Large air bubbles collected at the condenser surface near the vent and were periodically removed by opening the vent valve. This procedure was repeated until a vapor gap formed at the condenser surface and large quantities of vapor were seen to be rising into the liquid reservoir.

Due to some leaks in the enclosure and the presence of an air-liquid interface in the reservoir, complete degassing of the fluid could not be achieved. Consequently, in the course of a series of runs, an air bubble would form and slowly grow at the corner of the condenser surface in which the vent was located. Periodic opening of the vent valve allowed the accumulated air to escape and minimized the effect of the air on the condenser performance.

Following each series of runs, the flow of water through the cooling coil was stopped and the procedure described in the previous paragraph repeated.

B. 2 Operating Procedure

For each series of runs, the heat input at the selected heater configuration and, hence, the condenser and heater surface heat flux, was maintained constant. However, the flow rate of city water through the cooling coil was varied. The initial run of each series was made with the full flow of 1 gpm through the coil. When steady state was achieved, the condenser surface, heater surface, and bulk temperatures as well as the inlet and outlet water temperatures were recorded. As the water flow rate was decreased, the average water temperature in the coil increased and the heat transfer coefficient on the fluid side of the coil decreased. Consequently, the condenser surface temperature increased and a new data point was obtained.

This procedure was repeated until the condenser surface was blanketed by vapor and large quantities of vapor were seen to be rising into the liquid reservoir. At this point, the flow of cooling water was increased somewhat so as to slightly reduce the condenser surface temperature. This small change was performed so as to maintain the vapor gap at the condenser surface but reduce to a minimum the amount of vapor rising into the reservoir. This was defined as the condensive limit and any further increases in condenser surface temperature resulted in large scale vapor transfer into the reservoir and a rapidly falling liquid level in the enclosure.

BIOGRAPHY

Avram Markowitz was born in Brooklyn, N. Y. on January 19, 1946. He spent 8 of his childhood years in Israel and returned to the U. S. with his family, in time to enter the 7^{th} grade. After completing his high school education at the A. Lincoln High School in Brooklyn, he entered Massachusetts Institute of Technology in September 1963.

In 1966 he was admitted to the Mechanical Engineering Department Honors Program and completed his Bachelor and Master of Science degree jointly in June 1968. His Masters thesis investigation "Heat Transfer in Spray Towers" was supervised by Prof. Arthur E. Bergles. A paper based on the thesis has been published in the Chemical Engineering Progress, Symposium Series 102, Volume 66 (1970).

During his Sophmore year at MIT, he played in the goal for the MIT soccer team and won All-New England honors. Following the 1965 varsity season, he joined the Boston Tigers, a professional soccer team, and played for several years in the American Soccer League.

In September 1966 Avram was married in New York to Annette Pavony. The couple has a 4-month old son, Barak.